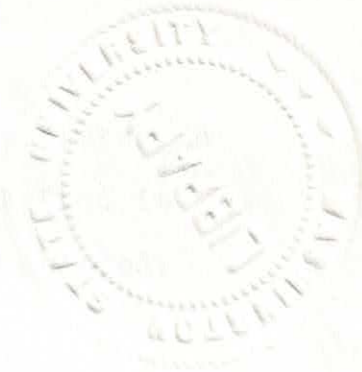
BERTHOLF

LONGITUDINAL ELASTIC WAVE PROPAGATION IN FINITE CYLINDRICAL BARS

LONGITUDINAL ELASTIC WAVE PROPAGATION IN FINITE CYLINDRICAL BARS

By

LARRY D. BERTHOLF



A thesis submitted in partial fulfillment of the requirements for the degree of

DOCTOR OF PHILOSOPHY IN

ENGINEERING SCIENCE

WASHINGTON STATE UNIVERSITY

1966

To the Resident Instructional Staff:

The members of the Committee appointed to examine the thesis of LARRY D. BERTHOLF find it satisfactory and recommend that it be accepted.

H. A. Sorensen
Chairman

John A. Shetland

George E. Worrall

Richard F. Fincher

887768

ACKNOWLEDGMENTS

The author would like to express his sincere gratitude to the following persons and organizations:

Professor George E. Duvall for the generous number of pleasant hours he spent giving me his advice, encouragement, and continual interest.

Professor John A. Smetana, for introducing me to the subject of elastic wave propagation and for giving me continual excellent guidance.

Professor Harry A. Sorenson for his interest and concrete advice.

Professor Richard F. Tinder for his help with this thesis.

Professor Ottis W. Rechard, Director of the Washington State University Computing Center, for his generous allotment of computer time.

The National Aeronautics and Space Administration for personal financial support.

Mr. Robert G. Colwell, my colleague and sounding board, for his suggestions, questions, and corrections.

My wife, Carol, who has done more to help me than anyone should be expected to do.

TABLE OF CONTENTS

	Page
ACKNOWLEDGMENTS	iii
LIST OF TABLES	vi
LIST OF ILLUSTRATIONS	vii
Chapter I. INTRODUCTION	1
Historical Background	1
Statement of the Problem	4
II. EQUATIONS OF MOTION AND THE BOUNDARY CONDITIONS FOR A SEMI-INFINITE BAR	6
Equation of Motion in Vector Form	6
Component Equations of Motion	8
Components of Stress and Strain	11
Boundary Conditions and Conditions for Proper Behavior	14
III. DIFFERENCE SCHEME FOR A SEMI-INFINITE BAR	18
Finite Difference Equations of Motion	20
Boundary Conditions in Difference Form	23
Stability of the Difference Equations	30
IV. POCHHAMMER-CHREE SOLUTION (P.C.S.) FOR THE INFINITE BAR	37
Pochhammer-Chree Method	37
Numerical Calculations	40
V. VALIDITY OF THE NUMERICAL SOLUTION AT POINTS REMOVED FROM THE END OF A SEMI-INFINITE BAR	46
Numerical Method	47
Comparison of the Numerical Solution with P.C.S.	56
Summary of Numerical Results	67
VI. VALIDITY OF THE NUMERICAL SOLUTION AT POINTS NEAR THE END OF A SEMI-INFINITE BAR	70
Boundary Conditions for a Pressure Applied at z = 0	72

Page

Chapter
VI.--Continued

Numerical Solution near the Loaded End for Small Values of Time. 76
Comparison between the Numerical Solution and Experimental Data at the Radial Surface of the Bar. 78

VII. NUMERICAL SOLUTION FOR REFLECTIONS IN FINITE CYLINDRICAL BARS. 90

Boundary Conditions for a Free End. 90
Boundary Conditions for a Fixed End 92
Summary of Numerical Results. 92

VIII. CONCLUSIONS AND RECOMMENDATIONS 100

Conclusions 100
Recommendations 101

LITERATURE CITED 103

APPENDIX
A. NOMENCLATURE. 108

B. JUSTIFICATION OF THE ACCELERATION APPROXIMATION 112

C. COMPUTER PROGRAM. 117

D. NUMERICAL VALUES FOR POCHHAMMER-CHREE SOLUTION. 128

ABSTRACT 133

LIST OF TABLES

Table		Page
1.	The Effect of Wave Length on the Phase Velocity in the P.C.S.	43
2.	Error between Numerical Solution and P.C.S.	66
3.	Physical Constants Used in the Numerical Procedure for a Step in Pressure	75
4.	Numerical Values for Pochhammer-Chree Solution	129

LIST OF ILLUSTRATIONS

Figure		Page
1.	The Stress Components in Cylindrical Polar Coordinates.	15
2.	The Deformations Necessary to Find the Deformation at the Next Time Step.	24
3.	Values of U(r,z) and W(r,z) Obtained from Equations (40)	25
4.	Values of U(r,z) and W(r,z) Obtained from the Boundary Conditions at r = 0 and z = 0	27
5.	The Stability Criteria for the Difference Equations.	35
6.	The Radial Distribution of u_r in the P.C.S.. . . .	44
7.	The Radial Distribution of u_z in the P.C.S.. . . .	45
8.	The Effect of Δz on the Accuracy of the Numerical Solution	52
9.	Error Introduced by Increasing Δz.	53
10.	The Effect of Δt on the Accuracy of the Numerical Solution	55
11.	Summary of Numerical Results at the Greatest Value of Time.	58
12.	Example of "Equivalent Nondimensional Phase Velocity" Determination at z = 6 cm and t = 40 μsec	60
13.	Values of the "Equivalent Nondimensional Phase Velocity".	61
14.	Deviation in the Radial Distribution of the Deformation for $d/\lambda' = 0.3$	63
15.	Deformation vs. Axial Distance at Various Times. .	68
16.	The Deformation as a Function of Time at z = 8 . .	69
17.	The "Core of Influence" as Determined by the Locus of Constant U(r,z,t)/W(r,z,t) Values	79

Figure Page

18. Growth of Axial Strain from One-Dimensional Strain to One-Dimensional Stress. 80

19. Time Records for Radial Displacement and Axial Strain as Obtained Experimentally by Miklowitz and Nisewanger 82

20. Comparison of Numerical Solution and Experimental Data at One Diameter from the Loaded End 84

21. Comparison of Numerical Solution and Experimental Data at Two Diameters from the Loaded End. . . . 85

22. Development of the "Spike" in the Axial Surface Strain with a Step of Pressure Applied at z = 0. 86

23. Effect of Δz on the Numerical Solution at One-Fourth of a Diameter from the Loaded End of the Bar 88

24. Surface Strain in a Two-Diameter Long Cylindrical Bar as a Function of Axial Position at the Indicated Values of Time 93

25. Radial Distribution of U at t = 14.7 μsec and Several Values of z in a Two-Diameter Long Bar . 94

26. Surface Strain in a One-Diameter Long Cylindrical Bar as a Function of Axial Position for Small Values of Time 95

27. Surface Strain in a One-Diameter Long Cylindrical Bar as a Function of Axial Position for Larger Values of Time 96

28. Surface Strain in a Two-Diameter Long Cylindrical Bar as a Function of Time at Different Axial Positions. 97

CHAPTER I

INTRODUCTION

Historical Background

In studying the history of almost any field of investigation there always seem to be certain efforts that particularly stand out as major contributions. In the field of longitudinal wave propagation in elastic bars such outstanding contributors include: Bernoulli [4],[1] Pochhammer [41], Chree [6], Bancroft [2], Davies [10], and Skalak [51].

Analytical Methods

Bernoulli obtained the most approximate solution to the cylindrical bar problem. This approximate solution does not account for the radial inertia of the bar and is commonly called the elementary stress wave solution. It is the solution of the one-dimensional wave equation where the phase velocity is the same for every frequency and equals $\sqrt{E/\rho}$.

Pochhammer and Chree independently applied the general three-dimensional differential equations of motion to the cylindrical bar problem. The equations of motion were transformed to cylindrical coordinates and solved for steady sinusoidal motion of an infinite bar. This solution demonstrates that the

---

[1]Numbers in brackets refer to references at the end of this paper.

phase velocity in the bar is frequency dependent and never greater than the very low frequency phase velocity $\sqrt{E/\rho}$.

Bancroft computed numerical values for the frequency equation given in the Pochhammer-Chree solution and plotted the phase velocity as a function of wave length for several Poisson ratios. The numerical solution of the frequency equation also allowed Bancroft to plot the axial deformation of the bar as a function of radial position in the bar for any wave length.

Whereas Bancroft was the first to describe numerically the exact solution to the infinite bar problem, Davies was the first to confirm experimentally the interdependence of frequency and phase velocity. In Davies' experiment a pulse composed of many waves with different frequencies was propagated in a very long bar and the dispersion of these waves was observed. He found close agreement with the P.C.S. (Pochhammer-Chree Solution) at long distances from the point of application of the pulse. Davies also pointed out that Bancroft made a numerical error in his calculations for the radial distribution of the axial deformation.

The first analytical solution to the problem of a bar with an end (semi-infinite) was obtained by Skalak. This solution was obtained by considering a collision of two semi-infinite cylindrical bars and using a double Fourier transform. Although the end conditions for this method are very restrictive (it was assumed that the impact results in a constant end velocity and caused a plane axial deformation at the

impact), the Fourier transform method has allowed other investigators [8,15,27,36] to obtain analytical solutions to more general problems. Solutions obtained by the Fourier transform method are expressed as integrals. The integrand is a very complicated function of time and position. The integration has been accomplished only for large values of time.

Experimental Studies

In experimental investigations of longitudinal wave propagation in bars, one of two methods is generally employed. The first is that of applying a stress pulse to one end of the bar and observing changes in strain at the surface. The other method is to produce standing waves in the bar by forcing the ends harmonically and observing surface nodes.

Both methods have produced a great deal of experimental data that verify the P.C.S. Some of these are: [8,11,12, 15,17,23,24,29,32,36,40,45,47,49,50,53).

The experimental studies of particular interest are those by Miklowitz and Nisewanger [32] and DeForest [12]. DeForest's experimental study was one of the first that utilized bonded strain gages. Also, it is one of the few that includes pictures of wave forms demonstrating reflections from the ends of a relatively short bar. In Miklowitz and Nisewanger's exhaustive experimental study, several pictures of wave forms are included. The wave forms were obtained at many locations on a long bar including points near the end of the bar where a step change in pressure is applied.

Statement of the Problem

Although there are many approximate theories [4,28,34, 43] that can be used for the solution of the finite bar problem, no exact analytical solution has yet been obtained.

In this study the exact theory is used and the complete differential equations of motion for an elastic solid are derived for cylindrical coordinates and written in terms of finite differences for solution on a digital computer. Depending upon the boundary conditions, the numerical solution to the finite difference equations will approximately describe any elastic wave propagation problem in this geometry from a nearly semi-infinite bar to a thin circular plate. It should be emphasized that the approximation involved is a result of solving the exact equations by approximating the derivatives with finite differences. In fact, with a sufficient amount of computer time this approximation can be made as refined as desired.

Axial symmetry is assumed because of the limited capacity of computing machinery. Since numerical solutions become more accurate as the increment sizes become smaller, it is desirable to use as many increments as possible for a given interval. The axi-symmetric case allows the elimination of one dimension and can be treated more accurately than the three-dimensional case. Although this limits the number of problems that can be solved, any type of longitudinal wave propagation can be considered and approximate solutions can be found at <u>every</u> point in the body including the ends.

The numerical solution is substantiated by showing that it asymptotically approaches the P.C.S. as the bar becomes very long and by showing that the solutions at the surface of a finite bar agree with those obtained in experiments.

Plates are not considered in this paper but the analysis could be easily extended to include longitudinal wave propagation in plates.

CHAPTER II

EQUATIONS OF MOTION AND THE BOUNDARY CONDITIONS FOR A SEMI-INFINITE BAR

Equation of Motion in Vector Form

The equation of motion for a three-dimensional elastic body is derived by using Hooke's Law and Newton's Second Law of Motion. In the absence of body forces only the surface forces need be considered in a force summation.

Since the surface force on a body is the stress times the area, Newton's Law can be written as follows:

$$\iint_A \vec{\vec{S}} \cdot d\vec{A} = \iiint_\tau \rho \frac{D\vec{V}}{Dt} \, d\tau \tag{1}$$

where A is the surface area, $\vec{\vec{S}}$ is the stress tensor, τ is a constant Eulerian volume, ρ is the mass density, $\vec{V}$ is the velocity vector, t is the time, and D/Dt denotes the substantial time derivative. If there are no singularities, the Gauss Integral Theorem may be applied to obtain equation (2):

$$\iiint_\tau \nabla \cdot \vec{\vec{S}} \, d\tau = \iiint_\tau \rho \frac{D\vec{V}}{Dt} \, d\tau. \tag{2}$$

But since the volume of the body is arbitrary:

$$\nabla \cdot \vec{\vec{S}} = \rho \frac{D\vec{V}}{Dt}. \tag{3}$$

Also for small displacements (see Appendix B) this reduces to:

$$\nabla \cdot \vec{\vec{S}} = \rho \frac{\partial^2 \vec{u}}{\partial t^2} \tag{4}$$

where $\vec{u}$ is the deformation vector.

For an elastic body, equation (4) can be written in the single variable $\vec{u}$ by employing Hooke's Law. Defining the dilation θ, as shown in equation (5), and assuming that the

$$\theta = \nabla \cdot \vec{u} \tag{5}$$

body is isotropic and homogeneous, Hooke's Law reduces to:

$$\sigma_{ij} = 2\mu\varepsilon_{ij} + \lambda\theta\delta_{ij} \tag{6}$$

where σ_{ij} are the components of the stress tensor, ε_{ij} are the components of the strain tensor, δ_{ij} is the Kronecker delta, and μ and λ are the Lamé constants. The Lamé constants can also be expressed in terms of Young's modulus (E) and the Poisson ratio (ν):

$$\mu = \frac{E}{2(1 + \nu)} \tag{7}$$

$$\lambda = \frac{E\nu}{(1 + \nu)(1 - 2\nu)}. \tag{8}$$

Equation (6) can also be written as a matrix equation as follows:

$$\vec{\vec{S}} = 2\mu\vec{\vec{E}} + \lambda\theta\vec{\vec{I}} \tag{9}$$

where $\vec{\vec{I}}$ is the unit or identity matrix and $\vec{\vec{E}}$ is the strain tensor which can be expressed in terms of the deformation as follows:

$$\overleftrightarrow{E} = \frac{1}{2}(\nabla\vec{u} + \widetilde{\nabla\vec{u}}). \tag{10}$$

In equation (10) the transpose of $\nabla\vec{u}$ is written as $\widetilde{\nabla\vec{u}}$.

Combining equations (4), (9), and (10), the equation of motion in the single variable $\vec{u}$ is obtained.

$$\rho\frac{\partial^2\vec{u}}{\partial t^2} = \mu\nabla\cdot(\nabla\vec{u} + \widetilde{\nabla\vec{u}}) + \lambda\nabla\cdot(\nabla\cdot\vec{u})\overleftrightarrow{I}. \tag{11}$$

Equation (11) can be written in a more convenient form by using the identities given in equations (12), (13), and (14) to obtain equation (15).

$$\nabla\cdot(\nabla\cdot\vec{u})\overleftrightarrow{I} = \nabla\nabla\cdot\vec{u} \tag{12}$$

$$\nabla\cdot(\widetilde{\nabla\vec{u}}) = \nabla\nabla\cdot\vec{u} \tag{13}$$

$$\nabla\cdot\nabla\vec{u} = \nabla\nabla\cdot\vec{u} - \nabla\times(\nabla\times\vec{u}) \tag{14}$$

$$\rho\frac{\partial^2\vec{u}}{\partial t^2} = (\lambda + 2\mu)\nabla\nabla\cdot\vec{u} - \mu\nabla\times(\nabla\times\vec{u}). \tag{15}$$

It should be noted that these equations are invariant for orthogonal transformations so long as care is used in the definitions of the operators [3].

Component Equations of Motion

The specific body to be considered in this work is a cylindrical bar. Thus, it is required to ultimately obtain the equations of motion, the boundary conditions, the stress components, and the strain components in the natural cylindrical polar coordinates. In order to write the component equations of motion it is convenient to introduce the rotation

vector $\vec{\omega}$ as defined in equation (16).

$$\vec{\omega} = \frac{1}{2}(\nabla x \vec{u}). \tag{16}$$

Substitution of equations (16) and (5) into equation (15) yields the following:

$$\rho\frac{\partial^2 \vec{u}}{\partial t^2} = (\lambda + 2\mu)\nabla\theta - 2\mu\nabla x\vec{\omega}. \tag{17}$$

Equation (17) can be written as three equations in cylindrical polar components as shown in equations (18), (19), and (20).

$$\rho\frac{\partial^2 u_r}{\partial t^2} = (\lambda + 2\mu)\frac{\partial\theta}{\partial r} - \frac{2\mu}{r}\left[\frac{\partial \omega_z}{\partial\varphi} - \frac{\partial}{\partial z}(r\omega_\varphi)\right] \tag{18}$$

$$\rho\frac{\partial^2 u_\varphi}{\partial t^2} = (\lambda + 2\mu)\frac{\partial\theta}{r\partial\varphi} - 2\mu\left[\frac{\partial \omega_r}{\partial z} - \frac{\partial \omega_z}{\partial r}\right] \tag{18}$$

$$\rho\frac{\partial^2 u_z}{\partial t^2} = (\lambda + 2\mu)\frac{\partial\theta}{\partial z} - \frac{2\mu}{r}\left[\frac{\partial}{\partial r}(r\omega_\varphi) + \frac{\partial \omega_r}{\partial\varphi}\right] \tag{18}$$

where,

$$\theta = \frac{1}{r}\frac{\partial u_\varphi}{\partial\varphi} + \frac{\partial u_z}{\partial z} + \frac{u_r}{r} + \frac{\partial u_r}{\partial r} \tag{19}$$

and,

$$2\omega_r = \frac{1}{r}\frac{\partial u_z}{\partial\varphi} - \frac{1}{r}\frac{\partial}{\partial z}(ru_\varphi) \tag{20}$$

$$2\omega_\varphi = \frac{\partial u_r}{\partial z} - \frac{\partial u_z}{\partial r} \tag{20}$$

$$2\omega_z = \frac{1}{r}\frac{\partial}{\partial r}(ru_\varphi) - \frac{1}{r}\frac{\partial u_r}{\partial\varphi}. \tag{20}$$

By allowing the bar to undergo only longitudinal vibrations, equations (18), (19), and (20) are greatly simplified.

It should be emphasized that longitudinal vibrations are not restricted to one-dimensional strain waves. The only restriction is that torsional and bending waves are forbidden. When flexural vibration is forbidden, it is evident that axial symmetry exists so that $\vec{u}$ is independent of φ. Also, if torsional vibration is forbidden, it is evident that u_φ is not a function of time. If a static torque is applied to the bar it can be shown that the angular deformation is $u_\varphi = \beta rz$ where β is constant. The resulting equations of motion and boundary conditions (thus the solution) are the same for $u_\varphi = \beta rz$ and $u_\varphi = 0$ and since the discussion is simplified for $u_\varphi = 0$, this will be assumed.

Employing these simplifications, equations (18), (19), and (20) become:

$$\theta = \frac{\partial u_z}{\partial z} + \frac{u_r}{r} + \frac{\partial u_r}{\partial r} \tag{21}$$

$$2\omega_r = 0 \tag{22}$$

$$2\omega_\varphi = \frac{\partial u_r}{\partial z} - \frac{\partial u_z}{\partial r} \tag{22}$$

$$2\omega_z = 0 \tag{22}$$

$$\rho\frac{\partial^2 u_r}{\partial t^2} = (\lambda + 2\mu)\frac{\partial \theta}{\partial r} + 2\mu\frac{\partial \omega_\varphi}{\partial z} \tag{23}$$

$$\rho\frac{\partial^2 u_\varphi}{\partial t^2} = 0 \tag{23}$$

$$\rho\frac{\partial^2 u_z}{\partial t^2} = (\lambda + 2\mu)\frac{\partial\theta}{\partial z} - \frac{2\mu}{r}\frac{\partial}{\partial r}(r\omega_\varphi). \tag{23}$$

Combining equations (21), (22), and (23) and expanding the derivatives the component equations of motion for longitudinal wave propagation are obtained:

$$\rho\frac{\partial^2 u_r}{\partial t^2} = (\lambda + 2\mu)\left[\frac{\partial^2 u_r}{\partial r^2} + \frac{1}{r}\frac{\partial u_r}{\partial r} - \frac{u_r}{r^2}\right] + (\lambda + \mu)\frac{\partial^2 u_z}{\partial r \partial z} + \mu\frac{\partial^2 u_r}{\partial z^2} \tag{24}$$

$$\rho\frac{\partial^2 u_z}{\partial t^2} = \mu\left[\frac{\partial^2 u_z}{\partial r^2} + \frac{1}{r}\frac{\partial u_z}{\partial r}\right] + (\lambda + 2\mu)\frac{\partial^2 u_z}{\partial z^2} + (\lambda + \mu)\left[\frac{\partial^2 u_r}{\partial r \partial z} + \frac{1}{r}\frac{\partial u_r}{\partial z}\right]. \tag{24}$$

Components of Stress and Strain

The components of stress and strain in cylindrical polar coordinates are directly obtained by using equations (6) and (10). By writing the elements of the matrices given in equation (10), the components of strain are found:

$$\nabla\vec{u} = \begin{pmatrix} \frac{\partial u_r}{\partial r} & \frac{\partial u_\varphi}{\partial r} & \frac{\partial u_z}{\partial r} \\ \frac{1}{r}\frac{\partial u_r}{\partial \varphi} - \frac{u_\varphi}{r} & \frac{u_r}{r} + \frac{1}{r}\frac{\partial u_\varphi}{\partial \varphi} & \frac{1}{r}\frac{\partial u_z}{\partial \varphi} \\ \frac{\partial u_r}{\partial z} & \frac{\partial u_\varphi}{\partial z} & \frac{\partial u_z}{\partial z} \end{pmatrix} \tag{25}$$

$$2\vec{E} = \begin{pmatrix} 2\frac{\partial u_r}{\partial r} & \frac{\partial u_\varphi}{\partial r} + \frac{1}{r}\frac{\partial u_r}{\partial \varphi} - \frac{u_\varphi}{r} & \frac{\partial u_r}{\partial z} + \frac{\partial u_z}{\partial r} \\ \frac{1}{r}\frac{\partial u_r}{\partial \varphi} - \frac{u_\varphi}{r} + \frac{\partial u_\varphi}{\partial r} & 2\frac{u_r}{r} + \frac{2}{r}\frac{\partial u_\varphi}{\partial \varphi} & \frac{\partial u_\varphi}{\partial z} + \frac{1}{r}\frac{\partial u_z}{\partial \varphi} \\ \frac{\partial u_z}{\partial r} + \frac{\partial u_r}{\partial z} & \frac{1}{r}\frac{\partial u_z}{\partial \varphi} + \frac{\partial u_\varphi}{\partial z} & 2\frac{\partial u_z}{\partial z} \end{pmatrix}. \quad (26)$$

Or, writing the strain components explicitly, equations (27) are obtained:

$$\varepsilon_{rr} = \frac{\partial u_r}{\partial r}; \qquad \varepsilon_{\varphi\varphi} = \frac{u_r}{r} + \frac{1}{r}\frac{\partial u_\varphi}{\partial \varphi}; \qquad \varepsilon_{zz} = \frac{\partial u_z}{\partial z} \quad (27)$$

$$\varepsilon_{r\varphi} = \varepsilon_{\varphi r} = \frac{1}{2}\left[\frac{\partial u_\varphi}{\partial r} + \frac{1}{r}\frac{\partial u_r}{\partial \varphi} - \frac{u_\varphi}{r}\right] \quad (27)$$

$$\varepsilon_{rz} = \varepsilon_{zr} = \frac{1}{2}\left[\frac{\partial u_z}{\partial r} + \frac{\partial u_r}{\partial z}\right] \quad (27)$$

$$\varepsilon_{\varphi z} = \varepsilon_{z\varphi} = \frac{1}{2}\left[\frac{1}{r}\frac{\partial u_z}{\partial \varphi} + \frac{\partial u_\varphi}{\partial z}\right]. \quad (27)$$

Then by using Hooke's Law as written in equation (6), the components of stress are easily obtained:

$$\sigma_{rr} = 2\mu\frac{\partial u_r}{\partial r} + \lambda\theta \quad (28)$$

$$\sigma_{\varphi\varphi} = 2\mu\left[\frac{u_r}{r} + \frac{1}{r}\frac{\partial u_\varphi}{\partial \varphi}\right] + \lambda\theta \quad (28)$$

$$\sigma_{zz} = 2\mu\frac{\partial u_z}{\partial z} + \lambda\theta \quad (28)$$

$$\sigma_{rz} = \sigma_{zr} = \mu\left[\frac{\partial u_z}{\partial r} + \frac{\partial u_r}{\partial z}\right] \quad (28)$$

$$\sigma_{r\varphi} = \sigma_{\varphi r} = \mu\left[\frac{\partial u_\varphi}{\partial r} + \frac{1}{r}\frac{\partial u_r}{\partial \varphi} - \frac{u_\varphi}{r}\right] \tag{28}$$

$$\sigma_{\varphi z} = \sigma_{z\varphi} = \mu\left[\frac{1}{r}\frac{\partial u_z}{\partial \varphi} + \frac{\partial u_\varphi}{\partial z}\right]. \tag{28}$$

Finally by using the definition of the dilation and considering only longitudinal waves ($u_\varphi = 0$ and $\partial/\partial\varphi = 0$), equations (27) and (28) can be written more simply as shown in equations (29) and (30).

$$\varepsilon_{rr} = \frac{\partial u_r}{\partial r}; \quad \varepsilon_{\varphi\varphi} = \frac{u_r}{r}; \quad \varepsilon_{zz} = \frac{\partial u_z}{\partial z} \tag{29}$$

$$\varepsilon_{r\varphi} = \varepsilon_{\varphi r} = \varepsilon_{\varphi z} = \varepsilon_{z\varphi} = 0 \tag{29}$$

$$\varepsilon_{rz} = \varepsilon_{zr} = \frac{1}{2}\left[\frac{\partial u_z}{\partial r} + \frac{\partial u_r}{\partial z}\right] \tag{29}$$

$$\sigma_{\varphi r} = \sigma_{r\varphi} = \sigma_{\varphi z} = \sigma_{z\varphi} = 0 \tag{30}$$

$$\sigma_{rr} = (\lambda + 2\mu)\frac{\partial u_r}{\partial r} + \lambda\left[\frac{u_r}{r} + \frac{\partial u_z}{\partial z}\right] \tag{30}$$

$$\sigma_{\varphi\varphi} = (\lambda + 2\mu)\frac{u_r}{r} + \lambda\left[\frac{\partial u_r}{\partial r} + \frac{\partial u_z}{\partial z}\right] \tag{30}$$

$$\sigma_{zz} = (\lambda + 2\mu)\frac{\partial u_z}{\partial z} + \lambda\left[\frac{\partial u_r}{\partial r} + \frac{u_r}{r}\right] \tag{30}$$

$$\sigma_{zr} = \sigma_{rz} = \mu\left[\frac{\partial u_z}{\partial r} + \frac{\partial u_r}{\partial z}\right]. \tag{30}$$

Boundary Conditions and Conditions for Proper Behavior

Boundary Conditions

The boundary conditions are determined by the stress at the surface of the cylindrical bar. For the sake of comparing the results of this work with other treatments and with experimental results it will be assumed that the radial surface of the bar is a free surface. Further it will be assumed that the only stress at the end of the bar is a normal stress.

By studying Fig. 1, the above assumptions yield the following boundary conditions:

$$\text{at } z = 0;\ \sigma_{z\varphi} = 0 \text{ and } \sigma_{zr} = 0 \tag{31}$$

$$\text{at } r = R;\ \sigma_{r\varphi} = 0,\ \sigma_{rz} = 0, \text{ and } \sigma_{rr} = 0. \tag{31}$$

Substituting equations (30) into equations (31), the boundary conditions for longitudinal wave propagation are obtained:

$$\text{at } z = 0;\ \frac{\partial u_z}{\partial r} + \frac{\partial u_r}{\partial z} = 0 \tag{32}$$

$$\text{at } r = R;\ \frac{\partial u_r}{\partial r} + \frac{\lambda}{\lambda + 2\mu}\left[\frac{u_r}{r} + \frac{\partial u_z}{\partial z}\right] = 0, \text{ and}$$

$$\frac{\partial u_z}{\partial r} + \frac{\partial u_r}{\partial z} = 0. \tag{32}$$

It should be noted that if a plane end condition is maintained at $z = 0$ the condition given at $z = 0$ in equation (32) would become $\partial u_r/\partial z = 0$ since $\partial u_z/\partial r = 0$. The boundary conditions for cases in which the ends are not plane will be discussed when they arise.

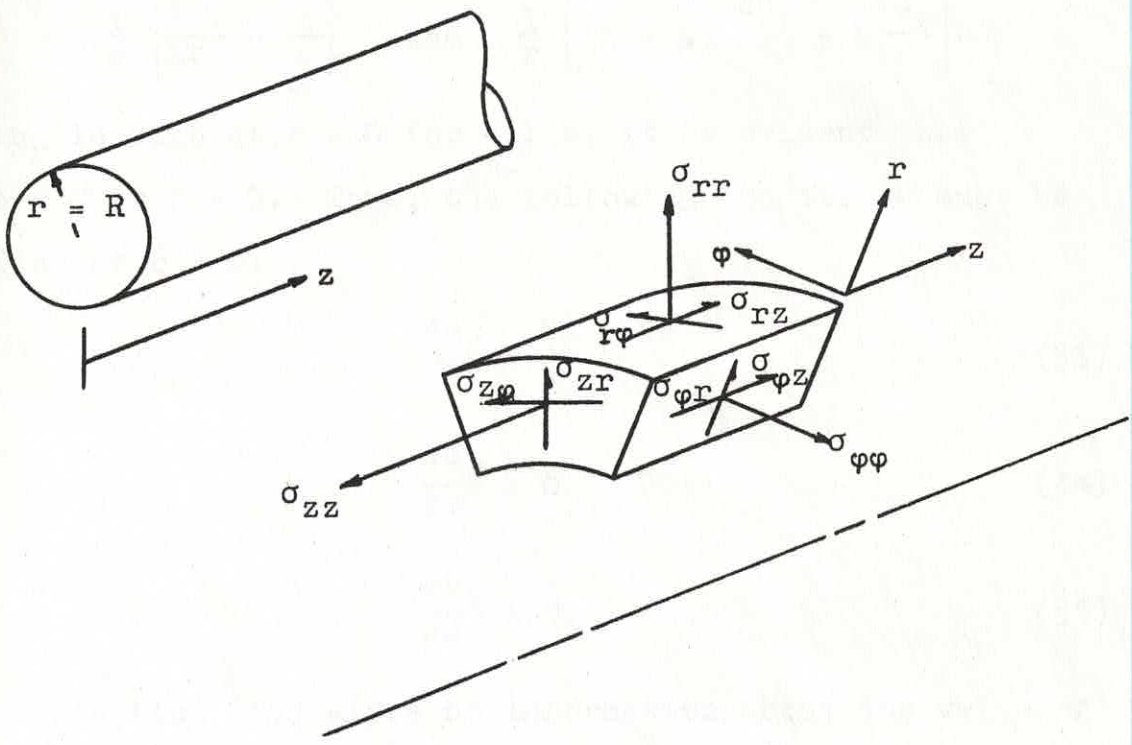


Fig. 1.--The Stress Components in Cylindrical Polar Coordinates.

Conditions for Proper Behavior

Besides the boundary conditions at the surface there are conditions that arise at the axis of the cylinder because of the coordinates used. The solution must be well behaved at the axis of the bar: the stresses and acceleration must be finite.

These conditions are easily obtained from equations (24) and (30). In order for the stresses (σ_{rr}, $\sigma_{\varphi\varphi}$, and σ_{zz}) to be finite at r = 0, it is necessary for u_r to be zero at r = 0. Also, in order for the accelerations to be finite at r = 0, the following terms must be finite:

$$\frac{1}{r}\left[\frac{\partial u_r}{\partial r} - \frac{u_r}{r}\right] \quad \text{and} \quad \frac{1}{r}\left[(\lambda + \mu)\frac{\partial u_r}{\partial z} + \mu\frac{\partial u_z}{\partial r}\right].$$

Since u_r is zero at $r = 0$ for all z, it is evident that $\partial u_r/\partial z = 0$ at $r = 0$. Thus, the following conditions must be satisfied at $r = 0$:

$$\frac{\partial u_r}{\partial r} = \frac{u_r}{r} \tag{33}$$

$$\frac{\partial u_r}{\partial z} = 0 \tag{34}$$

$$\frac{\partial u_z}{\partial r} = 0. \tag{35}$$

Equation (33) gives no information about the value of $\partial u_r/\partial r$ at $r = 0$. Since u_r is zero at $r = 0$, $\partial u_r/\partial r$ is indeterminate at $r = 0$. Thus, the pertinent conditions for proper solution behavior are as follows:

$$\text{at } r = 0; \quad u_r = 0 \quad \text{and} \quad \frac{\partial u_z}{\partial r} = 0. \tag{36}$$

In summary, the equations of motion and conditions on these equations for elastic longitudinal wave propagation in a semi-infinite bar, with axial symmetry and a plane displacement at $z = 0$ are as follows:

$$\rho\frac{\partial^2 u_r}{\partial t^2} = (\lambda + 2\mu)\left[\frac{\partial^2 u_r}{\partial r^2} + \frac{1}{r}\frac{\partial u_r}{\partial r} - \frac{u_r}{r^2}\right] + (\lambda + \mu)\frac{\partial^2 u_z}{\partial r \partial z} + \mu\frac{\partial^2 u_r}{\partial z^2} \tag{37}$$

$$\rho \frac{\partial^2 u_z}{\partial t^2} = \mu \left[\frac{\partial^2 u_z}{\partial r^2} + \frac{1}{r} \frac{\partial u_z}{\partial r} \right] + (\lambda + 2\mu) \frac{\partial^2 u_z}{\partial z^2}$$

$$+ (\lambda + \mu) \left[\frac{\partial^2 u_r}{\partial r \partial z} + \frac{1}{r} \frac{\partial u_r}{\partial z} \right] \tag{37}$$

$$\text{at } r = R; \quad \frac{\partial u_z}{\partial r} + \frac{\partial u_r}{\partial z} = 0 \quad \text{and}$$

$$\frac{\partial u_r}{\partial r} + \frac{\lambda}{\lambda + 2\mu} \left[\frac{u_r}{r} + \frac{\partial u_z}{\partial z} \right] = 0 \tag{37}$$

$$\text{at } z = 0; \quad \frac{\partial u_r}{\partial z} = 0 \tag{37}$$

$$\text{at } r = 0; \quad u_r = 0 \quad \text{and} \quad \frac{\partial u_z}{\partial r} = 0. \tag{37}$$

CHAPTER III

DIFFERENCE SCHEME FOR A SEMI-INFINITE BAR

By integrating the equations of motion and applying the boundary conditions, the solution to the problem of longitudinal elastic wave propagation in a semi-infinite bar would be obtained. However, the solution of the problem as stated in equations (37) is so complicated that this integration has not yet been achieved for every point in the bar.

There will be no attempt made in this work to write the solution of this problem in an integrated form. Instead, the solution will be obtained by using finite difference approximations to the differential equations for numerical integration.

Many difference schemes may be used to approximate a given differential equation. Any particular derivative can be approximated [16] by a forward difference, a backward difference, or a center difference. Also, the separate terms of the differential equation may be approximated by any one of the differencing methods.

The choice of a particular differencing scheme is based on the characteristics of the various differencing methods. These characteristics include the biasing effect, the effect of extraneous solutions and the stability of the method [18].

Exclusive use of forward or backward differences is less advantageous than the exclusive use of centered differences because a bias is introduced in the calculation. As an example of this bias, exclusive use of a forward-time difference would result in approximations to $(\partial/\partial t)_t$ that are not at the time t but at some time forward, that is, at a value greater than t.

The major disadvantage associated with exclusive use of centered differences is that this method may produce extraneous solutions which do not converge to the solution of the differential equations as the increment size tends to zero. That is, if a centered difference is used to approximate a first derivative, a second order difference (across two increments) is obtained. In order to solve a second order difference equation, two initial conditions are required, whereas only one initial condition is necessary for the first derivative that it approximates. If initial data are not sufficient, two conditions can not be determined and it is possible to generate an extraneous solution by an improper choice of the second condition [18].

Although an optimum differencing scheme is not obvious for a complicated differential equation, it is possible to determine the practicality of a scheme by using the von Neumann [37] stability criterion. The von Neumann stability criterion gives approximate necessary conditions for solution stability (a stable solution remains bounded for all positive values of time). If a particular differencing scheme gives

stability conditions that are not practical (a time increment that is too small for a given spatial increment) this scheme must be abandoned in favor of one that is more practical.

The centered differencing method was chosen for this problem. The choice is somewhat arbitrary but it is weighted by the fact that this method gives only one set of equations, whereas forward and backward differences, combined to reduce the bias, would yield many sets of equations depending on the particular difference used on each term. Furthermore, all of the first derivatives in the equations of motion (24) have corresponding second derivatives. The first derivatives are: $\partial u_z/\partial r$, $\partial u_z/\partial z$, $\partial u_r/\partial r$, and $\partial u_r/\partial z$, and there are second derivatives of all of these: $\partial^2 u_z/\partial r^2$, $\partial^2 u_z/\partial z^2$, $\partial^2 u_r/\partial r^2$, and $\partial^2 u_r/\partial z^2$. Since there must be enough conditions for the second derivatives, there must be enough conditions for the centered difference approximations to the first derivatives. That is, the use of centered differences does not, in this case, generate extraneous solutions.

Finite Difference Equations of Motion

The notation for difference equations is somewhat cumbersome. In order to reduce this encumbrance, the following change of notation will be used in the finite difference equations:

$$u_r \equiv U \text{ and } u_z \equiv W. \tag{38}$$

Also, the position in the r, z, t space will always be denoted in the same order, e.g., U(r,z,t). Furthermore, unless other-

wise specified, the value of time is $t + \Delta t$, e.g., $U(r,z) \equiv U(r,z,t+\Delta t)$.

Then using centered differences, where Δr, Δz, and Δt are the finite differences, the following finite difference approximations are obtained:

$$\frac{\partial^2 U}{\partial t^2} \rightarrow \frac{1}{(\Delta t)^2}\left[U(r,z,t+\Delta t) + U(r,z,t-\Delta t) - 2\,U(r,z,t)\right] \quad (39)$$

$$\frac{\partial^2 W}{\partial t^2} \rightarrow \frac{1}{(\Delta t)^2}\left[W(r,z,t+\Delta t) + W(r,z,t-\Delta t) - 2\,W(r,z,t)\right] \quad (39)$$

$$\frac{\partial^2 U}{\partial r^2} \rightarrow \frac{1}{(\Delta r)^2}\left[U(r+\Delta r,z,t) + U(r-\Delta r,z,t) - 2\,U(r,z,t)\right] \quad (39)$$

$$\frac{\partial^2 W}{\partial r^2} \rightarrow \frac{1}{(\Delta r)^2}\left[W(r+\Delta r,z,t) + W(r-\Delta r,z,t) - 2\,W(r,z,t)\right] \quad (39)$$

$$\frac{\partial^2 W}{\partial z^2} \rightarrow \frac{1}{(\Delta z)^2}\left[W(r,z+\Delta z,t) + W(r,z-\Delta z,t) - 2\,W(r,z,t)\right] \quad (39)$$

$$\frac{\partial^2 U}{\partial z^2} \rightarrow \frac{1}{(\Delta z)^2}\left[U(r,z+\Delta z,t) + U(r,z-\Delta z,t) - 2\,U(r,z,t)\right] \quad (39)$$

$$\frac{\partial U}{\partial r} \rightarrow \frac{1}{2(\Delta r)}\left[U(r+\Delta r,z,t) - U(r-\Delta r,z,t)\right] \quad (39)$$

$$\frac{\partial W}{\partial r} \rightarrow \frac{1}{2(\Delta r)}\left[W(r+\Delta r,z,t) - W(r-\Delta r,z,t)\right] \quad (39)$$

$$\frac{\partial U}{\partial z} \rightarrow \frac{1}{2(\Delta z)}\left[U(r,z+\Delta z,t) - U(r,z-\Delta z,t)\right] \quad (39)$$

$$\frac{\partial W}{\partial z} \rightarrow \frac{1}{2(\Delta z)}\left[W(r,z+\Delta z,t) - W(r,z-\Delta z,t)\right] \quad (39)$$

$$\frac{\partial^2 U}{\partial r \partial z} \rightarrow \frac{1}{4(\Delta z)(\Delta r)}\begin{bmatrix} U(r+\Delta r,z+\Delta z,t) - U(r-\Delta r,z+\Delta z,t) \\ -U(r+\Delta r,z-\Delta z,t) + U(r-\Delta r,z-\Delta z,t)\end{bmatrix} \quad (39)$$

$$\frac{\partial^2 W}{\partial r \partial z} \rightarrow \frac{1}{4(\Delta z)(\Delta r)} \begin{bmatrix} W(r+\Delta r, z+\Delta z, t) - W(r-\Delta r, z+\Delta z, t) \\ -W(r+\Delta r, z-\Delta z, t) + W(r-\Delta r, z-\Delta z, t) \end{bmatrix}. \qquad (39)$$

Substitution of equations (39) into equations (37) yields the difference equations of motion:

$$U(r,z) \equiv U(r,z,t+\Delta t) = 2\,U(r,z,t) - U(r,z,t-\Delta t)$$

$$- \frac{\lambda+2\mu}{\rho r^2} (\Delta t)^2\, U(r,z,t) - \frac{\lambda+\mu}{4\rho} \frac{(\Delta t)^2}{(\Delta r)(\Delta z)} W(r+\Delta r, z-\Delta z, t)$$

$$+ \frac{\lambda+2\mu}{\rho} \left(\frac{\Delta t}{\Delta r}\right)^2 \left[U(r+\Delta r, z, t) + U(r-\Delta r, z, t) - 2\,U(r,z,t)\right]$$

$$+ \frac{\lambda+\mu}{4\rho} \frac{(\Delta t)^2}{(\Delta r)(\Delta z)} \left[W(r+\Delta r, z+\Delta z, t) - W(r-\Delta r, z+\Delta z, t)\right]$$

$$+ \frac{\mu}{\rho} \left(\frac{\Delta t}{\Delta z}\right)^2 \left[U(r, z+\Delta z, t) + U(r, z-\Delta z, t) - 2\,U(r,z,t)\right]$$

$$+ \frac{\lambda+2\mu}{2\rho r} \frac{(\Delta t)^2}{(\Delta r)} \left[U(r+\Delta r, z, t) - U(r-\Delta r, z, t)\right]$$

$$+ \frac{\lambda+\mu}{4\rho} \frac{(\Delta t)^2}{(\Delta r)(\Delta z)} W(r-\Delta r, z-\Delta z, t) \qquad (40)$$

$$W(r,z) \equiv W(r,z,t+\Delta t) = 2\,W(r,z,t) - W(r,z,t-\Delta t)$$

$$+ \frac{\lambda+2\mu}{\rho} \left(\frac{\Delta t}{\Delta z}\right)^2 \left[W(r, z+\Delta z, t) + W(r, z-\Delta z, t) - 2\,W(r,z,t)\right]$$

$$+ \frac{\lambda+\mu}{4\rho} \frac{(\Delta t)^2}{(\Delta r)(\Delta z)} \left[U(r+\Delta r, z+\Delta z, t) - U(r-\Delta r, z+\Delta z, t)\right]$$

$$+ \frac{\lambda+\mu}{4\rho} \frac{(\Delta t)^2}{(\Delta r)(\Delta z)} \left[U(r-\Delta r, z-\Delta z, t) - U(r+\Delta r, z-\Delta z, t)\right]$$

$$+ \frac{\mu}{\rho}\left(\frac{\Delta t}{\Delta r}\right)^2 \left[W(r+\Delta r,z,t) + W(r-\Delta r,z,t) - 2\,W(r,z,t)\right]$$

$$+ \frac{\mu}{2\rho r}\frac{(\Delta t)^2}{\Delta r} \left[W(r+\Delta r,z,t) - W(r-\Delta r,z,t)\right]$$

$$+ \frac{\lambda+\mu}{2r\rho}\frac{(\Delta t)^2}{\Delta z} \left[U(r,z+\Delta z,t) - U(r,z-\Delta z,t)\right]. \qquad (40)$$

Boundary Conditions in Difference Form

The boundary conditions can be approximated with finite differences by substituting equations (39) into equations (37). However, there are a few subtleties involved. In order to adequately describe the tactics necessary to apply the boundary conditions in difference form it is necessary to describe the method for solving equations (40).

Equations (40) show that to determine $U(r,z) = U(r,z,t+\Delta t)$ and $W(r,z)$, it is necessary to know values of U and W at neighboring points and for earlier times. The required values are summarized in Fig. 2. For example, $U(r,z)$ as indicated by the square in the upper left hand diagram, can be calculated if the values of both U and W, shown in the squares, are known at previous times. Likewise, $W(r,z)$ as indicated by the solid circle in the upper right hand diagram, can be calculated if the values of both U and W, shown in the solid circles, are known at previous times.

All the values shown in Fig. 3 as cross-filled circles, can be calculated from equations (40). It is clear from Fig. 2 that the boundary values of $U(r,z)$ and $W(r,z)$ can not

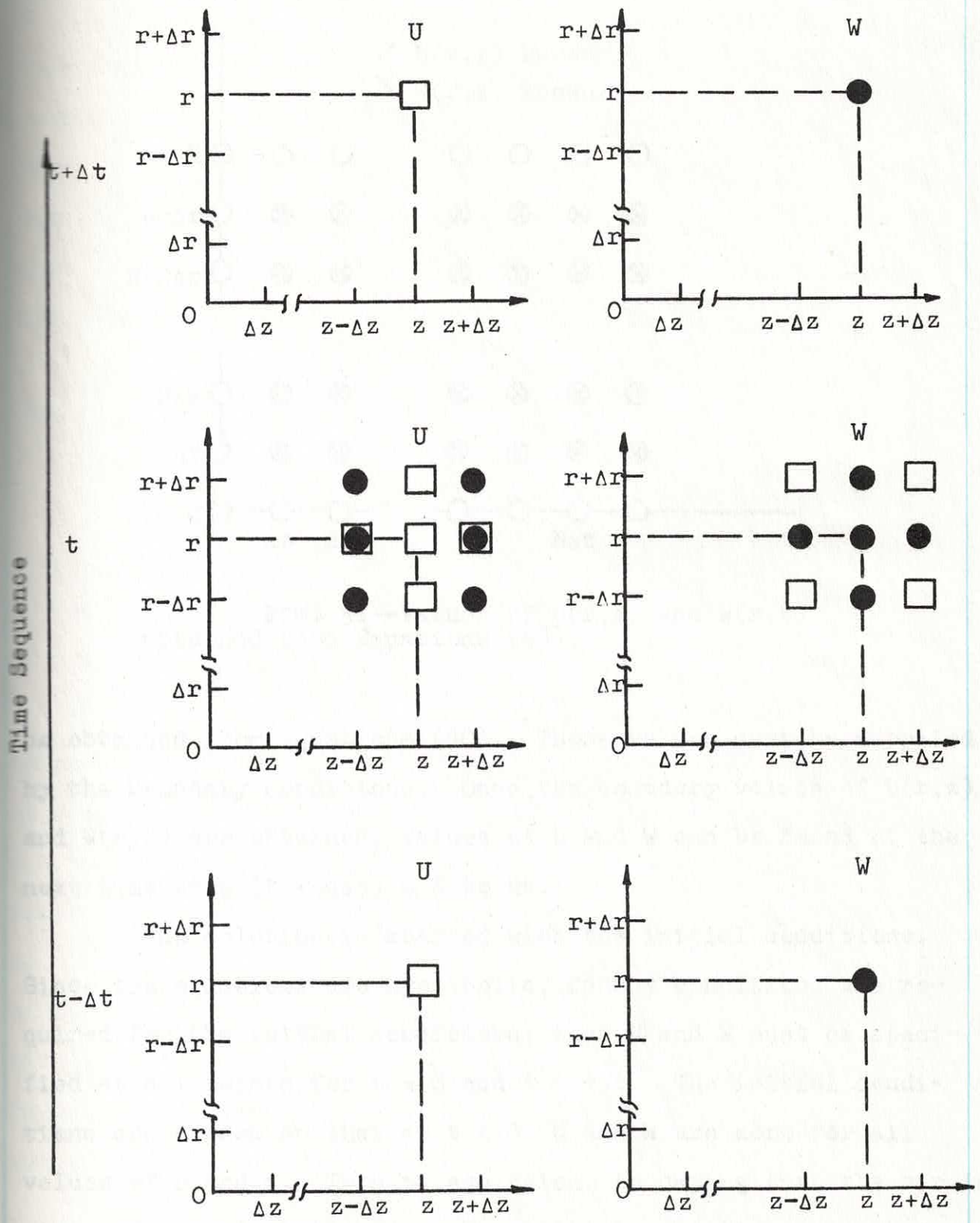


Fig. 2.--The Deformations Necessary to Find the Deformation at the Next Time Step.

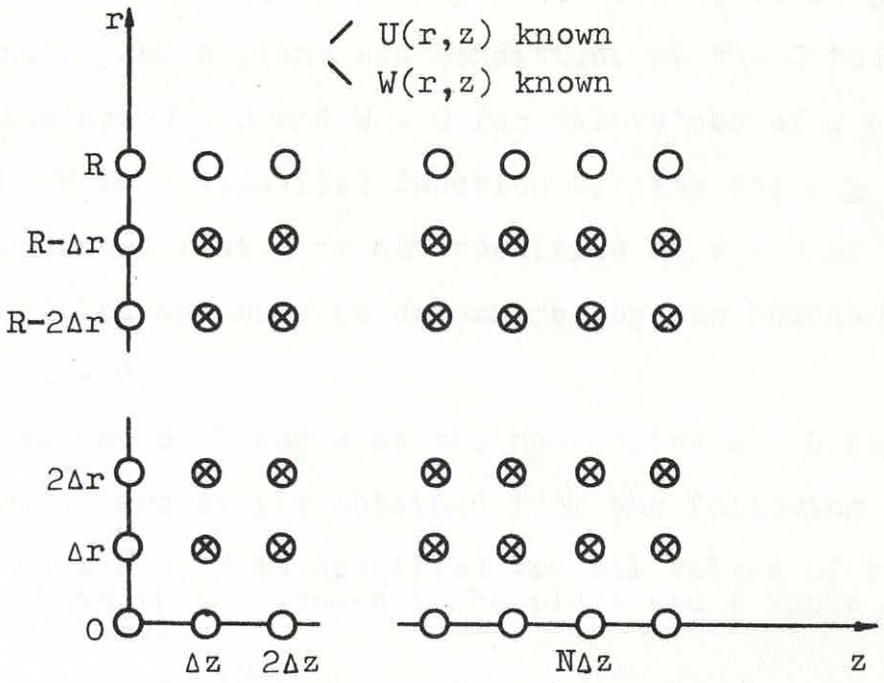


Fig. 3.--Values of U(r,z) and W(r,z) Obtained from Equations (40).

be obtained from equations (40). These values must be supplied by the boundary conditions. Once the boundary values of U(r,z) and W(r,z) are obtained, values of U and W can be found at the next time step ($t + 2\Delta t$) and so on.

The solution is started with the initial conditions. Since the equations are hyperbolic, Cauchy conditions are required for the initial conditions; thus U and W must be specified at all points for $t = 0$ and $t = -\Delta t$. The initial conditions are chosen so that at $t < 0$, U and W are zero for all values of r and z. This is equivalent to saying that the bar is stress free and stationary. The initial conditions are then completed by specifying U and W for all values of r and z at

$t = 0$. This condition will depend on the specific problem considered. For a plane end condition, at $t = 0$ the initial conditions are $U = 0$ and $W = 0$ for all values of r and $z > 0$. At $z = 0$, W is a specified function of time for $t \geq 0$. It should be noted that U is not specified at $z = 0$ by the initial condition and must be determined by the boundary conditions at $z = 0$.

Values of U and W at the boundaries $r = 0$ and $z = 0$ (see Fig. 4) are easily obtained from the following conditions:

1. At $z = 0$, W is specified for all values of t and r, since it is assumed to be plane and a known function of time.
2. At $z = 0$, $\frac{\partial U}{\partial z} = 0$.
3. At $r = 0$, $U = 0$.
4. At $r = 0$, $\frac{\partial W}{\partial r} = 0$.

Condition 1 explicitly determines W at $z = 0$ for all values of $r \leq R$. Also, condition 3 explicitly determines U at $r = 0$ for all values of z. The derivative conditions (2 and r) are approximated by finite differences to determine respectively, U at $z = 0$ for $0 < r < R$ and W at $r = 0$ for all values of $z > 0$. From Fig. 4 it is evident that no values of U or W exist for $r < 0$ or $z < 0$. Since these values do not exist, it is evident that neither backward nor centered differences can be used. Forward differences must be used for these conditions.

Using a forward difference on the second condition the following difference equation is obtained:

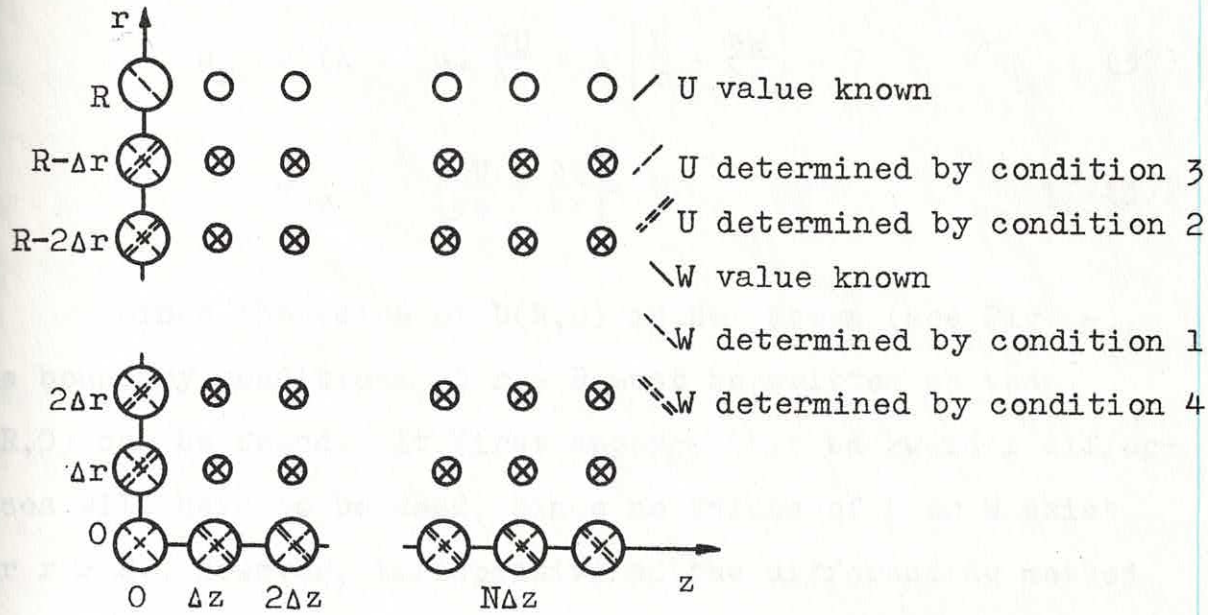


Fig. 4.--Values of U(r,z) and W(r,z) Obtained from the Boundary Conditions at r = 0 and z = 0.

$$\left(\frac{\partial U}{\partial z}\right)_{z=0} = \left[\frac{U(r,z+\Delta z) - U(r,z)}{\Delta z}\right]_{z=0} = 0. \qquad (41)$$

Thus, $U(r,0) = U(r,\Delta z)$ and since $U(r,\Delta z)$ for $0 < r < R$ is known from equation (40), $U(r,0)$ can be determined for $0 < r < R$.

Likewise a forward difference on the fourth condition yields the following difference equation:

$$\left(\frac{\partial W}{\partial r}\right)_{r=0} = \left[\frac{W(r+\Delta r,z) - W(r,z)}{\Delta r}\right]_{r=0} = 0. \qquad (42)$$

Thus, $W(0,z) = W(\Delta r,z)$ and since $W(\Delta r,z)$ for $z > 0$ is known from equation (40), $W(0,z)$ for $z > 0$ can be determined.

The values of U and W that remain to be calculated at $t + \Delta t$ are those at the radial surface $r = R$. These values are obtained by using the boundary conditions at $r = R$:

$$\sigma_{rr} = (\lambda + 2\mu) \frac{\partial U}{\partial r} + \lambda \left[\frac{U}{r} + \frac{\partial W}{\partial z}\right] = 0 \qquad (37)$$

$$\sigma_{rz} = \mu \left[\frac{\partial U}{\partial z} + \frac{\partial W}{\partial r}\right] = 0. \qquad (37)$$

Since the value of U(R,0) is not known (see Fig. 4), the boundary conditions at r = R must be written so that U(R,0) can be found. It first appears that backward r differences will have to be used, since no values of U or W exist for r > R. However, irrespective of the differencing method used for the derivatives with respect to z, the value of U(R,0) cannot be found with backward r differences. A forward z difference is the most encouraging and will be used to exemplify the attempts to find U(R,0) with backward r differences at z = 0 and r = R. Equations (37) become:

$$\frac{\lambda}{\lambda+2\mu} \left[\frac{U(R,0)}{R} + \frac{W(R,\Delta z) - W(R,0)}{\Delta z}\right]$$

$$+ \left[\frac{U(R,0) - U(R-\Delta r,0)}{\Delta r}\right] = 0 \qquad (40)$$

$$\left[\frac{U(R,\Delta z) - U(R,0)}{\Delta z}\right] + \left[\frac{W(R,0) - W(R-\Delta r,0)}{\Delta r}\right] = 0. \qquad (40)$$

There are three unknowns [U(R,0), U(R,Δz), and W(R,Δz)] and only two equations. Since a plane deformation is applied at z = 0, W(R,0) is equal to W(R-Δr,0). Therefore, U(R,Δz) is equal to U(R,0), but neither value can be found by using backward differences in the r-direction.

The only way that U(R,0) can be found is to avoid the use of backward differences in the r-direction. It is possible to use either forward or centered differences in the r-direction at r = R, if it is assumed that the bar has an outside radius of R + Δr.

With this assumption it is possible to find U(R,0) with either a forward or centered difference in the r-direction, if a forward difference is used in the z-direction. The centered r difference should be the better choice because it allows the boundary condition to be centered at the actual surface (r=R). Also, the use of a forward difference would result in two forward differences in the r-direction, since a forward difference must be used at r = 0.

Writing forward z differences and centered r differences and substituting them into equations (37), the difference approximation to the boundary conditions at r = R is obtained:

$$U(R+\Delta r,z) = U(R-\Delta r,z) - \left(\frac{2\Delta r\lambda}{\lambda+2\mu}\right)\left[\frac{U(R,z)}{R} + \frac{W(R,z+\Delta z) - W(R,z)}{\Delta z}\right] \qquad (44)$$

$$W(R+\Delta r,z) = W(R-\Delta r,z) + \left(\frac{2\Delta r}{\Delta z}\right)\left[U(R,z) - U(R,z+\Delta z)\right]. \qquad (44)$$

With this scheme, equation (40) is employed to calculate all values of U and W at t + Δt such that $0 < z$ and $0 < r < R + \Delta r$. The values of U and W at t + Δt for the pseudo-surface (r = R + Δr) at any value of z including z = 0 are

then found from equation (44). Notice that this method gives values at $R + \Delta r$ that have no physical meaning but allow the numerical calculation to proceed. Also, it should be noted that this method should give correct solutions since the difference equation of motion is satisfied at all points and the centered boundary conditions are satisfied at the real surface ($r = R$) and not at the pseudo-surface ($r = R + \Delta r$).

Stability of the Difference Equations

It is extremely important to investigate the stability of the difference equations. One reason is to justify that the solution of the difference equations converges to the actual solution. This is insured by the Lax Equivalence Theorem [44]. Another obvious reason is to insure that the numerical solution is bounded and well behaved.

Further, it is necessary to examine the stability of the difference equations to insure efficient use of the computing machine. That is, for fixed spatial increments (Δr and Δz), the time increment (Δt) should be given its maximum stable value so that the length of computing time is minimized.

A rigorous discussion of stability, including error analysis, for the finite difference equations given in equation (40) has not been achieved. However, by making reasonable assumptions and using the method suggested by von Neumann [37], an approximate criterion for stability can be developed. This condition will be necessary for stability, within the accuracy of the assumptions used, but not sufficient.

Although the only way to be certain of the stability of a complicated difference equation is to perform the actual numerical calculation, the von Neumann condition offers the best available guide. The method used by von Neumann is to consider stability in an infinite region so that boundary conditions do not enter and to assume that the dependent variables can be approximated by trigonometric functions. Then the solutions are of the following form:

$$U = U_o e^{i\ell r} e^{imz} e^{nt} \tag{45}$$

where ℓ, m, and n are integers and $i = \sqrt{-1}$. Also r, z, and t in this finite difference scheme are:

$$r = a\Delta r, \quad z = b\Delta z, \quad \text{and} \quad t = c'\Delta t \tag{46}$$

where a, b, and c' are integers.

Then by defining ζ, ψ, and η as follows:

$$\zeta = e^{i\ell\Delta r} = \cos \ell\Delta r + i \sin \ell\Delta r \tag{47}$$

$$\psi = e^{im\Delta z} = \cos m\Delta z + i \sin m\Delta z \tag{47}$$

$$\eta = e^{n\Delta t} \tag{47}$$

one obtains:

$$U(r,z,t) = U_o \zeta^a \psi^b \eta^{c'}. \tag{48}$$

It is evident that as time increases, c' increases. Thus, in order for U to be stable as time increases, it is necessary that $|\eta| \leq 1$.

It is necessary to eliminate either U or W from equations (40) or to make an estimate of their relative magnitudes.

The elimination of one of the variables in equations (40) would be tedious and since the entire argument is very approximate, an approximation to the relative magnitudes will be sufficient. It is thus assumed that $U = \nu W$.

Using this assumption and substituting equation (48) into equations (40) for U and dividing by $U_o \zeta^a \psi^b \eta^{c'}$, equation (49) is obtained:

$$\eta = 2 - \eta^{-1} + \frac{\lambda+\mu}{4\rho\nu} \frac{(\Delta t)^2}{(\Delta z)(\Delta r)} \left[\zeta\psi - \zeta^{-1}\psi - \zeta\psi^{-1} + \zeta^{-1}\psi^{-1}\right]$$

$$+ \frac{\mu}{\rho} \left(\frac{\Delta t}{\Delta z}\right)^2 \left[\psi + \psi^{-1} - 2\right] + \frac{\lambda+2\mu}{\rho} \left(\frac{\Delta t}{\Delta r}\right)^2 \left[\zeta + \zeta^{-1} + 2\right]$$

$$- \frac{\lambda+2\mu}{\rho r^2} (\Delta t)^2 + \frac{\lambda+2\mu}{2\rho r} \frac{(\Delta t)^2}{(\Delta r)} \left[\zeta - \zeta^{-1}\right]. \qquad (49)$$

Then defining α to be $\Delta z/\Delta r$, using $r = a\Delta r$, and rearranging equation (49), equation (50) is obtained:

$$\eta - 2 + \eta^{-1} = \left(\frac{\Delta t}{\Delta r}\right)^2 \left\{ \frac{\lambda+\mu}{4\rho\alpha\nu} \left[\zeta\psi - \zeta^{-1}\psi - \zeta\psi^{-1} + \zeta^{-1}\psi^{-1}\right] \right.$$

$$+ \frac{\mu}{\rho\alpha^2} \left[\psi + \psi^{-1} - 2\right] + \frac{\lambda+2\mu}{2\rho a} \left[\zeta - \zeta^{-1}\right]$$

$$\left. - \frac{\lambda+2\mu}{\rho a^2} + \frac{\lambda+2\mu}{\rho} \left[\zeta + \zeta^{-1} - 2\right] \right\}. \qquad (50)$$

Defining S as shown in equation (51), equation (52) can ultimately be obtained:

$$\eta - 2 + \eta^{-1} = -S \qquad (51)$$

$$\eta = \frac{2 - S}{2} \pm \sqrt{\left(\frac{2 - S}{2}\right)^2 - 1} \ .$$

For the magnitude of η to be less than unity it is necessary that $\left|\frac{2 - S}{2}\right| \leq 1$, thus $-4 \leq -S \leq 0$. Using these limits and the definition of S, equation (52) is obtained from equation (50):

$$-4 \leq \left(\frac{\Delta t}{\Delta r}\right)^2 \left\{ \frac{\lambda+\mu}{4\rho\alpha\nu} \left[\zeta\psi - \zeta^{-1}\psi - \zeta\psi^{-1} + \zeta^{-1}\psi^{-1}\right] - \frac{\lambda+2\mu}{\rho a^2} \right.$$

$$+ \frac{\mu}{\rho\alpha^2} \left[\psi + \psi^{-1} - 2\right] + \frac{\lambda+2\mu}{2\rho a} \left[\zeta - \zeta^{-1}\right]$$

$$\left. + \frac{\lambda+2\mu}{\rho} \left[\zeta + \zeta^{-1} - 2\right] \right\} \leq 0. \qquad (52)$$

Equation (52) is simplified by using the definitions of ζ and η and considering only their real parts as follows:

$$-4 \leq \left(\frac{\Delta t}{\Delta r}\right)^2 \left\{ \frac{\mu}{\alpha^2\rho} \left[2 \cos m\alpha\Delta r - 2\right] + \frac{\lambda+2\mu}{\rho} \left[2 \cos \ell\Delta r - 2 - \frac{1}{a^2}\right] \right.$$

$$\left. + \frac{\lambda+\mu}{4\rho\nu\alpha} \left[2 \cos (m\alpha\Delta r + \ell\Delta r) - 2 \cos (m\alpha\Delta r - \ell\Delta r)\right] \right\} \leq 0. \qquad (53)$$

If B is defined as shown in equation (54);

$$B = \frac{\lambda+\mu}{4\rho\nu\alpha} \left[-2 \cos (m\alpha\Delta r + \ell\Delta r) + 2 \cos (m\alpha\Delta r - \ell\Delta r)\right]$$

$$+ \frac{\lambda+2\mu}{\rho a^2} + \frac{\mu}{\alpha^2\rho} \left[2 - 2 \cos m\alpha\Delta r\right] + \frac{\lambda+2\mu}{\rho} \left[2 - 2 \cos \ell\Delta r\right] \qquad (54)$$

equation (53) can be written as shown in equation (55):

$$0 \leq \left(\frac{\Delta t}{\Delta r}\right)^2 B \leq 4. \qquad (55)$$

The upper stable bound of $(\Delta t/\Delta r)^2$ that will satisfy equation (55) for any value of ℓ, m, α, or a can be obtained by finding the maximum possible value of B. If $(\Delta t/\Delta r)$ is

computed from equation (55) using a value equal to or greater than the maximum value of B, certainly that value of $(\Delta t/\Delta r)$ will always satisfy the necessary condition for stability. Since the minimum value of a is unity (values at r = 0 are not calculated in the difference equation of motion), equation (56) can be obtained:

$$\left(\frac{\Delta t}{\Delta r}\right)^2 B \leq \left(\frac{\Delta t}{\Delta r}\right)^2 B_{max}.$$

Also,

$$B_{max} \leq \begin{Bmatrix}\text{the sum of the maximum values}\\ \text{of each term of equation (54)}\end{Bmatrix}.$$

Thus,

$$\left(\frac{\Delta t}{\Delta r}\right)^2 B \leq \left(\frac{\Delta t}{\Delta r}\right)^2 \left\{\frac{\lambda+\mu}{\rho\nu\alpha} + \frac{4\mu}{\alpha^2\rho} + \frac{\lambda+2\mu}{\rho} + 4\,\frac{\lambda+2\mu}{\rho}\right\} \leq 4$$

or,

$$\frac{\Delta t}{\Delta r} \leq \left[\frac{\lambda+\mu}{4\rho\nu\alpha} + \frac{\mu}{\alpha^2\rho} + \frac{5}{4}\,\frac{\lambda+2\mu}{\rho}\right]^{-1/2}. \qquad (56)$$

This is the stability criterion for the U equation in equation (40).

The same method is used for the W equation and the following stability criterion is obtained:

$$\frac{\Delta t}{\Delta r} \leq \left[\frac{\lambda+2\mu}{\alpha^2\rho} + \frac{(\lambda+\mu)\nu}{4\rho\alpha} + \frac{\mu}{\rho}\right]^{-1/2}. \qquad (57)$$

For the special case of E = 2 Mbar, ν = 0.25, and ρ = 8 gm/cc, equations (56) and (57) are plotted in Fig. 5 and the approximate stable region is indicated.

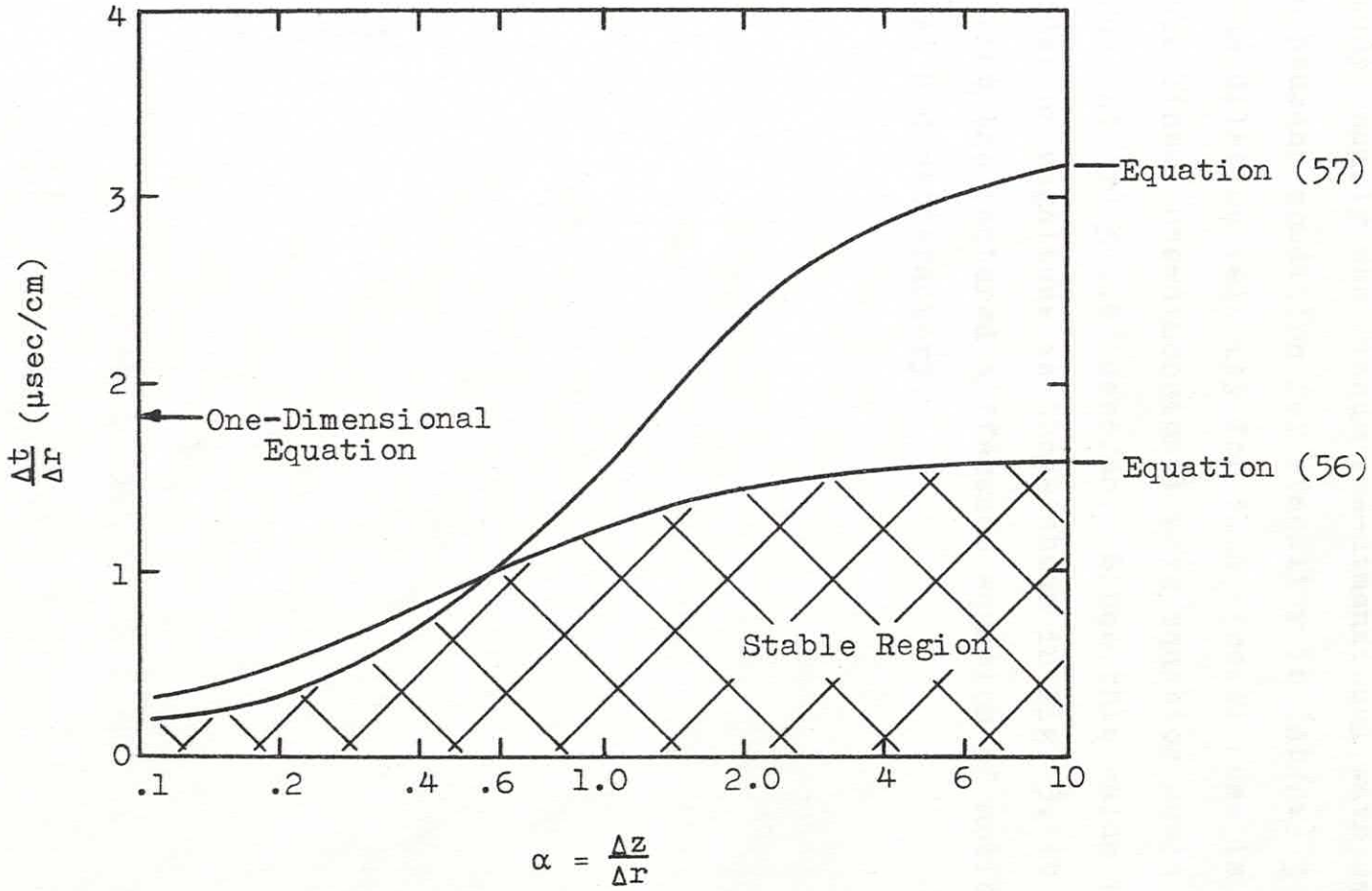


Fig. 5.--The Stability Criteria for the Difference Equations

For a much simpler equation than the one considered in this study, namely the linear one-dimensional wave equation, the von Neumann condition for stability is $(\Delta t/\Delta x) \leq 1/c$.[1] Since the dilation velocity for this special case is 0.548 cm/μsec, the linear one-dimensional wave equation would have the condition $(\Delta t/\Delta x) \leq 1.82$ μsec/cm. Since this value is the same order of magnitude as those shown in Fig. 5, it is concluded that the centered difference equation of motion is practical and satisfactory.

[1]This criterion is based on the difference equations recommended by Richtmyer [44] for the numerical solution of the linear wave equation.

CHAPTER IV

POCHHAMMER-CHREE SOLUTION (P.C.S.) FOR THE INFINITE BAR

The P.C.S. for the infinite bar was obtained by Pochhammer [41] in 1876 and by Chree [6] in 1889. However, numerical values for the frequency equation were not obtained until Bancroft's [2] computations in 1941. The values obtained by Bancroft for the phase velocity are correct, but as Davies [10] pointed out in 1948, the values obtained by Bancroft for the axial deformation of the bar as a function of radial position in the bar are incorrect.

Davies obtained the axial deformation, radial deformation, axial stress, radial stress, and the shear stress in the bar as functions of the radial position for two values of d/λ' where d is the diameter of the bar and λ' is the wave length.

Davies considered radial variations for only two values of d/λ' (more numerical values for the P.C.S. are obtained in this chapter). This allows an extension of Davies' considerations and a correction of Bancroft's values.

Pochhammer-Chree Method

The method given for the analytical solution can be found in Kolsky [26] but it is included in this discussion so

that the method employed for the numerical solution will have a convenient foundation.

The equation of motion for the infinite cylindrical bar is equation (17) which was developed in Chapter II.

$$\rho \frac{\partial^2 \vec{u}}{\partial t^2} = (\lambda + 2\mu) \nabla\theta - 2\mu \nabla x \vec{\omega}. \tag{17}$$

Also, for longitudinal elastic waves, equation (17) can be written component equations and simplified as shown in equations (23):

$$\rho \frac{\partial^2 u_r}{\partial t^2} = (\lambda+2\mu) \frac{\partial \theta}{\partial r} + 2\mu \frac{\partial \omega_\varphi}{\partial z} \tag{23}$$

$$\rho \frac{\partial^2 u_z}{\partial t^2} = (\lambda+2\mu) \frac{\partial \theta}{\partial z} - \frac{2\mu}{r} \frac{\partial (r\omega_\varphi)}{\partial r} \tag{23}$$

where

$$\theta = \frac{1}{r} \frac{\partial}{\partial r} (ru_r) + \frac{\partial u_z}{\partial z}$$

and

$$2\omega_\varphi = \frac{\partial u_r}{\partial z} - \frac{\partial u_z}{\partial r}.$$

In the P.C.S. it is assumed that an infinite train of sinusoidal waves is propagated along the entire infinite length of the bar such that the deformation at each point is a simple harmonic function of z as well as of t. If this simple harmonic condition exists, the deformations can be expressed as shown in equations (58) where γ is the wave number and p is the frequency.

$$u_r = \tilde{U}(r) \exp [i (\gamma z + pt)] \tag{58}$$

$$u_z = \tilde{W}(r) \exp [i (\gamma z + pt)]. \tag{58}$$

Then by substituting equations (58) into equations (23) it can be shown that $\tilde{U}(r)$ and $\tilde{W}(r)$ are as shown in equations (59) where A and C are to be determined from the boundary conditions

$$\tilde{U}(r) = A \frac{d}{dr} J_o(h'r) + C \gamma J_1(k'r) \tag{59}$$

$$\tilde{W}(r) = A\, i\, \gamma\, J_o(h'r) + C \frac{i}{r} \frac{d}{dr} [rJ_1(k'r)] \tag{59}$$

and where h' and k' are defined as shown in equations (60):

$$h'^2 = \frac{\rho p^2}{\lambda+2\mu} - \gamma^2 \tag{60}$$

$$k'^2 = \frac{\rho p^2}{\mu} - \gamma^2. \tag{60}$$

By carrying out the differentiations indicated in equations (59), equations (61) are obtained:

$$\tilde{U}(r) = - A\, h'\, J_1(h'r) + C \gamma J_1(k'r) \tag{61}$$

$$\tilde{W}(r) = A\, i\, \gamma\, J_o(h'r) + C\, i\, k'\, J_o(k'r). \tag{61}$$

The definitions of the stress components as given in equations (30) along with equations (58) and (61) are used with the boundary conditions given in equations (62):

$$\text{at } r = R;\ \sigma_{rr} = \sigma_{rz} = 0. \tag{62}$$

This results in two simultaneous equations as shown in equations (63):

$$0 = A \left\{ [J_o(h'R)] \left[\frac{-\lambda \rho p^2}{\lambda+2\mu} - 2\, \mu\, h'^2 \right] + \frac{2\mu h'}{R} J_1(h'R) \right\}$$

$$+ C \left\{ 2\mu\gamma k' \left[J_o(k'R) - \frac{J_1(k'R)}{k'R} \right] \right\} \tag{63}$$

$$0 = A\,[-2\gamma h'\,J_1(h'R)] + C\left[2\gamma^2 - \frac{\rho p^2}{\mu}\right] J_1(k'R). \qquad (63)$$

Numerical Calculations

For a given bar, the unknowns in equations (63) are A/C and $p/\gamma = c$. These values are obtained numerically by writing the ratio of A/C in both of these equations as shown in equations (64) and using the following procedure:

$$\left(\frac{A}{C}\right)_1 = \frac{2\mu\gamma k'\left[J_0(k'R) - \dfrac{J_1(k'R)}{k'R}\right]}{J_0(h'R)\left[\dfrac{\lambda\rho p^2}{\lambda+2\mu} + 2\mu h'^2\right] - \dfrac{2\mu h'}{R}\,J_1(h'R)} \qquad (64)$$

$$\left(\frac{A}{C}\right)_2 = \frac{\left[2\,\gamma^2 - \dfrac{\rho p^2}{\mu}\right] J_1(k'R)}{2\,\gamma\,h'\,J_1(h'R)}\,. \qquad (64)$$

Choose ρ and E so that c_o is specified, then for a given value of ν, μ and λ can be found. Also, for a given value of d/λ', γ can be found using the relation $\gamma = 2\pi/\lambda'$. Then the value of p is systematically varied until $(A/C)_1$ and $(A/C)_2$ are equal. When they are equal p is known and $c = p/\gamma$ can be found. This allows c/c_o to be calculated for the given ν and d/λ'. Also, by knowing the correct value of A/C the radial distribution of u_r and u_z is found from equations (61).

Although this method is somewhat crude analytically, it can be easily used with a digital computer. A routine for computing Bessel functions of integer order was written for real arguments. Since h' and k' are not real for all values

of d/λ', it is necessary to rewrite equations (61) and (64) in terms of modified Bessel functions of the first kind with real arguments. This is accomplished by using the identify given in equation (65):

$$I_n(x) = i^{-n} J_n(ix). \tag{65}$$

To determine when h' and k' are real, equation (60) is rewritten as shown in equation (66) where c_D is the phase velocity of dilation waves and c_S is the phase velocity of shear

$$h'^2 = p^2 \left[\frac{1}{c_D^2} - \frac{1}{c^2}\right] \tag{66}$$

$$k'^2 = p^2 \left[\frac{1}{c_S^2} - \frac{1}{c^2}\right] \tag{66}$$

or distortion waves. Since $c_D > c_o$ and $c_o \geq c$ for all values of d/λ' and positive ν values, it is evident that h' is always imaginary. Also, for sufficiently large values of d/λ' ($d/\lambda' > 1.1$ to $d/\lambda' > 1.4$ depending on the Poisson ratio) both h' and k' are imaginary. For this case the substitutions given in equations (67) are used in equations (61) and (64) to obtain equations (68) and (69), respectively.

$$h' = ih \tag{67}$$

$$k' = ik \tag{67}$$

$$\tilde{U}(r) = C \left[\gamma I_1(kr) + \frac{A}{C} h\, I_1(hr)\right] \tag{68}$$

$$\tilde{W}(r) = C \left[\frac{A}{C} \gamma I_o(hr) + k\, I_o(kr)\right] \tag{68}$$

$$\left(\frac{A}{C}\right)_1 = \frac{2\mu\gamma k\left[I_o(kR) - \frac{I_1(kR)}{kR}\right]}{2\mu\,\frac{h}{r}\,I_1(hR) + I_o(hR)\left[\frac{\lambda\rho p^2}{\lambda+2\mu} - 2\mu h^2\right]} \tag{69}$$

$$\left(\frac{A}{C}\right)_2 = \frac{\left[\frac{p^2\rho}{\mu} - 2\gamma^2\right] I_1(kR)}{2\gamma h\, I_1(hR)}. \tag{69}$$

The results of the numerical computations are given in Table 1, Figs. 6 and 7, and Appendix D. In Figs. 6 and 7, U_{max} and W_{max} are computed for each value of d/λ' and the maximum values of the nondimensional ordinates are unity. The value of U_{max} is the extreme value of U(r) and W_{max} is the extreme value of W(r).

The values of c/c_o given in Table 1 for $\nu = 0.25$ agree with Bancroft's values to the limit of his accuracy (five significant figures are given by Bancroft). Also, although the values of deformation are not plotted for $\nu = 0.29$, the results agree with Davies' calculations. The correct values for the deformation are shown in Appendix D and plotted in Figs. 6 and 7. Bancroft's curves for deformation are incorrect and should be as shown in Fig. 7.

TABLE 1

The Effect of Wave Length on the Phase Velocity in the P.C.S.

d/λ'	ν	c/c_o	W_{max}/U_{max}
0.30	0.25	0.98336589	3.9112716
0.35	0.25	0.97572510	3.2604134
0.40	0.25	0.96558601	2.7681523
0.45	0.25	0.95220241	2.3863680
0.50	0.25	0.93479171	2.0874038
0.55	0.25	0.91287711	1.8538694
0.60	0.25	0.88680975	1.6726878
0.90	0.25	0.72825505	1.0817076
1.20	0.25	0.64711607	0.78446712
1.50	0.25	0.61163106	0.57280688
2.00	0.25	0.58932206	-0.55047086
5.00	0.25	0.57829007	-0.64882154
10.00	0.25	0.57938007	-0.66524453
0.3936	0.29	0.95818679	2.5910168
1.8701	0.29	0.58969409	-0.50533807

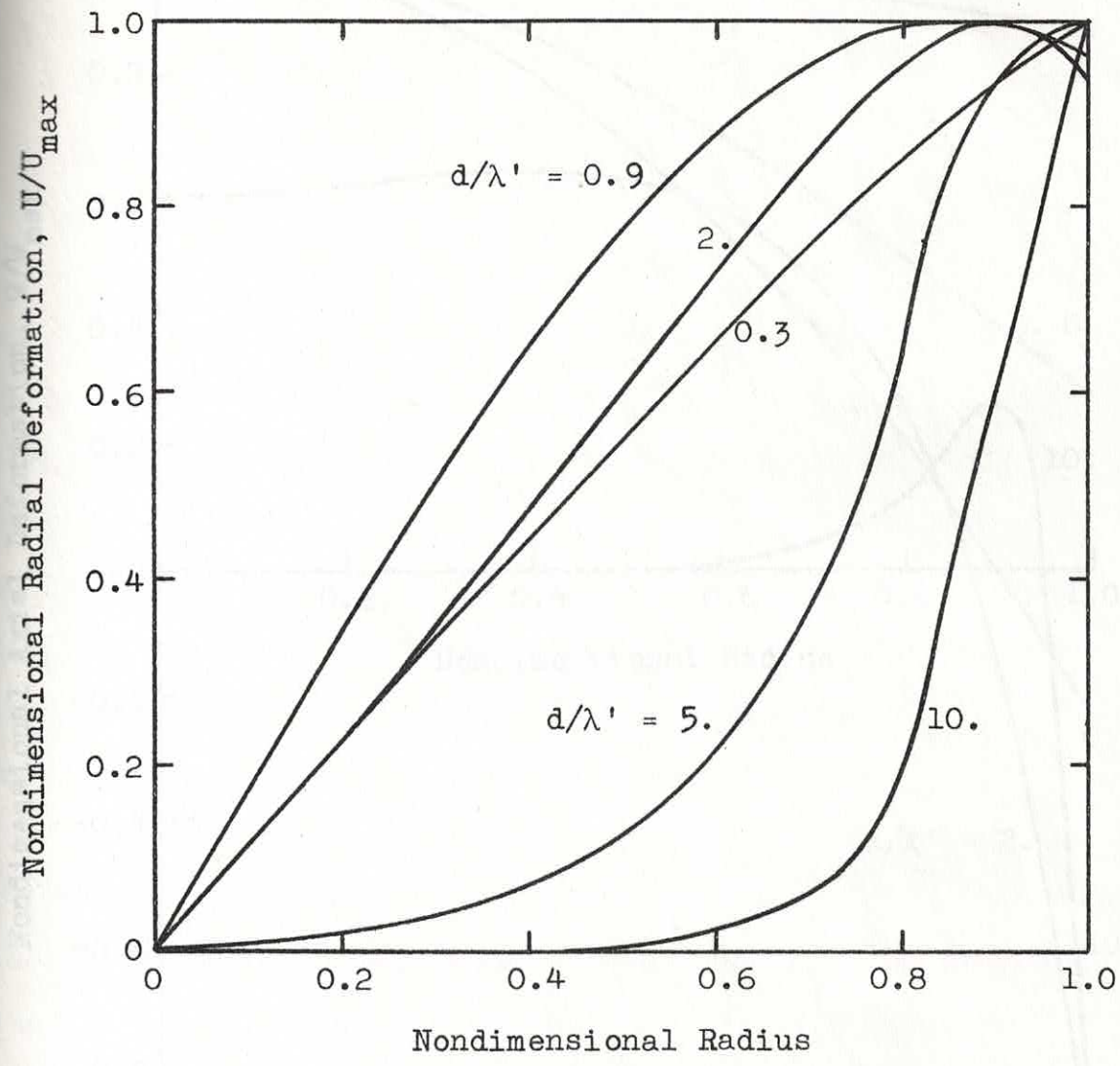


Fig. 6.--The Radial Distribution of u_r in the P.C.S.

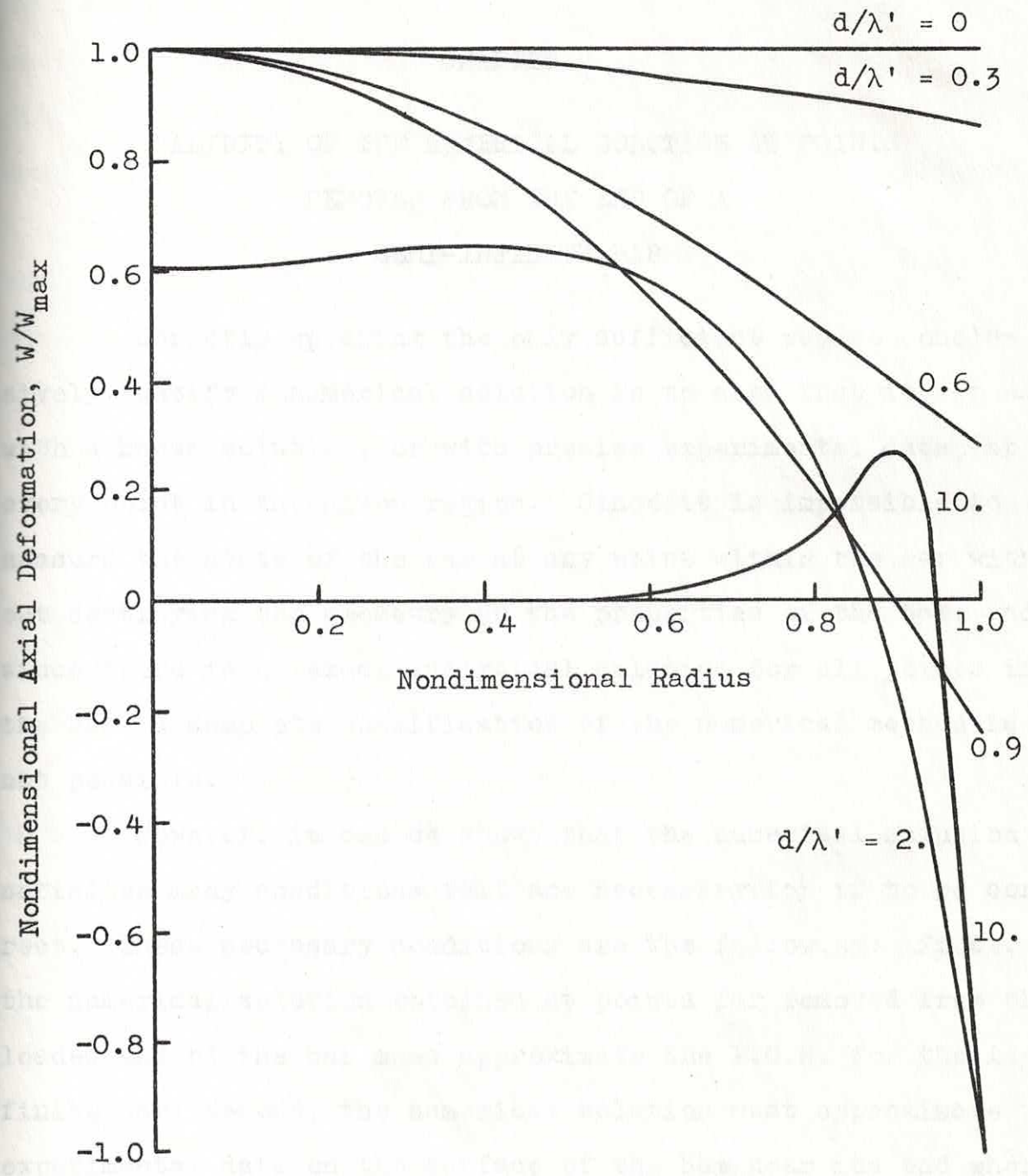


Fig. 7.--The Radial Distribution of u_z in the P.C.S.

CHAPTER V

VALIDITY OF THE NUMERICAL SOLUTION AT POINTS REMOVED FROM THE END OF A SEMI-INFINITE BAR

Strictly speaking the only sufficient way to conclusively justify a numerical solution is to show that it agrees with a known solution, or with precise experimental data, at every point in the given region. Since it is impossible to measure the state of the bar at any point within the bar without destroying the geometry or the properties of the bar, and since there is no exact analytical solution for all points in the bar; a complete justification of the numerical method is not possible.

However, it can be shown that the numerical solution satisfies many conditions that are necessary for it to be correct. These necessary conditions are the following: first, the numerical solution obtained at points far removed from the loaded end of the bar must approximate the P.C.S. for the infinite bar; second, the numerical solution must approximate experimental data on the surface of the bar near its end where no analytic solution is known; finally, the solution near the driven face must agree with the uni-axial strain solution within the "core of influence."

These necessary conditions are very strong conditions. In fact, without an exact analytic solution, no other significant condition can be advanced. Also, the strength of the condition resulting from the comparison with the P.C.S. cannot be over emphasized.

A numerical solution that is started at the end of the bar will involve a large number of calculations before it can approach the region in which the P.C.S. is valid. In addition, any appreciable errors or instabilities in the numerical procedure will become more evident as the number of calculations increases. Furthermore, since the P.C.S. yields the state of the bar for all radial points (not just at the surface), the comparison of it with the numerical solution allows a very strong test of the validity of the numerical solution.

Thus, if the approximate numerical solution satisfies all of the above necessary conditions it will be assumed here that it is valid for every point in the bar.

At points far removed from the end of the bar the P.C.S. is valid. For a given frequency, this region can be determined by comparing the P.C.S. to a correct numerical solution.

Numerical Method

In order to compare the numerical solution with the P.C.S., a disturbance that is periodic in time must be applied at some point in the bar. Far removed from the point of application, a favorable comparison can be made, if the frequency components of the resulting disturbance travel with the proper

velocity and if these components are harmonic along the bar axis.

In this chapter the finite difference boundary conditions developed in Chapter III are used with $W = \sin \omega t$ at $z = 0$. The harmonic disturbance is easier to use than a periodic, nonharmonic disturbance because the general periodic disturbance would have to be analyzed by Fourier analysis. Also, the harmonic disturbance can be more accurately studied with less computer time and storage.

The choice of the particular frequency of the displacement is influenced by many factors. First of all, it is desirable to choose a frequency that allows a severe test on the numerical solution. Probably the most reasonable criterion for the severity of the test would be that the wave length ought to be chosen so that the two-dimensional effect is most predominant.

The P.C.S. (see Fig. 7) indicates that the two-dimensional effect is evident for a frequency that yields $d/\lambda' = 0.30$ and becomes more pronounced until $d/\lambda' = 1.7$. Thus, from this standpoint, the frequency of the disturbance should be chosen so that d/λ' is equal to 1.7.

However, the capacity of the computer, the accuracy of the solution, and the amount of computing time necessary must be considered. The IBM 709 computer allows about 18,000 numbers to be stored in dimensioned arrays when FORTRAN IV is used. Furthermore, with the numerical procedure used it is necessary to store the values of U and W for three time

increments, a fixed number of radial increments, and a fixed number of axial increments. If it is assumed that there are I increments in the radial direction and J increments in the axial direction, then equation (70) can be written:

$$(2)\ (3)\ (I)\ (J) \leq 18{,}000, \qquad (70)$$

where 2 is the number of variables and 3 is the number of time increments. Thus, the product of the number of radial increments and the number of axial increments must be no larger than 3,000.

A total of 3,000 points in the body seems like a very adequate number. However, for the problem of the long bar, this number is quite restrictive. That is, for a reasonable degree of accuracy, the number of axial increments, the number of radial increments, and the d/λ' ratio must be chosen with care.

There are two major factors that influence the accuracy of the numerical procedure. First, it is expected that a larger number of radial increments will be necessary for a given accuracy when the deformation changes more rapidly along the radius. Second, if it is assumed that a given level of accuracy is established by the number of points used to represent a wave length, it is evident that for this accuracy, the number of axial increments will increase with the frequency of the disturbance.

Since the P.C.S. indicates that high frequencies yield large changes of the deformation in the radial direction, it is evident that for a fixed number of increments, the higher the

frequency the more inaccurate the numerical procedure will be. In order to have a sufficiently accurate solution and yet demonstrate the two-dimensional effect, the frequency is chosen so that d/λ' is equal to 0.3. This frequency is calculated by using the phase velocity given by the P.C.S. as follows:

$$d/\lambda' = 0.3$$

$$\lambda' = 2\pi/k$$

$$k = \omega/c$$

$$c/c_o = 0.98336$$

$$0.3 = d/\lambda' = dk/2\pi = d\omega c_o/2\pi c c_o.$$

Therefore,

$$\omega = 1.8535898\ c_o/d.$$

For $d/\lambda' = 0.3$, it was found that the accuracy of the numerical solution is not appreciably increased by using more than 12 increments. Thus, 12 radial zones are used and since the total number of points is 3,000, this leaves 250 axial zones.

A numerical solution can be performed for a specific case only. In comparing the numerical solution to the P.C.S., the following specific case is considered:

$$E = 2.0 \text{ Mbar}, \rho = 8.0 \text{ gm/cc}, \text{ and } \nu = 0.25.$$

Also, the radial increment size is arbitrarily chosen to be 0.1 cm and this results in a bar diameter of 2 cm. The low-

frequency phase velocity is easily computed to be 0.5 cm/μsec and this along with d = 2.0 yields the desired value of the frequency (ω = 0.4633974 rad/μsec).

The size of the axial increment is chosen to allow both an accurate solution and a solution that yields values at distances "far removed" from the end of the bar. It is assumed that "far removed" from the end is a distance greater than 10 diameters from the end; or it is assumed that the P.C.S. is valid at 10 diameters from the end of the semi-infinite bar. With d/λ' = 0.3 the bar velocity is 0.49168 cm/μsec and the dilation velocity is approximately 0.548 cm/μsec. Thus, the time required for a wave to propagate 10 diameters or 20 cm at the bar velocity is 40.75 μsec. At the dilation velocity the front of the wave would propagate approximately 22.4 cm in this time.

Since there is room for only 250 axial zones in the machine memory, the smallest Δz that can be used is 0.0895 cm. The size of the axial increment is chosen to be 0.2 cm. To determine how much this limits the accuracy of the numerical solution, several numerical solutions (at distances close to the bar end) were performed for Δr = 0.1, Δt = 0.075 and various values of Δz. The results of these calculations are shown in Figs. 8 and 9.

These figures, especially Fig. 9, show that the most accurate solution is obtained with the smallest Δz. From the curves for W in Fig. 9, it can be seen that the estimated error for Δz = 0.05 is about 0.6%, for Δz = 0.10 it is about 2%, for

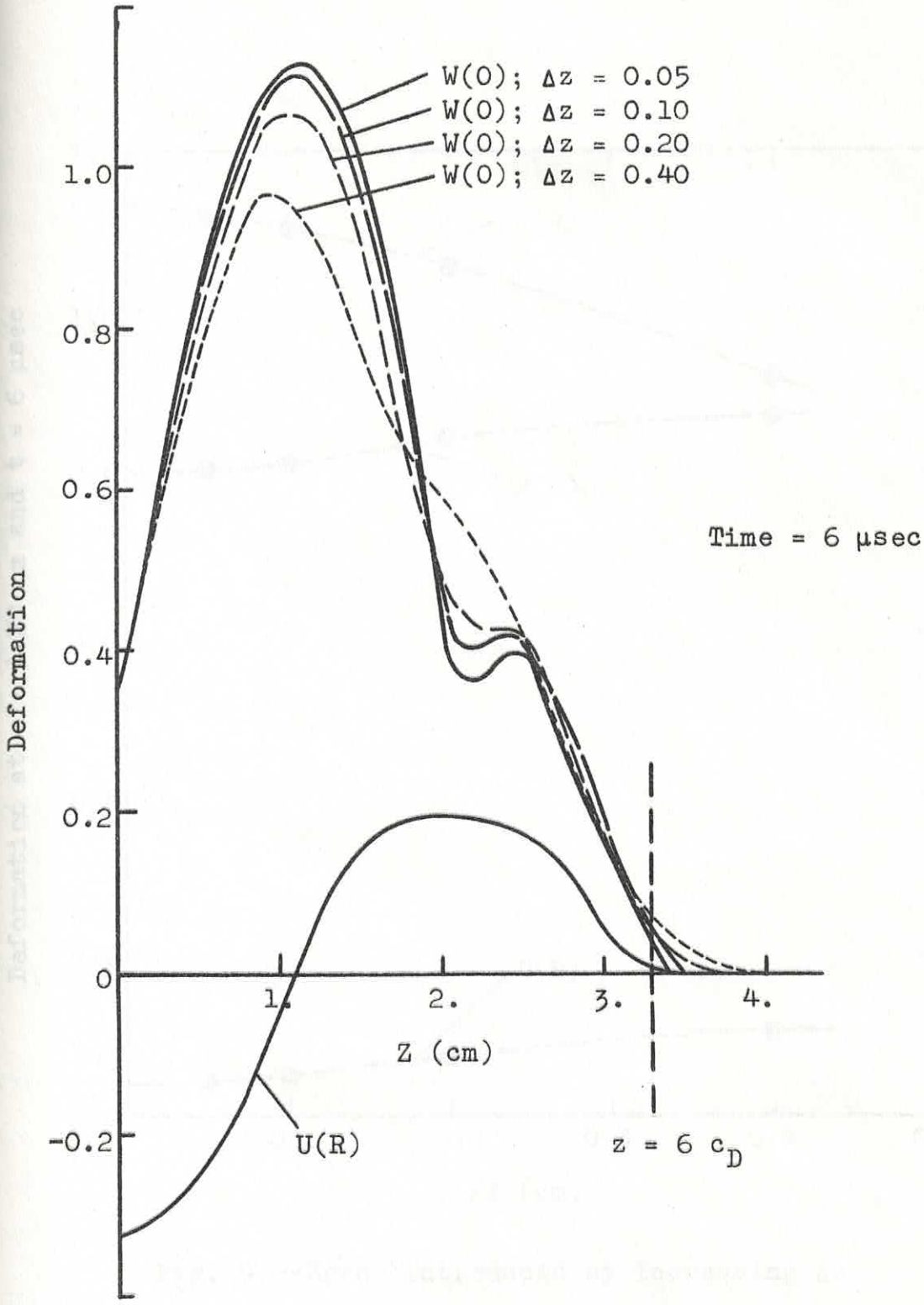


Fig. 8.--The Effect of Δz on the Accuracy of the Numerical Solution.

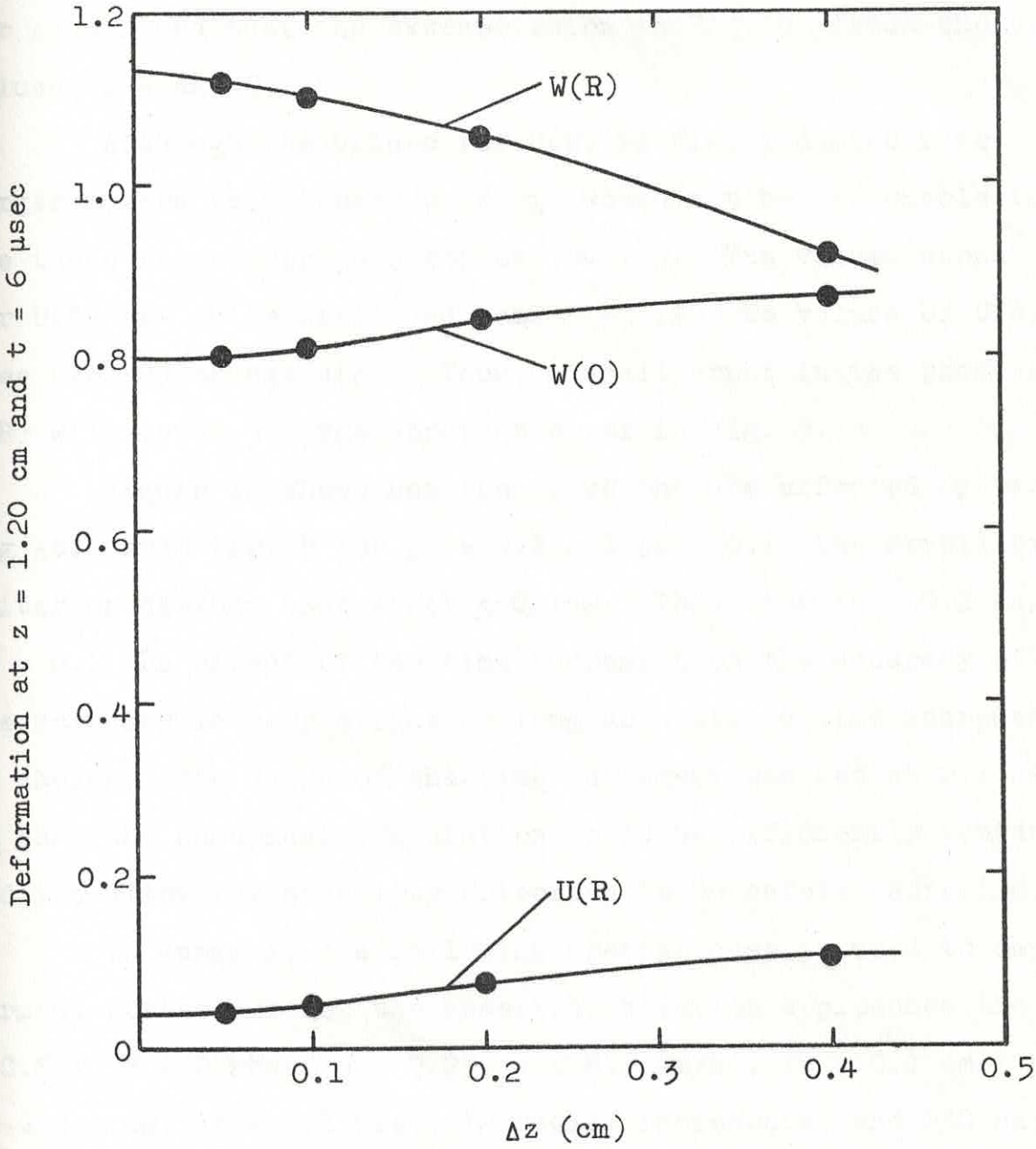


Fig. 9.--Error Introduced by Increasing Δz

$\Delta z = 0.2$ it is about 7%, and for $\Delta z = 0.4$ it is an unreasonable 19%. These error estimates are calculated by assuming that the values of the deformation smoothly approach the values for $\Delta z = 0$ and that the extrapolation in Fig. 9 yields the true values of W and U.

Although the values for U(R) in Fig. 9 demonstrate larger errors than those for W, it would not be reasonable to use these values for an error estimation. The values shown for U(R) are quite small and near z = 1.20 the values of U(R) (see Fig. 8) change sign. Thus, a small error in the phase of U(R) will cause a large apparent error in Fig. 9.

Figure 10 shows how the solutions are affected by varying Δt. From Fig. 5 for $\Delta z = 0.2$ and $\Delta r = 0.1$, the stability criterion demands that $\Delta t/\Delta r \leq 0.142$. Thus, for $\Delta z = 0.2$ and $\Delta r = 0.1$ the effect of the time increment on the accuracy of the solution is very slight so long as a stable time increment is chosen. The value of the time increment was set at 0.1 μsec so that the numerical computation could be efficiently achieved and yet allow the stability criterion to be safely satisfied.

In summary, the following special case is used to determine whether or not the numerical solution approaches the P.C.S.: E = 2 Mbar, $\nu = 0.25$, $\rho = 8.0$ gm/cc, $\Delta r = 0.1$ cm, $\Delta z = 0.2$ cm, $\Delta t = 0.1$ μsec, 12 radial increments, and 250 axial increments with $d/\lambda' = 0.3$. The value of $\Delta z = 0.2$ is used in the solution because the estimated error is not extremely large (7%) and this solution should approach the P.C.S. if any numerical solution does. Furthermore, the solution for $\Delta z =$

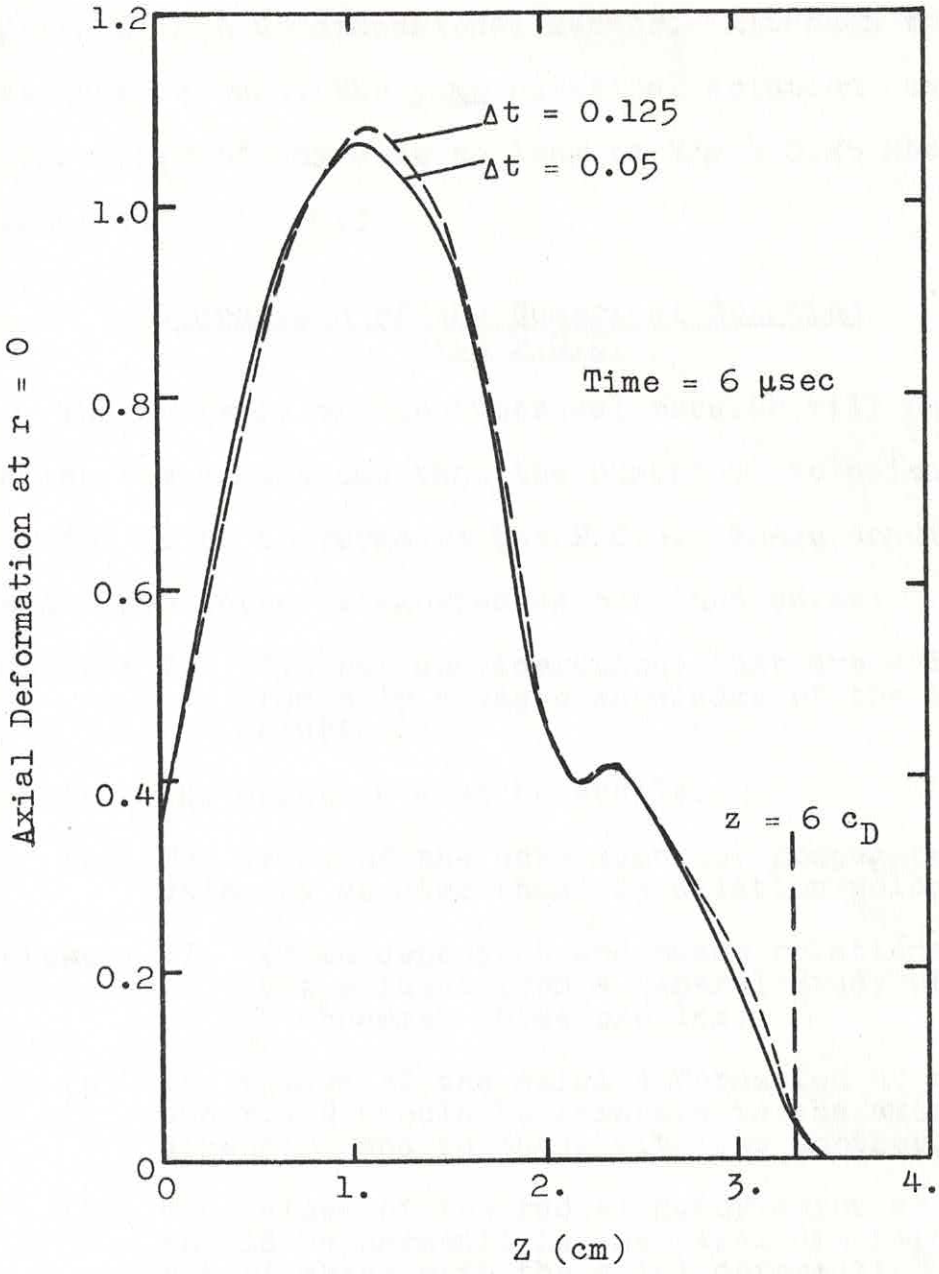


Fig. 10.--The Effect of Δt on the Accuracy of the Numerical Solution.

1.2 takes approximately 1.8 hours of IBM 709 time and a more accurate solution would take an unreasonable length of time.

It should be emphasized that the numerical solution is accomplished in a nondimensional manner. Although the above special case is used, the same numerical solution can be applied for a bar of any size so long as $E/\rho = 0.25$ Mbar-cc/gm, $\nu = 0.25$, and $d/\lambda' = 0.3$.

Comparison of the Numerical Solution with P.C.S.

The analysis of the numerical results will be initiated by stating the conditions that the numerical solution must satisfy for it to converge to the P.C.S. These conditions are separated into three categories as outlined below:

Category I. (General considerations that are evident from only a vague knowledge of the true solution)

(a) The solution must be stable.

(b) The front of the wave must not propagate at a velocity greater than the dilation velocity.

Category II. (Time dependent and phase relations that are evident from a general study of the Pochhammer-Chree problem)

(a) The values of the axial deformation at $r = 0$ and $r = R$ should be harmonic in the axial dimension and in phase with one another.

(b) The values of the radial deformation at $r = R$ should be harmonic in the axial dimension and out of phase with the axial deformation by $\pm 90^{\circ}$.

Category III. (Conditions that are evident only after the solution to the Pochhammer-Chree problem has been studied in detail)

(a) For $d/\lambda' = 0.3$, the harmonic amplitudes of the maximum axial deformation (at $r = 0$) and the maximum radial deformation (at $r = R$) should be as predicted by the P.C.S., namely, $W_{max}/U_{max} = 3.91127$.

(b) By using the driving frequency that was computed from the P.C.S. for $d/\lambda' = 0.3$, the wave length for the numerical solution should yield $d/\lambda' = 0.3$.

(c) The nondimensional phase velocity (c/c_o) for the wave should be 0.98337.

(d) The radial distribution of the axial deformation should be as given in Fig. 6 for $d/\lambda' = 0.3$.

(e) The radial distribution of the radial deformation should be as shown in Fig. 7 for $d/\lambda' = 0.3$.

The analysis of the numerical results is greatly simplified by using these three categories. If Category I is not satisfied there is no reason to continue the analysis. Also, provided that Category I is satisfied, Category II can be easily tested to determine whether or not there is any expectation that the numerical solution will converge to the P.C.S. Finally, if the first two Categories are satisfied, Category III can be applied to find where the numerical solution and the P.C.S. agree best and to determine how well they agree.

The satisfaction of Category I is easily tested by plotting the displacement at $r = 0$ as a function of the axial position for the final time increment calculated as shown in Fig. 11. Since the solution is stable and the front of the wave is propagating at the dilation velocity, Category II can be tested. This is accomplished by plotting the curves for the axial and radial deformations at $r = R$ as shown in Fig. 11.

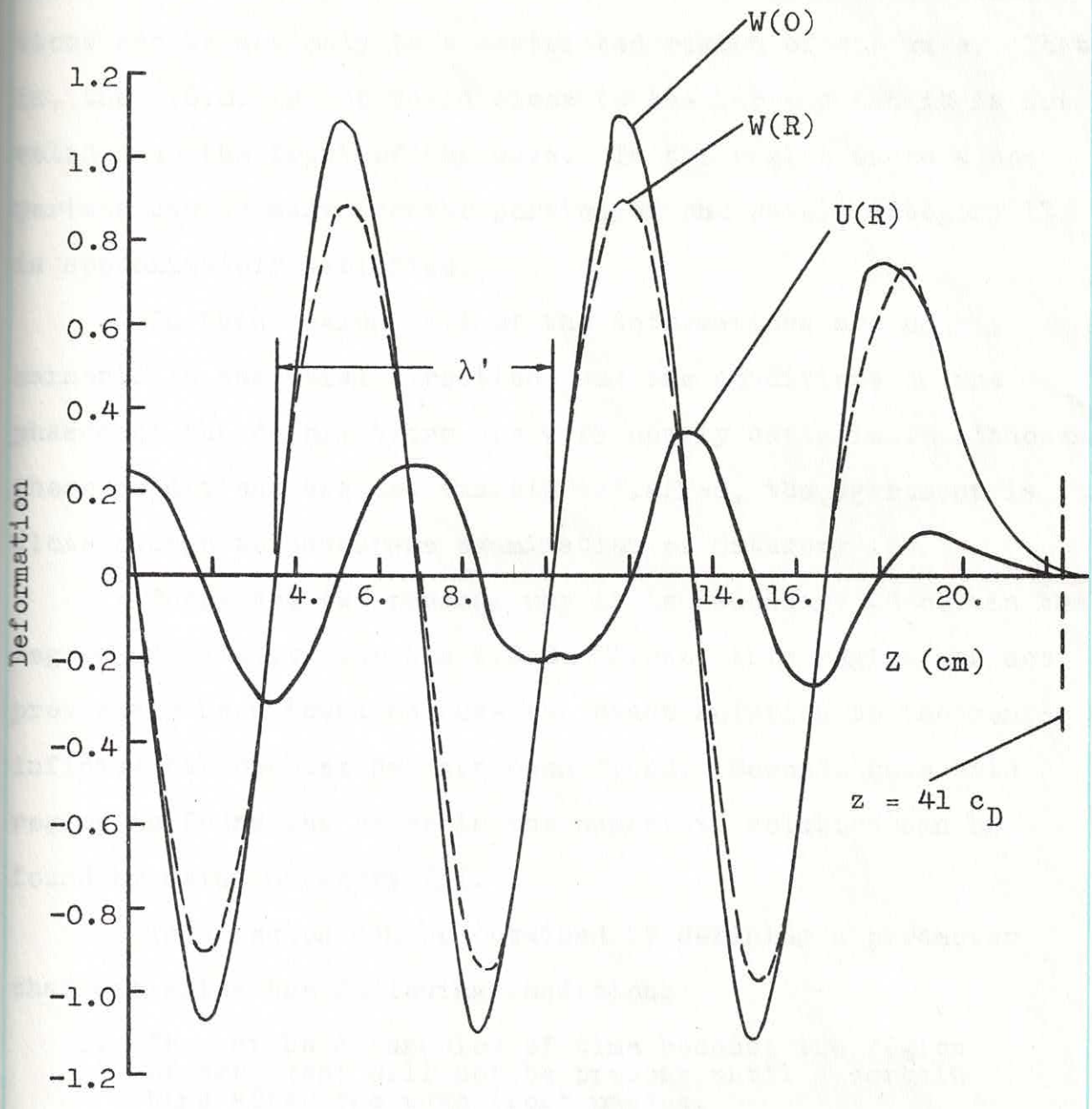


Fig. 11.--Summary of Numerical Results at the Greatest Value of Time (t = 41 μsec).

Before a conclusion can be reached concerning the satisfaction of Category II, it must be realized that these conditions can be met only in a restricted region of the wave. That is, the P.C.S. is not valid close to the bar end and it is not valid near the front of the wave. In the region where a comparison can be made (center portion of the wave), Category II is approximately satisfied.

In this region, all of the deformations are nearly harmonic in the axial direction, and the conditions on the phases of the deformations are very nearly satisfied. Although these conditions are not exactly satisfied, the agreement is close enough to encourage examination of Category III.

There are two reasons why it is necessary to obtain the region of validity for the P.C.S. First, this region has not previously been found because the exact solution to the semi-infinite bar problem has not been found. Second, once this region is found the error in the numerical solution can be found by using Category III.

This region can be obtained by defining a parameter that satisfies the following conditions:

1. It must be a function of time because the region of agreement will not be present until a certain <u>time</u> after the wave front passes.
2. It must be a function of the distance (z) because the region of agreement will be a certain <u>distance</u> from the end of the bar.
3. It must be related to the details of the P.C.S. and Category III.

The most convenient parameter that satisfies the above requirements is the nondimensional phase velocity. An "Equivalent Nondimensional Phase Velocity," as defined and computed in Fig. 12, was computed for many times and distances. In the example shown, the equivalent phase velocity is (0.98 cm)/(41 - 39) μsec = 0.49 cm/μsec and the "Equivalent Nondimensional Phase Velocity" is 0.49/0.50 = 0.98.

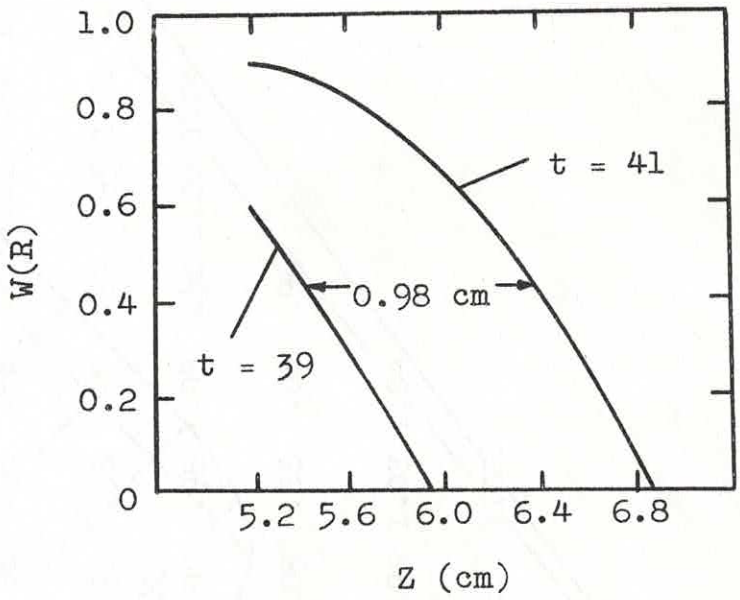


Fig. 12.--Example of "Equivalent Nondimensional Phase Velocity" Determination at z = 6 cm and t = 40 μsec.

The results of these calculations are shown in Fig. 13. The region of best agreement is also suggested here. The points of best agreement are those between z = 5 and z = 9 cm for a time greater than 40 μsec. In this region, the satisfaction of the other conditions in Category III can now be investigated.

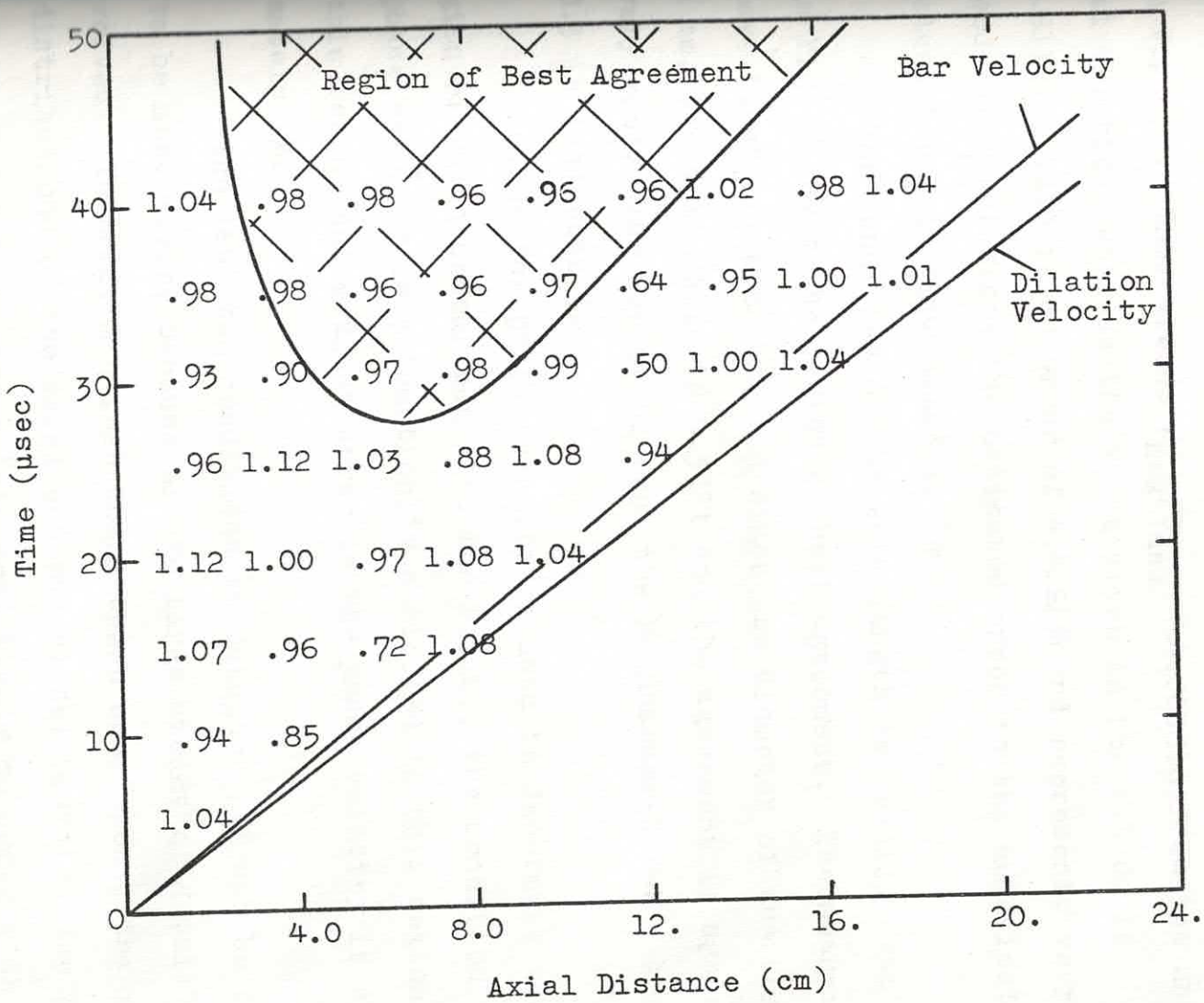


Fig. 13.--Values of the "Equivalent Nondimensional Phase Velocity."

The condition on the harmonic amplitudes is easily checked at t = 41 μsec by using $W(r = 0, z = 5.2) = W_{max} = 1.0811253$ and $U(r = R, z = 6.8) = U_{max} = 0.26473070$ as shown in Fig. 11. This yields $W_{max}/U_{max} = 4.083868$ from the numerical solution, whereas the value given in the P.C.S. is 3.91127. This is an error of 4.4128% and represents very good agreement since the estimated error in the numerical calculations is approximately 7%.

The condition on the wave length is readily examined in Fig. 11 over the region of best agreement. The measured wave length is 6.62 cm, and since the diameter of the bar is 2 cm, the d/λ' ratio is 0.3021 and the agreement is again very good. The deviation from the Pochhammer-Chree value of 0.3 is less than 1%.

Since the phase velocity is used to determine the region of valid comparison with the P.C.S., the condition on the phase velocity is automatically satisfied in this region. In this region the maximum error in the phase velocity is approximately 2%.

The last two conditions in Category III can be expected to be most severe because of the large amount of detail involved. To perform a test using these conditions, the radial distributions of the axial and radial deformations are plotted in Fig. 14 for the two points most likely to agree with the distributions obtained from the P.C.S. (z = 6 and z = 8 cm for t = 41 μsec).

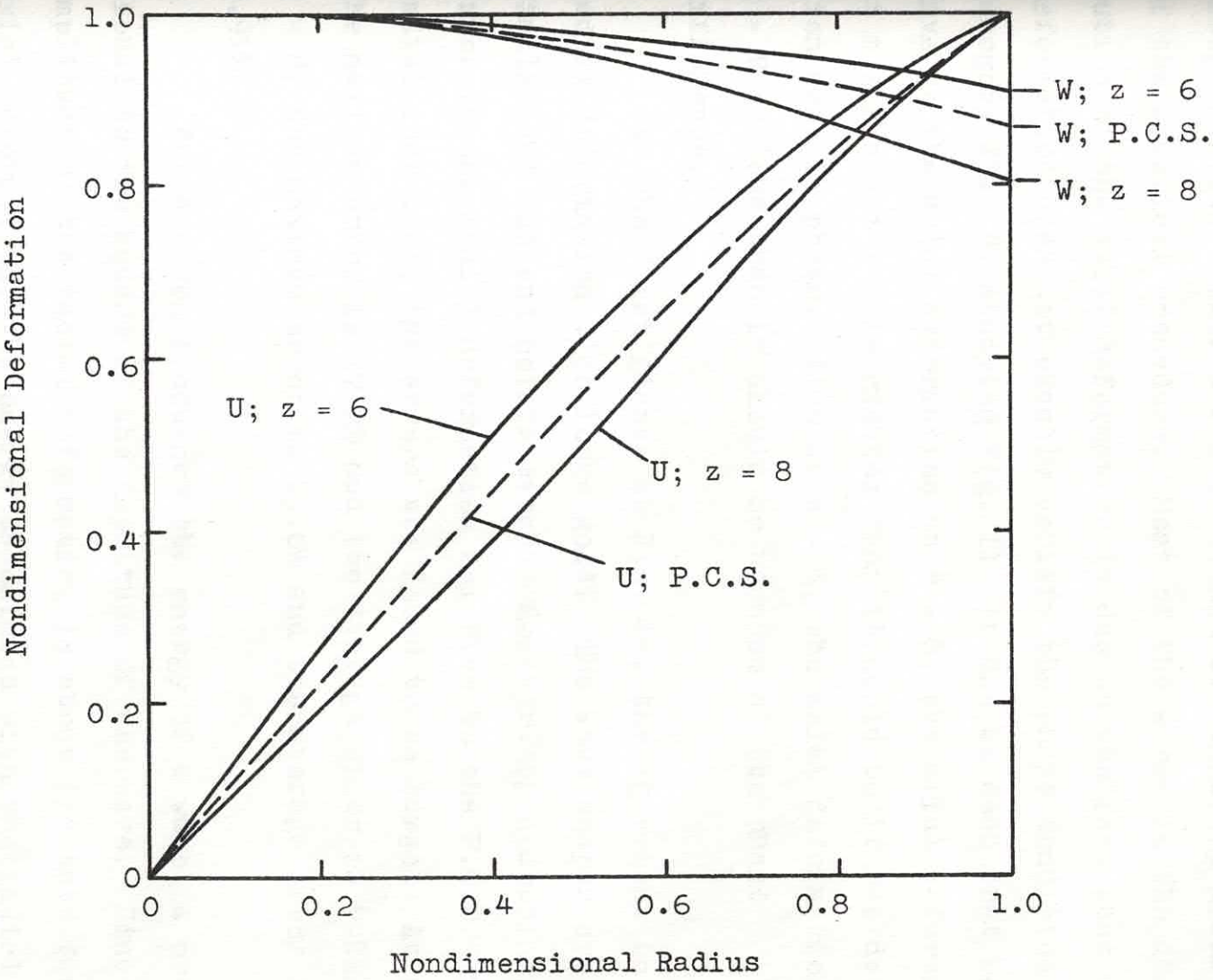


Fig. 14.--Deviation in the Radial Distribution of the Deformation for $d/\lambda' = 0.3$.

The maximum error in the distribution for the axial deformation at z = 6 is 4.73% and for z = 8 cm, the maximum error is 7.04%. This error is within the expected accuracy of the numerical procedure. Most of the error in the distribution of the axial deformation is due to the fact that this deformation does not exactly satisfy the phase condition of Category II. By studying Fig. 11, it can be seen that relative to the axial deformation at r = 0, the axial deformation at r = R and z = 6 is greater than it would be if the deformation were in phase. Also at z = 8, the axial deformation at r = R is less than it should be because of the phase difference.

At the first glance at Fig. 14, the agreement in the radial deformation also looks good. The wave shapes are quite similar and the end points match. However, by computing the error in the radial deformation relative to the P.C.S. at each radial increment, the errors are found to be large. At z = 6, the maximum error is 17.2% and the average error is 9.22%. At z = 8, the maximum error is 13.6% and the average error is 5.91%.

For a given frequency the energy of a wave is proportional to the square of the amplitude of the wave. Since the amplitude of the radial deformation is about 1/4 that for the axial deformation, the energy associated with the radial deformation is only about 1/16 of that for the axial deformation. Thus, a large error in the radial deformation can be present without causing an appreciable effect in the remainder of the

solution. Furthermore, the maximum percent errors in the radial deformations occur at low wave amplitudes and thus the average amount of error in the amplitude based on the energy associated with the radial deformation will be much less than the error values calculated.

Since energy E(r) is proportional to the amplitude squared $[A(r)]^2$, the energy associated with the radial deformation can be written as follows:

$$\int_0^R E(r)\, dr \sim \int_0^R [A(r)]^2\, dr.$$

By the trapezoidal rule, this is approximately equal to:

$$1/2 \left[A_o^2 + 2A_1^2 + 2A_2^2 + \cdots + 2A_{N-1}^2 + A_N^2\right] \delta r$$

where $\delta r = (R - 0)/N$. Using N = 10 and R = 1, the following relative energies are obtained for the radial deformations: Pochhammer-Chree = 0.3721, numerical at z = 6 is 0.4134, and numerical at z = 8 is 0.3465. The average value of the amplitude for each case is computed as follows:

$$\int_0^R E(r)\, dr = \int_0^R [A(r)]^2\, dr = A_{avg}^2\, R.$$

This yields the following average amplitudes: Pochhammer-Chree is 0.610, numerical at z = 6 is 0.634, and numerical at z = 8 is 0.589. Thus, the error in the average amplitude is 5.46% at z = 6 and 3.45% at z = 8.

In the region where agreement is expected, the approximate amount of error associated with each of the conditions in Category III is summarized in Table 2.

TABLE 2

Error between Numerical Solution and P.C.S.

Condition	Percentage of Error
W_{max}/U_{max}.....	4.4127
d/λ'.....	0.7
c/c_o.....	2.0 (max.)
W(r).....	7.04 (max.)
Average U(r).....	5.46 (max.)

Since the numerical solution is expected to have an error of approximately 7%, there is no reasonable doubt that the numerical solution is converging to the P.C.S. However, these differences can be caused either by the fact that the convergence is not yet complete or by the errors in the numerical procedure. The only way this can be determined is to obtain a more accurate numerical solution. This can be done by using a smaller Δz, but it would take an unreasonable amount of machine time. The solution for $\Delta z = 0.2$ represents the compromise that was made between accuracy and cost.

Even so, it can be reasonably concluded that for a plane harmonic deformation at $z = 0$ and for $d/\lambda' = 0.3$, the P.C.S. is very nearly valid at distances of more than 4 diameters from the end of the bar for times greater than $(z + 6d)/c_o$ (see Fig. 13).

Summary of Numerical Results

In the comparison between the numerical solution and the P.C.S., the numerical results were closely examined at $t = 41$ μsec. The numerical results for $t < 41$ μsec are also of interest and are summarized in Figs. 15 and 16. Figures 11 and 15 indicate how the deformations approach the conditions of Category II as the time increases. In Fig. 16, the indicated deformations are plotted at the point where the best agreement with the P.C.S. is expected. It is evident from Fig. 16 that as time increases the conditions of Category II are more and more closely satisfied.

The dashed vertical lines in Figs. 11, 15, and 16 indicate the ordinate values that correspond to the dilation velocity. Also, these figures show that the wave front is one-dimensional. The value of U approaches zero and the axial deformation becomes planar. Thus, the wave front is a dilation wave.

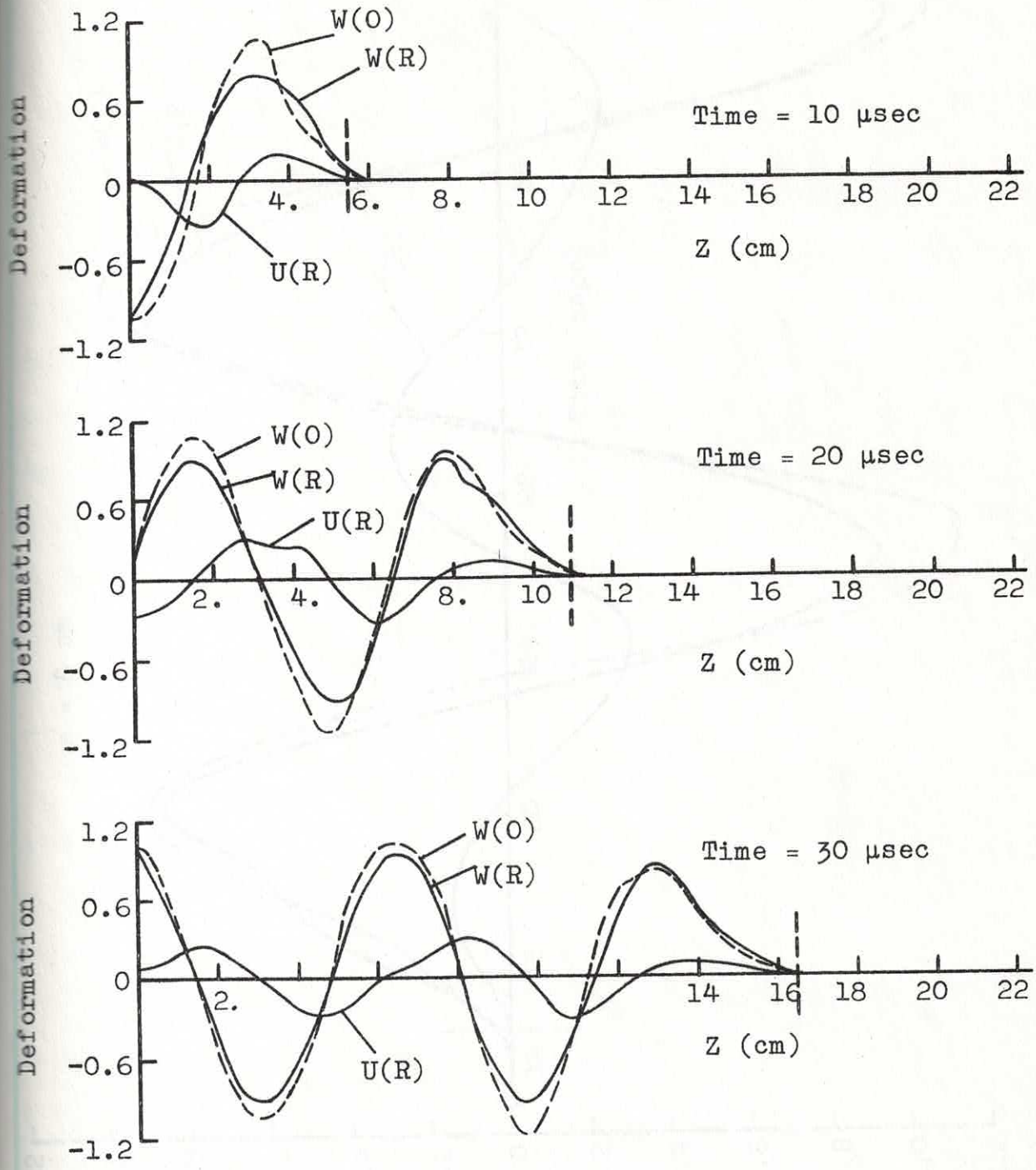


Fig. 15.--Deformation vs. Axial Position at Various Times

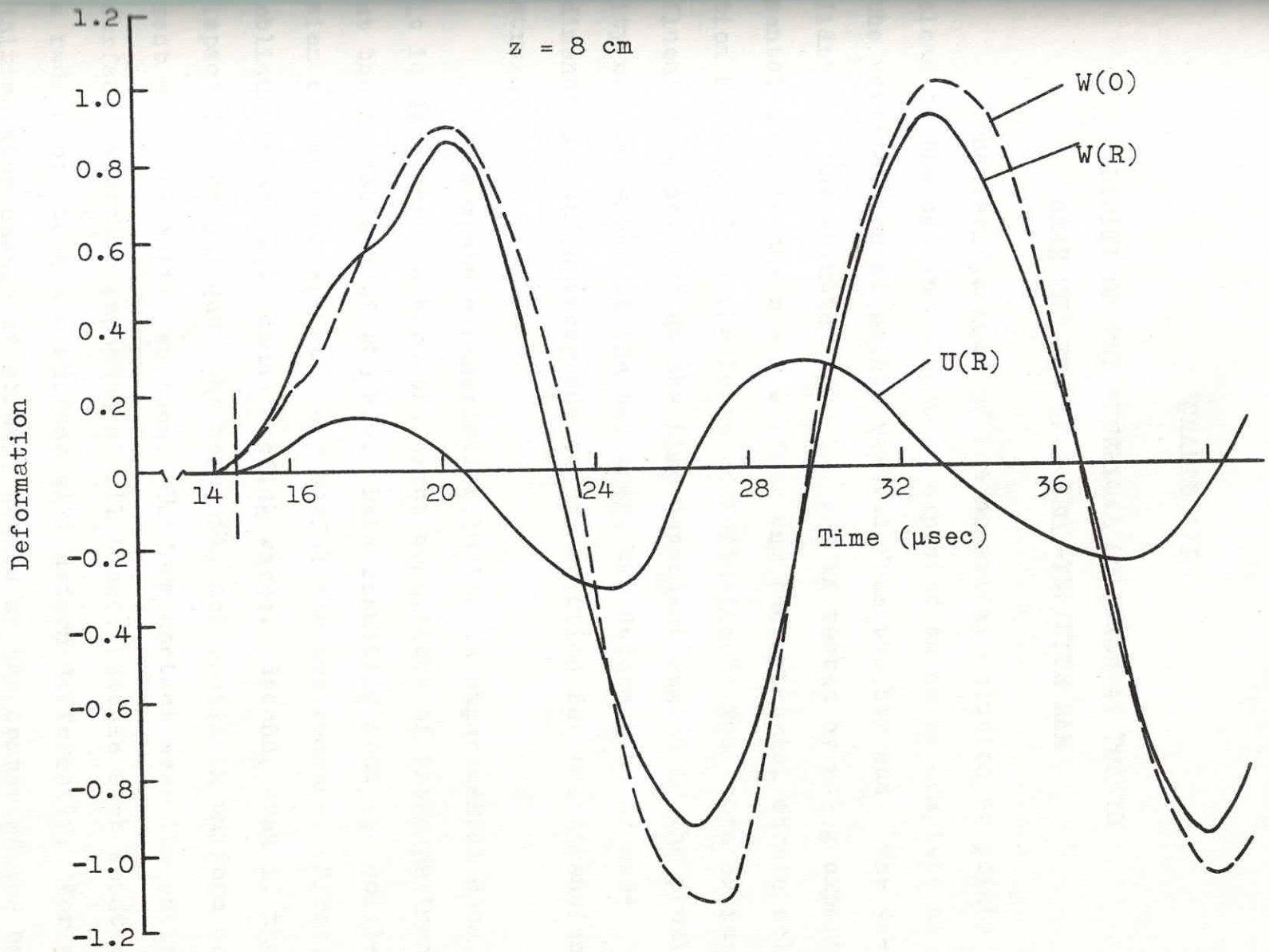


Fig. 16.--The Deformation as a Function of Time at z = 8

CHAPTER VI

VALIDITY OF THE NUMERICAL SOLUTION AT POINTS NEAR THE END OF A SEMI-INFINITE BAR

The verification of the numerical solution at points close to the bar end cannot be expected to be as complete as the verification at points removed from the bar end. The validity of the solution near the end is tested by using experimental data at the r = R surface and the uni-axial strain solution near r = 0 in the "core of influence." The "core of influence" is defined as the time dependent region in the proximity of the center of the bar where the deformation is one-dimensional and corresponds to the solution for one-dimensional strain.

To compare a numerical solution to experimental data, it is necessary to know the exact conditions of the experiment at the impact end of the bar. Data resulting from the collision of two bars are not very useful for two reasons. First, oblique impact will cause bending waves. Second, even if the impact is not oblique, the bars will not remain in uniform contact over the entire surface. Uniform contact over the entire surface cannot be expected at all times, because each point on a radius of the z = 0 surface will deform differently. For an initial step change of stress, points at the center of the bar will initially deform as if the radius of the bar were infinite.

That is, at the center the bar will initially deform as it would for a one-dimensional strain. The axial deformation at the outside of the rod will initially be larger than the one-dimensional strain value because the radial normal stress is equal to zero at r = R. Although the larger deformation at r = R will decrease the stress there and tend to make the deformation plane again, it is evident that an exact solution would depend on a time dependent boundary condition at z = 0 which, in turn, depends on the solution.

Many recent experimenters have used either ultrasonic pulses [23,29,53] or a shock tube [15,32]. Because of the characteristics of an ultrasonic transducer, the initial amplitude of the wave is also time dependent. Thus, the experimental arrangement that produces the best defined boundary conditions is one that utilizes a shock tube. When the gas shock wave contacts the end of the elastic bar, the stress on the end of the bar will be very nearly a step change from zero to a constant value. The change of stress will be nearly immediate because the length of the shock front is very small and the velocity of the shock wave is large. Furthermore, this yields a pressure that is nearly constant over the diameter of the bar.

Miklowitz and Nisewanger [32] performed this type of experiment and obtained very useful data. The reader is referred to this paper for the details of the experiment. They obtained data for both the radial deformation and the axial strain on the radial surface at points near the end of the bar.

These data appear to be very reliable and will be used for a check on the numerical procedure.

Boundary Conditions for a Pressure Applied at z = 0

In determining the validity of the numerical procedure at points removed from the end of the bar, the boundary conditions at z = 0 were not important because the numerical solution was examined at points where the end conditions were not significant. However, to compare a numerical solution with experimental data close to the bar end it is obvious that the boundary conditions of the experiment must be reproduced, if agreement is to be obtained.

For the experiment of Miklowitz and Nisewanger, the boundary conditions at z = 0 are: $\sigma_{zz} = -P$ and $\sigma_{rz} = 0$, where the initial conditions are U = 0 and W = 0. Also, since the radial surface is free,[1] $\sigma_{rr} = 0$ at r = R and z = 0. Furthermore, at r = 0, the conditions for proper behavior of the equations of motion must be satisfied.

By using equations (30) for the components of stress, the boundary conditions at z = 0 for an applied pressure are obtained:

$$\text{at } r = R;\ \sigma_{rr} = 0 = (\lambda+2\mu)\frac{\partial U}{\partial r} + \lambda\left[\frac{\partial W}{\partial z} + \frac{U}{r}\right] \qquad (71)$$

---

[1] The seal around the bar at the shock tube probably introduces some radial constraint, but the mounting is not described and the effect of the seal will be omitted in the numerical solution. This may be expected to produce small differences between the numerical and experimental results.

$$\text{for } 0 \leq r \leq R;\ \sigma_{rz} = 0 = \mu \left[\frac{\partial U}{\partial z} + \frac{\partial W}{\partial r}\right] \tag{72}$$

$$\text{for } 0 \leq r \leq R;\ \sigma_{zz} = -P = (\lambda + 2\mu)\frac{\partial W}{\partial z} + \lambda\left[\frac{U}{r} + \frac{\partial U}{\partial r}\right] \tag{73}$$

$$\text{at } r = 0;\ \frac{U}{r} = \frac{\partial U}{\partial r},\ U = 0, \text{ and } \frac{\partial W}{\partial r} = 0. \tag{74}$$

Since values of U and W for $r < 0$ are nonexistent, the finite difference approximation to equations (71), (72), (73), and (74) must be written in forward r differences. By the same token forward z differences must be used. Equations (71) and (72) are easily written in forward finite differences as follows:

$$0 = \left[\frac{U(R+\Delta r,0) - U(R,0)}{\Delta r}\right] + G\left[\frac{U(R,0)}{R} + \frac{W(R,\Delta z) - W(R,0)}{\Delta z}\right] \tag{75}$$

for $0 \leq r \leq R$;

$$0 = \left[\frac{W(r+\Delta r,0) - W(r,0)}{\Delta r}\right] + \left[\frac{U(r,\Delta z) - U(r,0)}{\Delta z}\right] \tag{76}$$

where $G = \lambda/(\lambda + 2\mu)$.

For $0 < r \leq R$, equation (73) can be written in forward differences as follows:

$$-\frac{PG}{\lambda} = \left[\frac{W(r,\Delta z) - W(r,0)}{\Delta z}\right] + G\left[\frac{U(r,0)}{r} + \frac{U(r+\Delta r,0) - U(r,0)}{\Delta r}\right]. \tag{77}$$

Also, by using the first of equations (74), equation (73) can be written as follows:

$$-P = (\lambda + 2\mu)\left(\frac{\partial W}{\partial z}\right)_{r=0} + 2\lambda\left(\frac{\partial U}{\partial r}\right)_{r=0} \tag{78}$$

and for forward differences this becomes:

$$-\frac{PG}{\lambda} = \left[\frac{W(0,\Delta z) - W(0,0)}{\Delta z}\right] + 2G\left[\frac{U(\Delta r,0) - U(0,0)}{\Delta r}\right]. \quad (79)$$

The remaining equations are easily written in differences as follows:

$$U(0,0) = 0 \text{ and } W(\Delta r,0) = W(0,0). \quad (80)$$

Since equation (76) is identically satisfied at $r = 0$, difference equations (79), (77), (76), and (75), respectively, can be written as follows:

$$-\frac{PG\Delta z}{\lambda} - W(0,\Delta z) = 2G\,\frac{\Delta z}{\Delta r}\,U(\Delta r,0) - W(\Delta r,0) \quad (81)$$

$$\text{for } 0 < r \leq R; \quad -\frac{PG\Delta z}{\lambda} - W(r,\Delta z) = G\,\frac{\Delta z}{\Delta r}\,U(r+\Delta r,0)$$

$$+ G\,\Delta z\left[\frac{1}{r} - \frac{1}{\Delta r}\right]U(r,0) - W(r,0) \quad (81)$$

$$\text{for } 0 < r \leq R; \quad U(r,\Delta z) = U(r,0) + \frac{\Delta z}{\Delta r}\,W(r,0)$$

$$-\frac{\Delta z}{\Delta r}\,W(r+\Delta r,0) \quad (81)$$

$$-G\,\frac{\Delta r}{\Delta z}\,W(R,\Delta z) =$$

$$U(R+\Delta r,0) + U(R,0)\left[G\,\frac{\Delta r}{R} - 1\right] - G\,\frac{\Delta r}{\Delta z}\,W(R,0) \quad (81)$$

where equations (80) were used to eliminate $U(0,0)$ and $W(0,0)$.

For $R = N\Delta r$, equations (81) are a system of $2(N + 1)$ linear equations with $2(N + 1)$ unknowns. Since the values of $U(r,\Delta z)$ and $W(r,\Delta z)$ for $0 < r \leq R$ are obtained from

equations (40), the unknowns are $U(M\Delta r,0)$ and $W(M\Delta r,0)$ for $M = 1, 2, \cdots N, N + 1$.

In the numerical procedure, this system of equations is solved at each time step. Then the value of $W(0,0)$ is computed from equation (80). The computer time required to solve this system of $2(N + 1)$ equations for every time step is minimized by inverting the matrix of coefficients at the start and using this inverse, which does not change with time, at each subsequent time step.

This numerical procedure is used for a step change in the stress at $z = 0$ for a bar with the same diameter and material constants as were used in the experiment of Miklowitz and Nisewanger. These constants are summarized in Table 3.

TABLE 3

Physical Constants Used in the Numerical Procedure for a Step in Pressure

Property	Value
Bar material.....	24S-T aluminum
Bar diameter.....	1 inch
E	0.72395 Mbar
ρ	2.7135 gm/cc
ν	0.3125
Bar velocity.....	0.51654 cm/μsec
Dilation velocity....	0.60965 cm/μsec

Miklowitz and Nisewanger used SR-4 type C-19 resistance strain gages that have a gage length of 1/16 inch. Although these gages are short, their high frequency response is limited by their length. Even if the recording system had an infinite frequency response and even if the strain gages had no inertia, the strain gage must measure average strain over its length.

If it is assumed that a gage of length L' is placed on a bar in which a harmonic wave of wave length λ' is travelling, the ratio of the measured average strain to the actual strain at any point can easily be found to be:

$$\varepsilon_m/\varepsilon_a = \frac{\lambda'}{\pi L'} \sin \frac{\pi L'}{\lambda'}. \qquad (82)$$

If a maximum error of 10% is arbitrarily allowed, L'/λ' can be no greater than 1/4. Thus, for a gage length of 1/16 inch, the wave length can be no shorter than 0.635 cm if the experimental error is to be less than 10%.

The numerical solution is necessarily approximate, and since it is desired to compare the experimental data and the numerical solution, there is no need to make the numerical solution significantly more accurate than the experiment. Thus, Δr is set equal to 0.127 cm, Δz is set at 0.127 cm, and a time increment of 0.1 μsec is used.

Numerical Solution near the Loaded End for Small Values of Time

It has been previously mentioned that an initial step change of stress at z = 0 will cause a deformation that is a function of radial position at z = 0. The particles at r = R

will be subjected to the zero radial stress condition. Also, at t = 0, the radial deformation will be zero throughout the bar. Since $\varepsilon_{\varphi\varphi} = U/r$, the conditions at r = R, z = 0, and t = 0 are as follows:

$$\sigma_{rr} = 0, \quad \sigma_{zz} = -P, \quad \text{and} \quad \varepsilon_{\varphi\varphi} = 0.$$

By using Hooke's Law, equations (6), the axial strain at this point is easily obtained:

$$\varepsilon_{zz} = \frac{-PG}{\lambda(1 - G^2)}.$$

Since the effect of the free surface at r = R travels inward at the dilation velocity, the particles near r = 0 will initially deform as though the free surface were not present.

If the numerical procedure for a step in stress at z = 0 is a correct one, the core of influence must exist. Also, the radius of the core of influence must decrease with time at z = 0 as the effect of the free surface at r = R is felt. Furthermore, the strain in the core of influence at z = 0 must initially be the one-dimensional value $[\sigma_{zz}/(\lambda + 2\mu)]$ and it must increase toward the one-dimensional stress value (σ_{zz}/E) as time progresses. Also, the axial strain at z = 0, r = R, and t = 0 must equal $-PG/\lambda(1 - G^2)$.

For the one-inch aluminum bar, the numerical procedure for the step in stress at z = 0 is tested to determine if it satisfies the above conditions. The values of U(r,z,t), W(r,z,t), $\varepsilon_{zz}(r,z,t)$, and U(r,z,t)/W(r,z,t) are computed for $t \leq 1.90$ μsec with $\Delta r = 0.127$ cm, $\Delta z = 0.127$ cm, and $\Delta t =$

0.100 μsec. These results are summarized in Figs. 17 and 18.

In Fig. 17 the values of $U(r,z,t)/W(r,z,t)$ are plotted in the r-z plane for different values of t. The curves on the r-z plane indicate the locus of constant U/W values at that time. The dashed vertical lines in the figure indicate the value of z corresponding to $z = c_D t$ for that time.

The values of U/W in Fig. 17 do not define a definite boundary on the core of influence. The numerical procedure causes a smoothing effect and yields small (nonzero) values in the region where the U values are expected to be zero. However, the core of influence can be drawn by arbitrarily choosing a value of U/W = 0.003 to be the boundary of the core. The core of influence is indicated by the cross-hatched area in Fig. 17.

The results of the numerical calculations are as would be expected. Figure 17 indicates that the core of influence is present and that it behaves as expected. Figure 18 indicates that the strain at z = 0 and r = 0 is initially equal to the one-dimensional strain value and as time proceeds the strain begins to increase toward the one-dimensional stress value. Figure 18 also indicates that at z = 0, r = R, and t = 0:

$$\varepsilon_{zz} = \sigma_{zz} G/(1 - G^2).$$

Comparison between the Numerical Solution and Experimental Data at the Radial Surface of the Bar

The numerical solution for a step in pressure at z = 0 behaves properly in the core of influence, and it is very

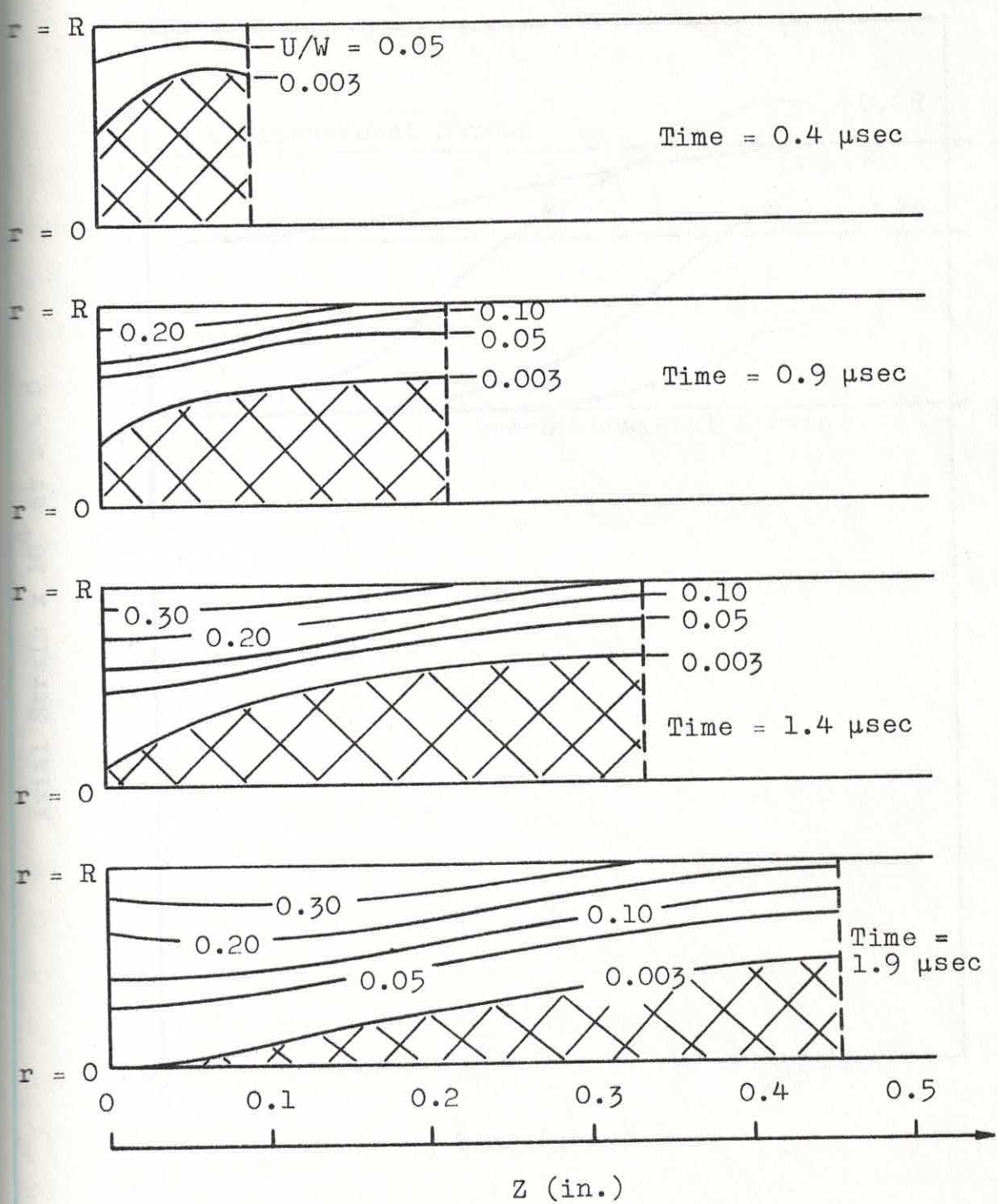


Fig. 17.--The "Core of Influence" as Determined by the Locus of Constant U(r,z,t)/W(r,z,t) Values.

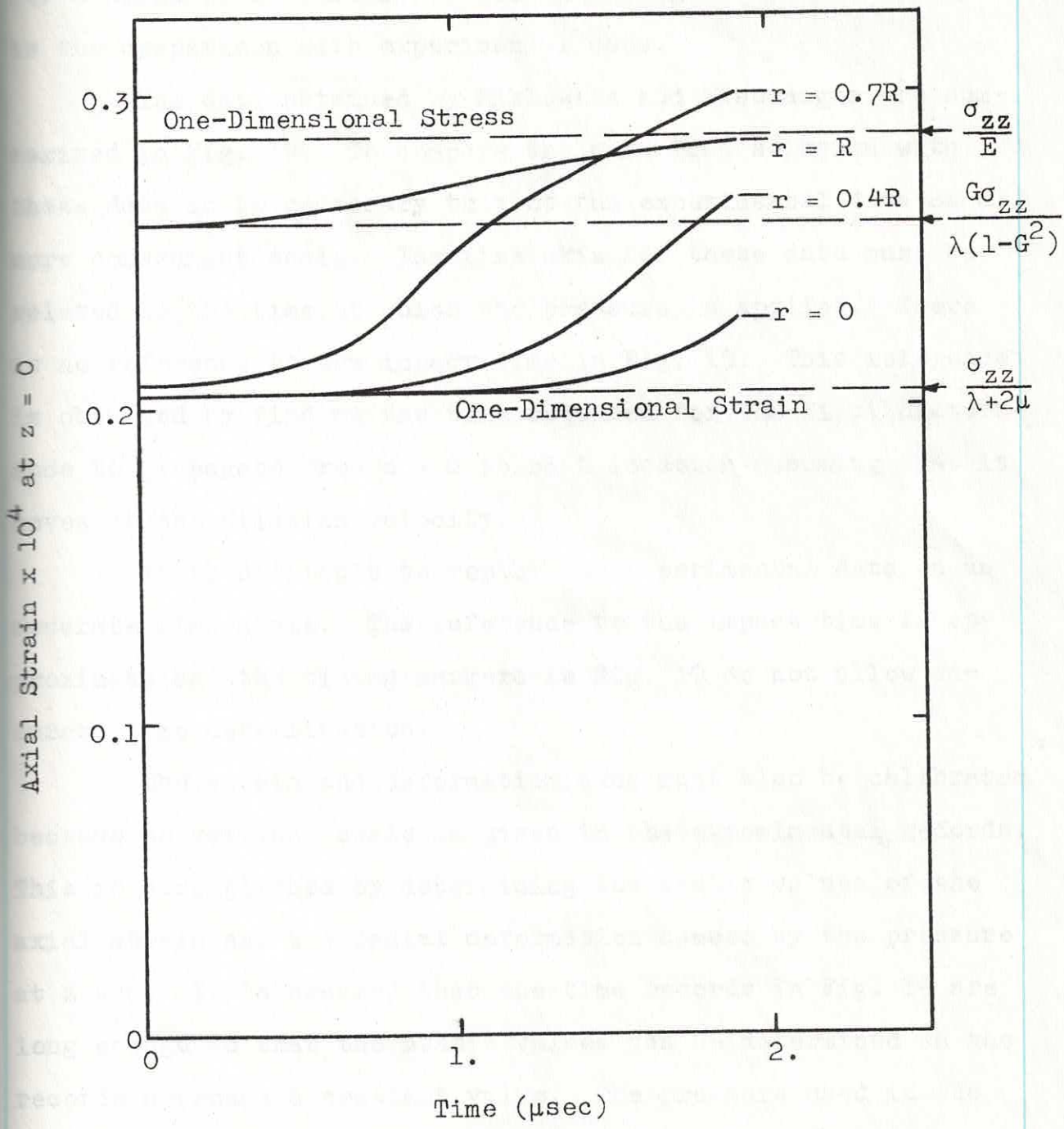


Fig. 18.--Growth of Axial Strain from One-Dimensional Strain to One-Dimensional Stress.

nearly correct at points far removed from the end of the bar for a harmonic disturbance. The remaining test to be applied is the comparison with experimental data.

The data obtained by Miklowitz and Nisewanger are summarized in Fig. 19. To compare the numerical solution with these data it is necessary to plot the experimental data on a more convenient scale. The time axis for these data must be related to the time at which the pressure is applied. There is no reference to the impact time in Fig. 19. This reference is obtained by finding the time required for the first disturbance to propagate from $z = 0$ to that location assuming that it moves at the dilation velocity.

It is difficult to replot the experimental data on an accurate time scale. The reference to the impact time is approximate and the timing markers in Fig. 19 do not allow accurate time determination.

The strain and deformation axes must also be calibrated because no vertical scale is given in the experimental records. This is accomplished by determining the static values of the axial strain and the radial deformation caused by the pressure at $z = 0$. It is assumed that the time records in Fig. 19 are long enough so that the static values can be determined as the records approach a constant value. The pressure used in the experiment was "approximately 300 psi," thus the static value of the axial strain is $-P/E = -0.286 \times 10^{-4}$ cm/cm and the static value of the radial deformation at the radial surface is 0.1136×10^{-5} cm.

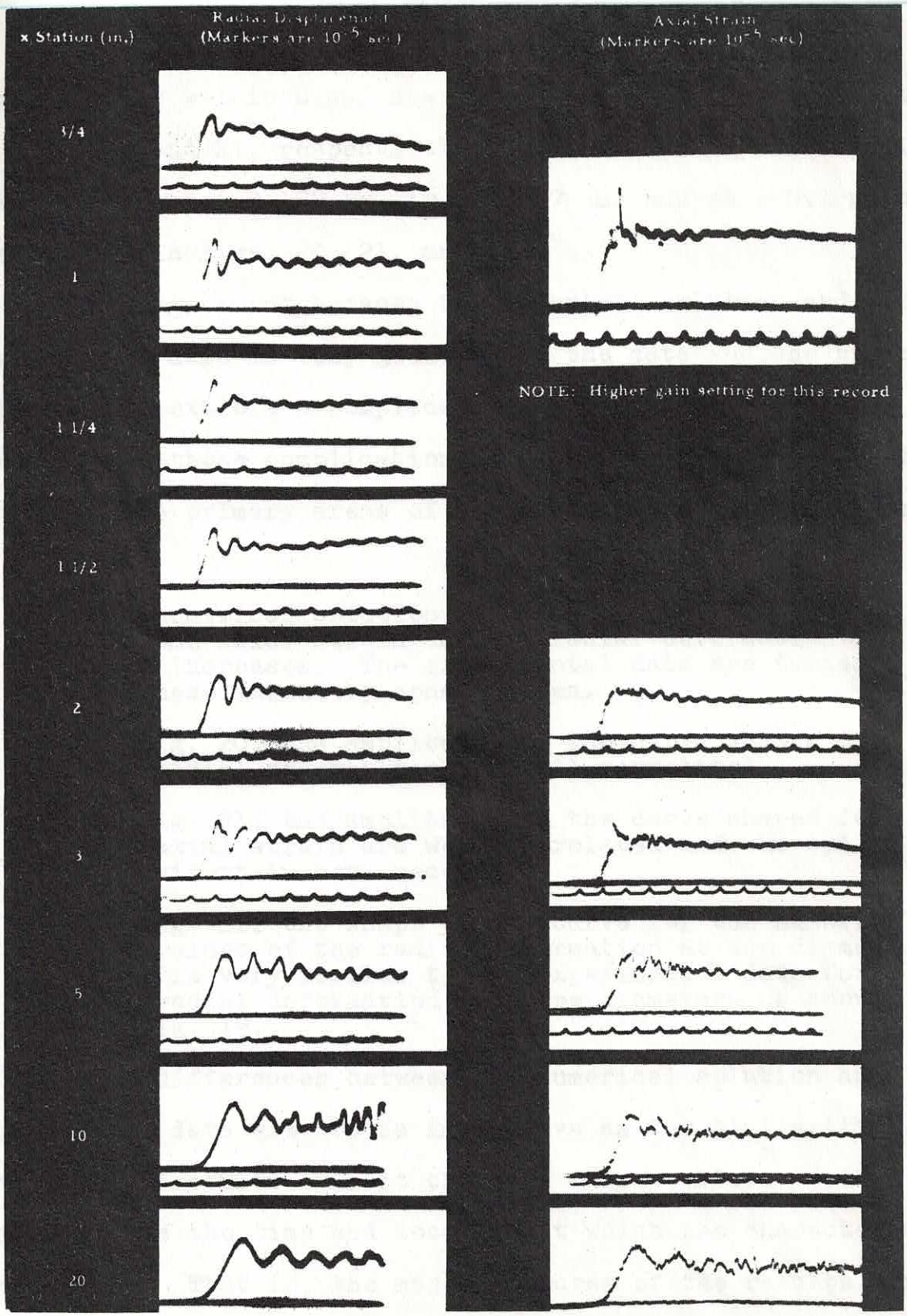


Fig. 19.--Time Records for Radial Displacement and Axial Strain as Obtained Experimentally by Miklowitz and Nisewanger [32].

These scale factors were applied to the records of Fig. 19 for z = 1 inch and z = 2 inch. The results are plotted in Figs. 20 and 21, respectively. The results of the numerical solution for Δz = 0.127 cm, Δr = 0.127 cm, and Δt = 0.1 μsec are plotted in Figs. 20, 21, and 22.

The agreement between the numerical solution and the experimental data is very good. Both the data and the numerical solution exhibit a complicated response to the step of pressure and these complications are similar in both sets of results. The primary areas of agreement and similarities are as follows:

1. The numerical solution approaches the static values for the axial strain and the radial deformation as time increases. The experimental data are forced to these values by construction.

2. In Fig. 20, the amplitude and the curve shapes for the radial deformation are well correlated.

3. In Fig. 21, the amplitude and the curve shapes for the axial strain are well correlated and the spike is evident in both records.

4. In Fig. 21, the shape of the curve for the numerical values of the radial deformation at two diameters is very similar to the experimental data for the radial deformation at three diameters as shown in Fig. 19.

The differences between the numerical solution and the experimental data are not as impressive as the similarities. Both sets of results exhibit the same characteristics--the difference is the time and location at which the characteristics appear. That is, the major features of the results agree but they occur at different times or in different regions. These differences are as follows: The numerical results in

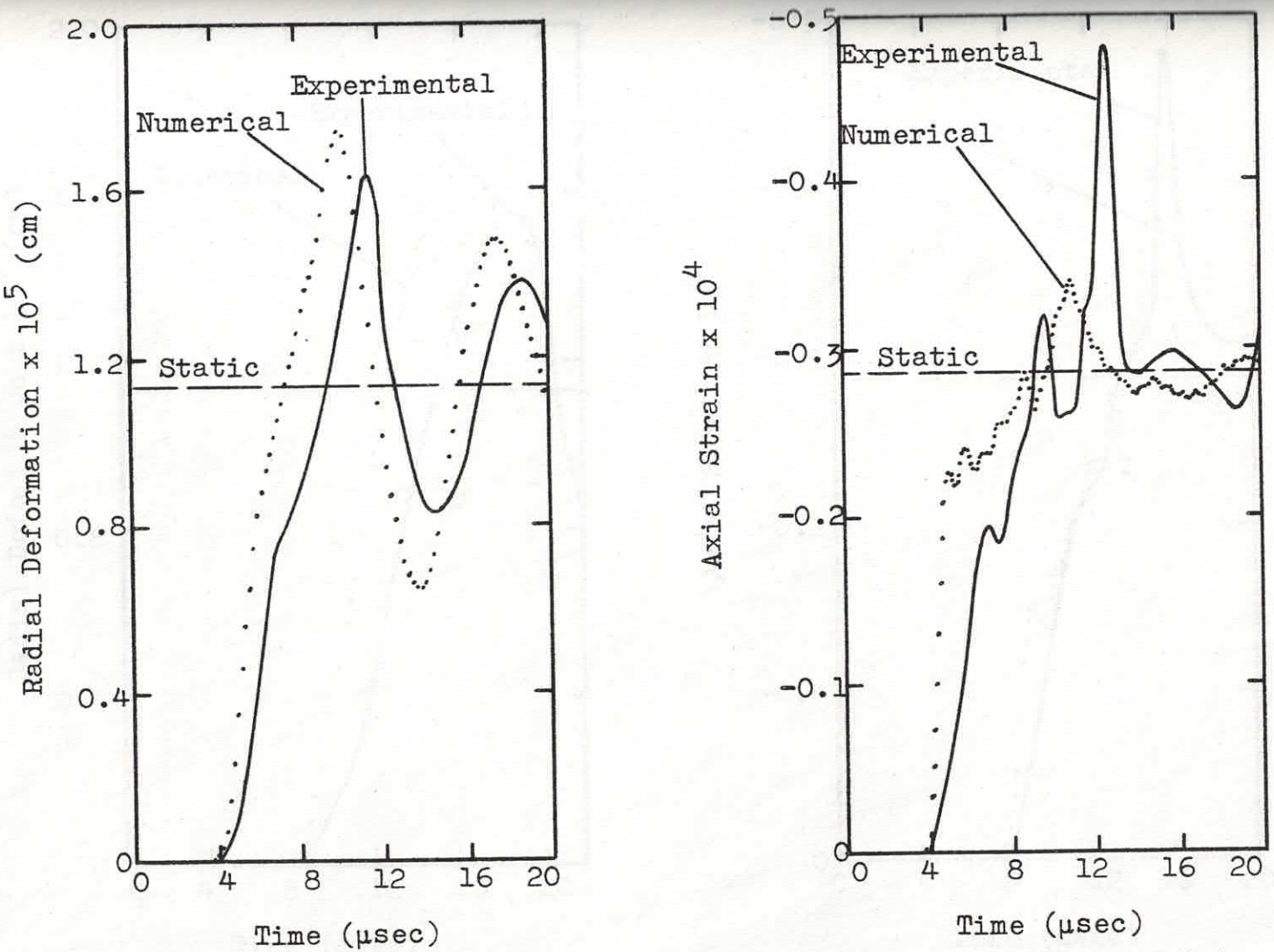


Fig. 20.--Comparison of Numerical Solution and Experimental Data at One Diameter from the Loaded End.

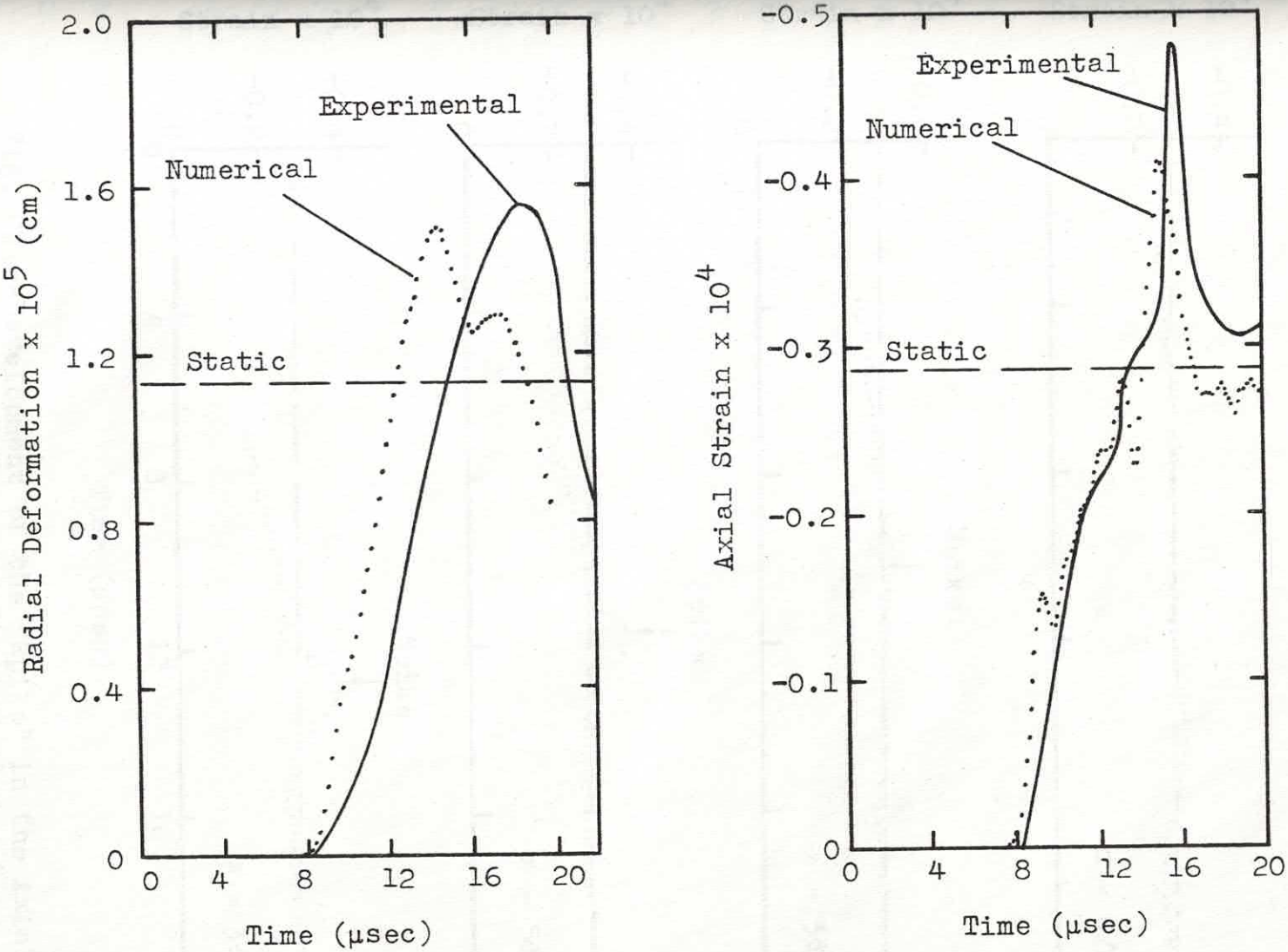


Fig. 21.--Comparison of Numerical Solution and Experimental Data at Two Diameters from the Loaded End.

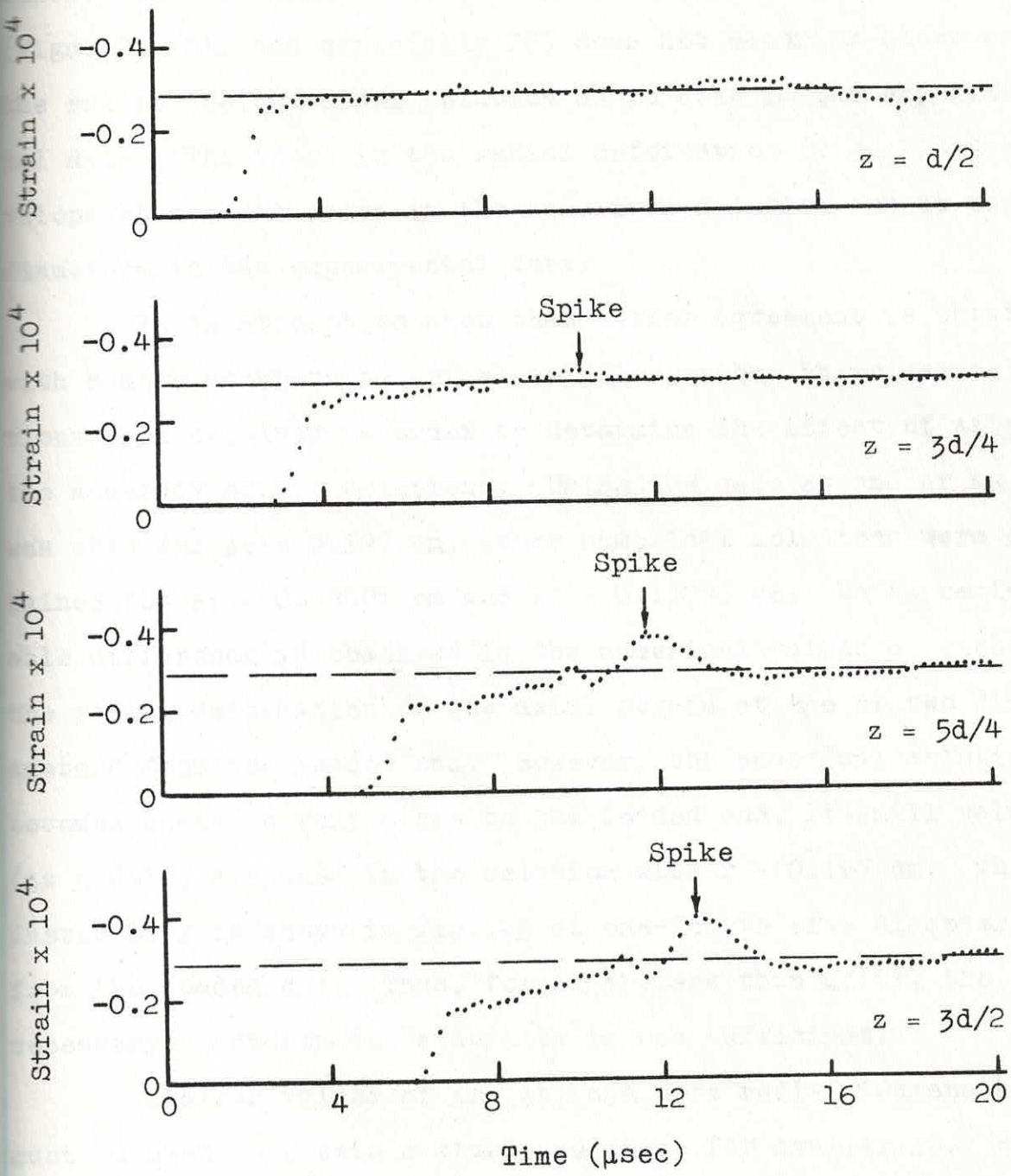


Fig. 22.--Development of the "Spike" in the Axial Surface Strain with a Step of Pressure Applied at z = 0.

Figs. 20 and 21 are ahead (in time) of the experimental results. The development of the spike in the axial strain (Figs. 20, 21, and especially 22) does not occur as close to the end in the numerical solution as it does in the experimental data. The "jog" in the radial deformation (Fig. 21) develops at two diameters in the numerical solution and at three diameters in the experimental data.

In an attempt to show that better agreement is obtained with a more accurate numerical solution, other numerical solutions were obtained in order to determine the effect of Δz on the accuracy of the solutions. Using the same Δt and Δr as was used for $\Delta z = 0.127$ cm, other numerical solutions were obtained for $\Delta z = 0.09071$ cm and $\Delta z = 0.15875$ cm. No appreciable difference is observed in the numerical values of either the radial deformation or the axial strain at one or two diameters from the loaded end. However, the numerical solution becomes unstable very close to the loaded end, if small values ($\Delta z \leq 0.10$) are used in the solution with r = 0.127 cm. This instability is shown in Fig. 23 at one-fourth of a diameter from the loaded end. Thus, for $\Delta z/\Delta r$ less than unity, the necessary condition for stability is not sufficient.

Smaller values of Δr, Δt, and more radial increments must be used to obtain a stable solution for smaller Δz. But the numerical solution is not appreciably affected by changes in stable values of Δz. Thus, a significantly more accurate solution could be obtained only with very small Δz, Δt, and Δr with many radial increments. This would require a very

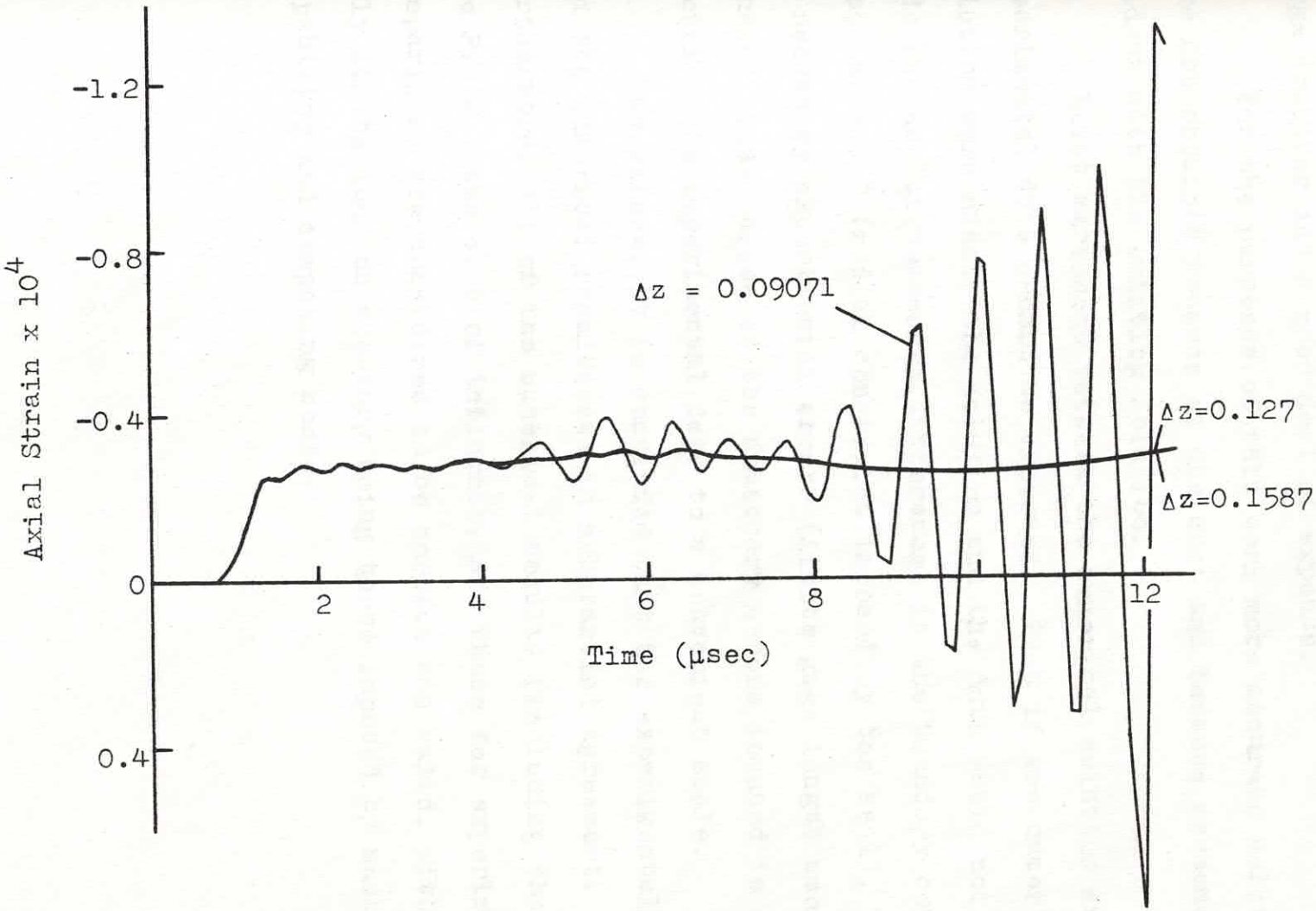


Fig. 23.--Effect of Δz on the Numerical Solution at One-Fourth of a Diameter from the Loaded End of the Bar.

large computer and a good deal of expense.

For the purposes of this work more accurate solutions were not obtained because of the cost and because agreement is evident with the existing solution.

Exact agreement between the numerical solution and the experimental data cannot be expected. Even if the numerical solution were exact, the solution and the data would not coincide because of necessary differences in the boundary conditions at $z = 0$ (radial constraint imposed by the seal), because of necessary experimental errors (finite gage length among others), and because of the necessary errors induced in replotting the experimental data to a convenient scale.

Therefore, it is concluded that the experimental data and the numerical results are in substantial agreement. Furthermore, all of the numerical results (including those for the P.C.S., the core of influence, and those for experimental comparison) are considered to be correct and valid, with the only limitations on accuracy being those imposed by machine capability and computing costs.

CHAPTER VII

NUMERICAL SOLUTION FOR REFLECTIONS IN FINITE CYLINDRICAL BARS

The numerical procedure developed in the last chapter for a step increase in pressure is applied in this chapter. The same properties of the bar as well as the same increment sizes are used.

For the finite bar, two different end conditions are considered at the z = L end of the bar. The first case is a stress-free end (free end) and the second corresponds to a rigid surface at z = L (fixed end).

Boundary Conditions for a Free End

For a stress-free surface at z = L, the boundary conditions are:

$$\sigma_{rz} = 0 \text{ and } \sigma_{zz} = 0. \tag{83}$$

Furthermore, the boundary condition at r = R is:

$$\sigma_{rr} = 0. \tag{84}$$

Also, the conditions for proper behavior must be satisfied at r = 0:

$$U = 0, \frac{\partial U}{\partial r} = \frac{U}{r}, \text{ and } \frac{\partial W}{\partial r} = 0. \tag{85}$$

Although the pressure is zero at $z = L$, equations (83), (84), and (85) are the same conditions as those for a constant pressure at $z = 0$. The finite difference procedure for these conditions is also the same except that backward differences must be used in the z-direction at $z = L$. Using this method, the following system of linear equations (similar to the system for a constant pressure at $z = 0$) is obtained:

$$U(0,L) = 0 \tag{86}$$

$$W(\Delta r,L) = W(0,L) \tag{86}$$

$$W(0,L-\Delta z) = W(0,L) + 2G \frac{\Delta z}{\Delta r} U(\Delta r,L) \tag{86}$$

for $0 < r \leq R$; $W(r,L-\Delta z) = W(r,L)$

$$+ G \frac{\Delta z}{\Delta r} U(r+\Delta r,L) + G \left[\frac{\Delta z}{r} - \frac{\Delta z}{\Delta r}\right] U(r,L) \tag{86}$$

for $0 < r \leq R$; $U(r,L-\Delta z) = U(r,L) + \frac{\Delta z}{\Delta r} W(r+\Delta r,L)$

$$- \frac{\Delta z}{\Delta r} W(r,L) \tag{86}$$

$$G \frac{\Delta r}{\Delta z} W(R,L-\Delta z) = U(R+\Delta r,L) + \left[\frac{G\Delta r}{R} - 1\right] U(R,L) + \frac{G\Delta r}{\Delta z} W(R,L). \tag{86}$$

In the same way as before, the values of U and W for $0 \leq z < L$ and $0 \leq r \leq R + \Delta r$ are obtained and the same method is used to solve equations (86)--the values of U and W at $z = L$ are found by inverting the matrix of coefficients at the start and this inverse is used at each subsequent time step.

Boundary Conditions for a Fixed End

For a fixed end at z = L it is assumed that the end of the bar is in contact with a greased rigid surface. For this case the boundary conditions at z = L are:

$$W = 0 \text{ and } \sigma_{rz} = \mu \left[\frac{\partial W}{\partial r} + \frac{\partial U}{\partial z}\right] = 0. \tag{87}$$

These conditions are easily written in finite differences as follows:

$$\text{for } 0 \leq r \leq R + \Delta r; \quad W(r,L) = 0 \tag{88}$$

$$\text{for } 0 \leq r \leq R; \quad U(r,L) = U(r,L-\Delta z). \tag{88}$$

Since the values of U and W for $0 \leq z < L$ and $0 \leq r < R + \Delta r$ are obtained in the same way as before, all the values of U and W are known except $U(R+\Delta r,L)$. This value is easily obtained by using $\sigma_{rr} = 0$ at r = R and z = L. This results in the following difference equation:

$$U(R+\Delta r,L) = \left[1 - \frac{G\Delta r}{R}\right] U(R,L) - \frac{G\Delta r}{\Delta z}\left[W(R,L) - W(R,L-\Delta z)\right]. \tag{89}$$

Summary of Numerical Results

Numerical results are obtained for two different bar lengths. Values for a bar length of two diameters are summarized in Figs. 24, 25, and 28. For a length of one diameter, multiple reflections are observed and these results are summarized in Figs. 26 and 27.

The numerical results are compared with the elementary one-dimensional stress approximation which is indicated by the

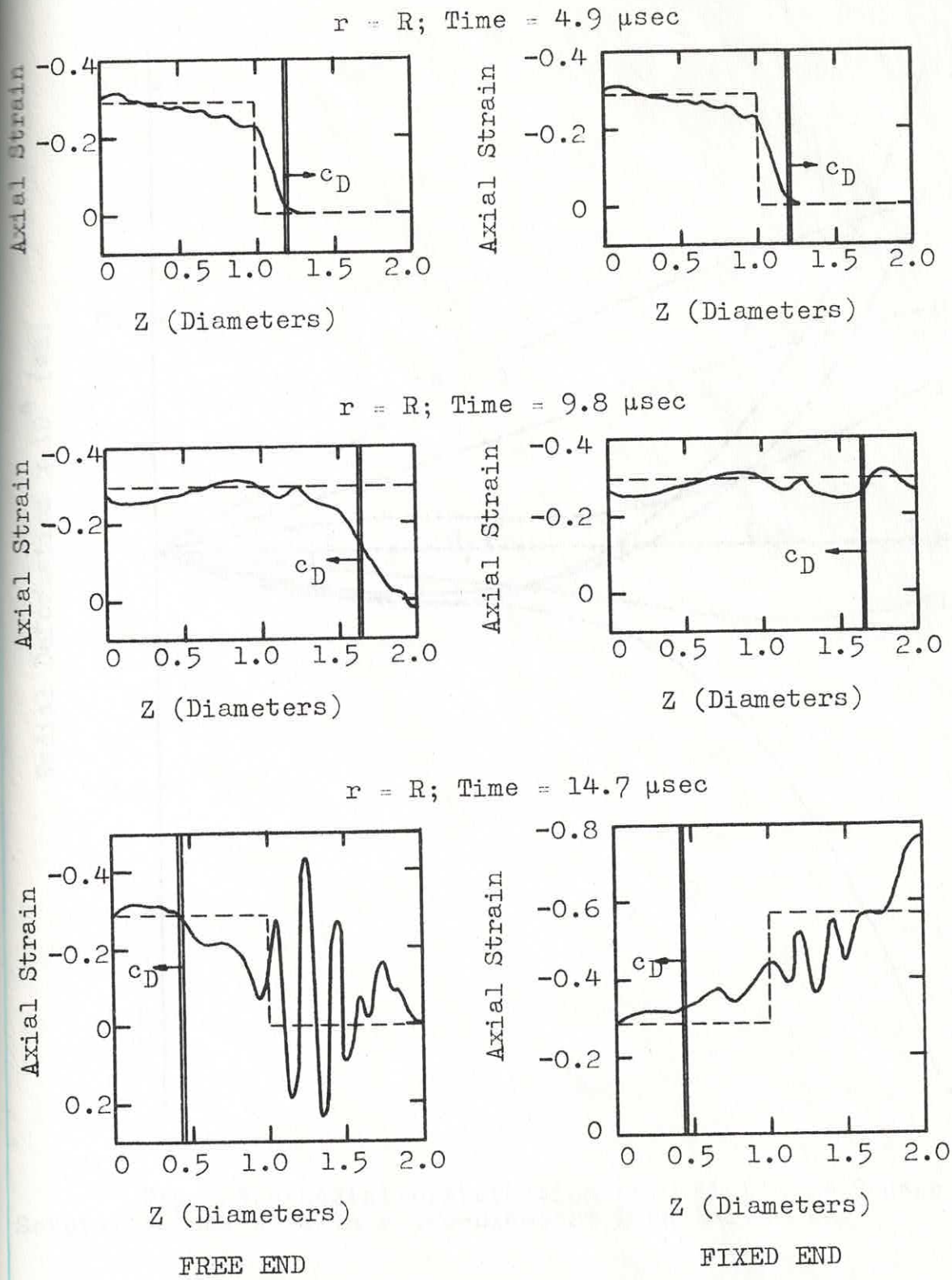


Fig. 24.--Surface Strain in a Two-Diameter Long Cylindrical Bar as a Function of Axial Position at the Indicated Values of Time.

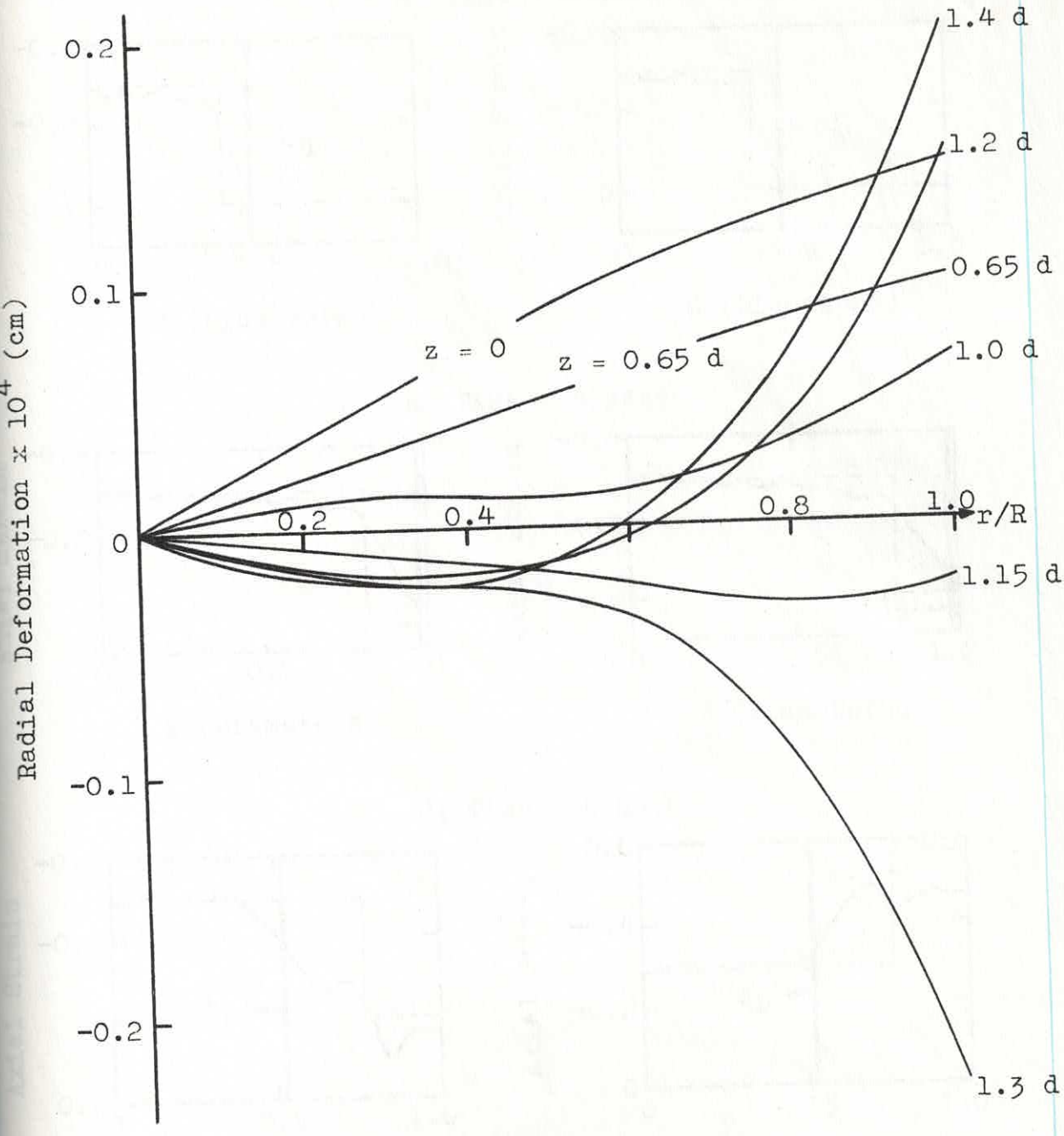


Fig. 25.--Radial Distribution of U at t = 14.7 μsec and Several Values of z in a Two-Diameter Long Bar.

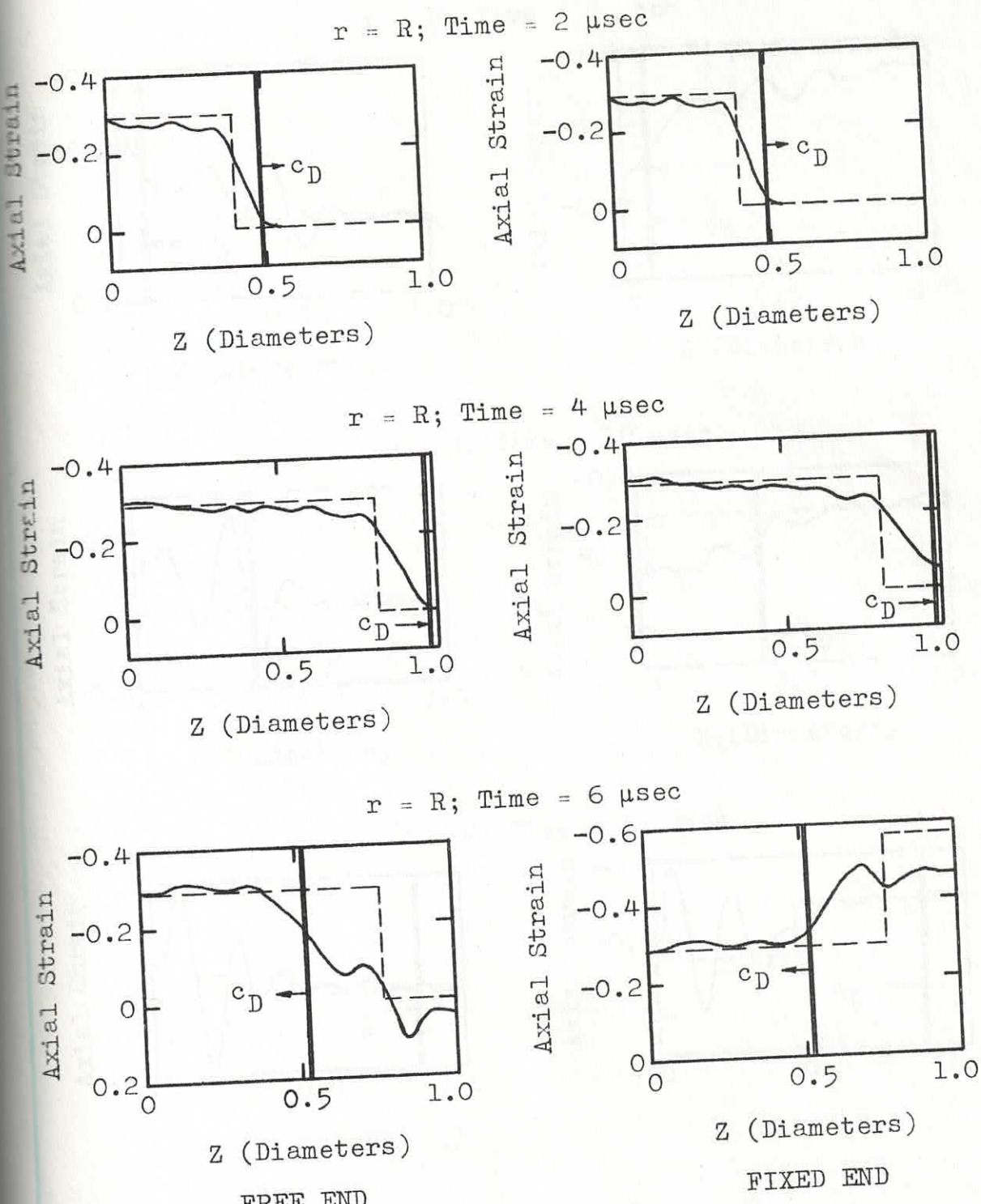


Fig. 26.--Surface Strain in a One-Diameter Long Cylindrical Bar as a Function of Axial Position for Small Values of Time.

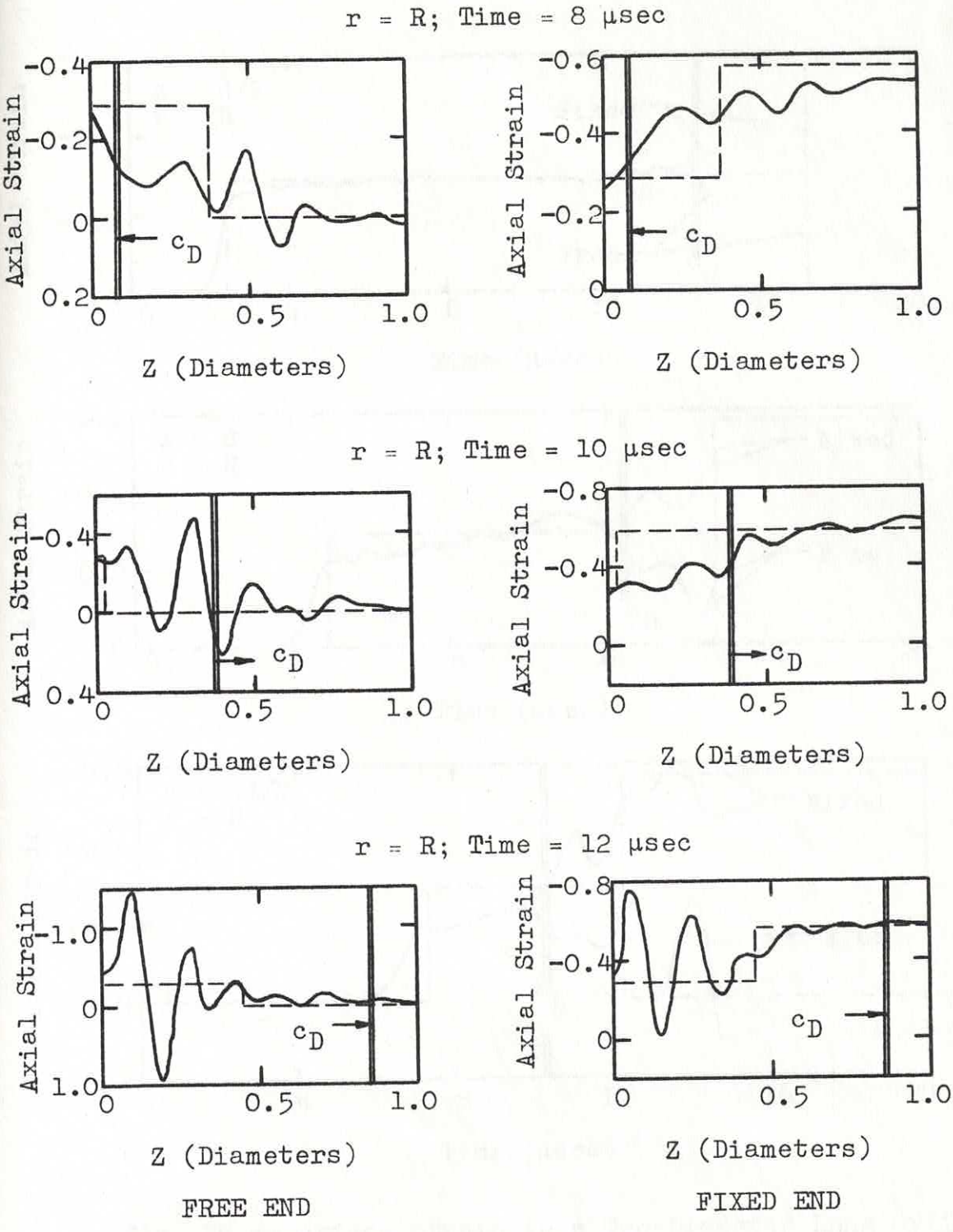


Fig. 27.--Surface Strain in a One-Diameter Long Cylindrical Bar as a Function of Axial Position for Larger Values of Time.

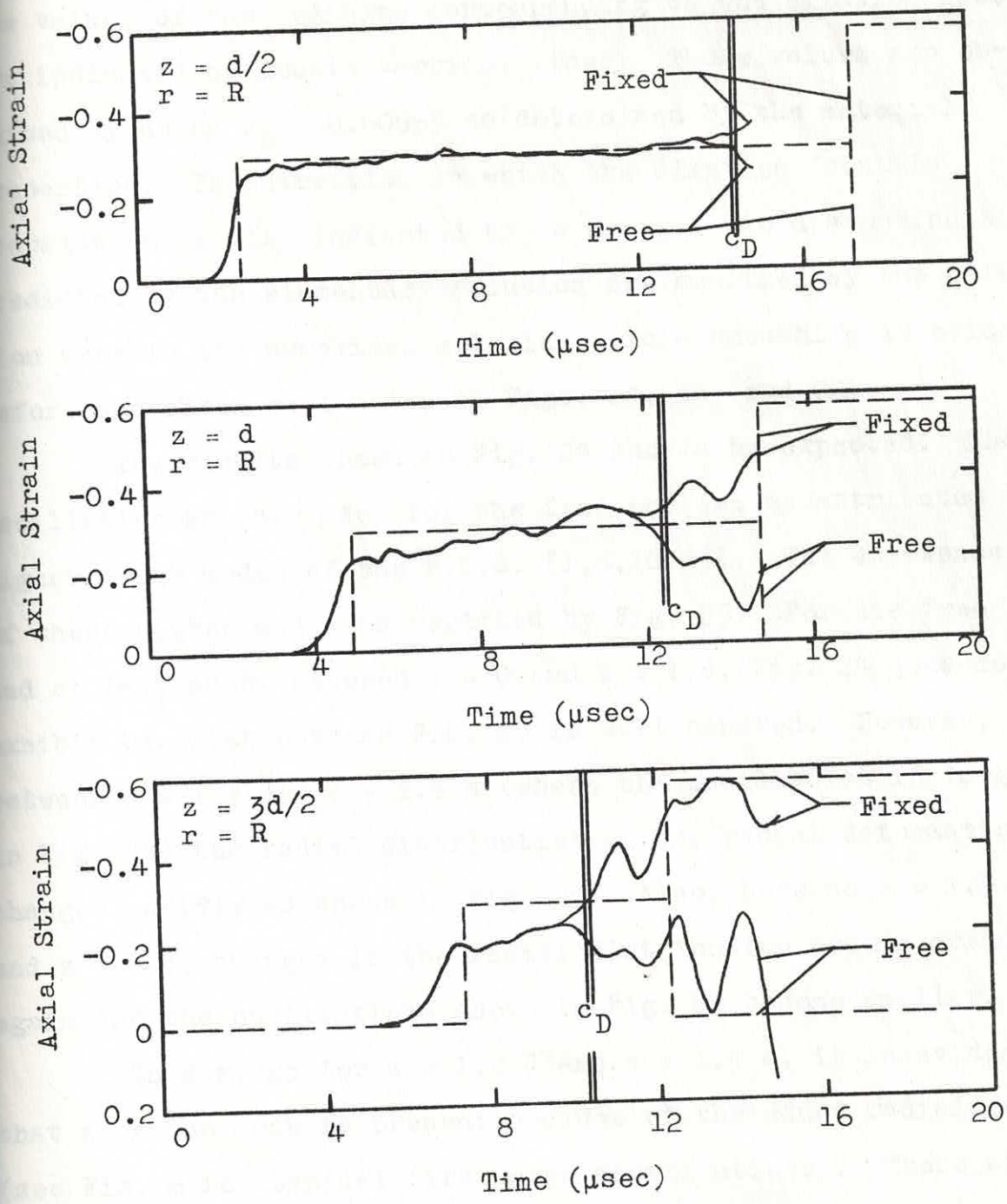


Fig. 28.--Surface Strain in a Two-Diameter Long Cylindrical Bar as a Function of Time at Different Axial Positions.

dashed lines in Figs. 24, 26, 27, and 28. In these figures, the values of the ordinate corresponding to the dilation front are indicated by double vertical lines. These values are obtained by using $c_D = 0.60965$ as determined by the material properties. The direction in which the dilation front is propagating is also indicated by an arrow. The discontinuities predicted by the elementary solution are smoothed by the dilation wave in the numerical solution. This smoothing is evident before and after reflection in Figs. 24, 26, and 28.

The results shown in Fig. 24 should be expected. The oscillation at 14.7 μsec for the free end can be attributed to higher order modes of the P.C.S. [1,8,10,25]. The existence of these higher modes is verified by Fig. 25. For the free end at 14.7 μsec, between z = 0 and z = 1 d, Fig. 24 does not exhibit oscillations and Fig. 25 is well behaved. However, between z = 1 d and z = 1.5 d (where the oscillation is largest in Fig. 24) the radial distribution of the radial deformation changes rapidly as shown in Fig. 25. Also, between z = 1.5 d and z = 2 d, changes in the radial distribution become gradual again and the oscillations shown in Fig. 24 become smaller.

In Fig. 25 for z = 1.2 d and z = 1.4 d, it is evident that a second mode is present because of the added radial node (see Fig. 6 for typical first mode distributions). There are probably higher modes but the second order mode is conspicuous in Fig. 25.

In Figs. 26 and 27, the numerical values for the axial strain at the radial surface are plotted as functions of axial

position for six different values of time. These figures show how multiple reflections affect the numerical solution. The wave front is reflected from the z = L surface (both cases--fixed and free) and then reflected from the z = 0 surface.

In Fig. 28, the numerical values for the surface strain are plotted as functions of time for three axial positions. These results appear reasonable, and if experimental data were available, the numerical results could be easily compared with them.

It should be noted that all of the numerical values presented in this chapter are approximate, and although these results are reasonable, experimental data and more accurate numerical solutions will certainly be welcomed.

CHAPTER VIII

CONCLUSIONS AND RECOMMENDATIONS

Conclusions

Stable and accurate numerical solutions for longitudinal elastic wave propagation have been obtained. By formulating the difference equations in terms of deformations and without using the artificial viscosity approximation [37], solutions have been obtained for continuous and discontinuous loadings at the end of the bar.

For the plane deformation $u_z = \sin \omega t$ at $z = 0$, the numerical solution converges to the Pochhammer-Chree solution for the infinite bar. If ω is chosen so that $d/\lambda' = 0.3$, the convergence is nearly complete at distances of more than 4 diameters from the end of the bar for a time greater than $(z + 6\ d)/c_o$.

With the application of a step change of stress at $z = 0$, the numerical results exhibit a time dependent region that corresponds to the one-dimensional strain solution. For a given value of z, the radius of this region decreases with time. The numerical solution approaches the one-dimensional stress solution for large values of time.

The numerical solution and experimental data near $z = 0$ are in reasonable agreement. The important features of the experimental data are evident in the numerical solution.

The numerical solution for reflections in bars of finite length yields complicated results. The important features of reflection, indicated by the one-dimensional stress solution, are still evident despite these complexities.

Recommendations

Numerous extensions for the study of two-dimensional elastic wave propagation are possible. Many of these can be investigated with the existing program or with minor changes to this program.

With no appreciable changes of the existing program, the following problems can be approached:

1. Study transmission and reflection of waves by using different (partial impedance match) end conditions at $z = L$.

2. Study the effects of different frequencies for the plane harmonic disturbance at $z = 0$ on the region of agreement between the numerical solution and the P.C.S.

3. Study the effects of different radial distributions of axi-symmetric harmonic loadings at $z = 0$ on the region of agreement between the numerical solution and the P.C.S.

4. Study the effects of different radial distributions of axi-symmetric step increases in pressure at $z = 0$. This would result in a study of the Dynamic St. Venant Principle for a two-dimensional bar.

5. Study the validity of existing and new approximate theories.

With minor changes in the existing program the following problems could be studied:

1. Study two-dimensional wave propagation in the following geometries: plates, tubes, cones, and bars with changes in cross-sections such as notches or swells.

2. Study torsional wave propagation in a two-dimensional bar.

In the future (with the advent of larger and faster computing machines) it will be feasible to obtain accurate numerical solutions to the general elastic wave propagation problem. Then, a program can be developed to simultaneously include bending, torsion, and longitudinal waves.

Besides the application of the computer there is an obvious need for experimental data. Very few data are available for the neighborhood of the loaded end of long bars and no data could be found for reflections in very short bars.

LITERATURE CITED

1. Abramson, H., Plass, H., and Ripperger, E. "Stress Wave Propagation in Rods and Beams," Advances in Applied Mechanics, V (1958), 111.

2. Bancroft, D. "The Velocity of Longitudinal Waves in Cylindrical Bars," Phys. Rev., LIX (1941), 588.

3. Band, W. Introduction to Mathematical Physics. p. 70. Princeton, New Jersey: D. Van Nostrand Company, Inc., 1960.

4. Bernoulli, D. "De Vibrationibus et Sono Laminarum Elasticum Commentiationes Physico-Geometricae," Commentarii Academiae Scientiarum Imperialis Petropolitanae, XIII (1751), 105. (See Todhunter, I., and Pearson, K. A History of the Theory of Elasticity and the Strength of Materials, II, part 1, p. 325. Cambridge: Cambridge University Press, 1893.)

5. Bertholf, L. "Use of Elementary Stress Wave Theory for Prediction of Dynamic Strain in Wood," Washington State University Institute of Technology Bulletin 291, 1965.

6. Chree, C. "The Equations of an Isotropic Elastic Solid in Polar and Cylindrical Coordinates, Their Solution and Application," Trans. Camb. Phil. Soc., XIV (1889), 351.

7. Cooper, J. L. B. "The Propagation of Elastic Waves in a Rod," Phil. Mag., XXXVIII, Ser. 7 (1947), 1-22.

8. Curtis, C. W. "Propagation of an Elastic Strain Pulse in a Semi-Infinite Bar," International Symposium on Stress Wave Propagation in Materials. p. 10. Edited by Norman Davids. New York: Interscience Publishers, Inc., 1960.

9. Davids, N., and Mehta, P. "Computer Analysis Methods in Dynamics," Penn. State Univ. Engr. Res. Bulletin B-92, May 1965.

10. Davies, R. M. "A Critical Study of the Hopkinson Pressure Bar," Trans. Roy. Phil. Soc. London, Ser. A, CCXL (1948), 375.

11. Davies, R. M. "Stress Waves in Solids," Surveys in Mechanics. p. 64. Edited by Batchelor, G. K., and Davies, R. M. Cambridge: Cambridge University Press, 1956.

12. DeForest, A. V. "The Measurement of Impact Strains," Fifth Int. Cong. Appl. Mech. p. 673. New York: John Wiley and Sons, Inc., 1938.

13. Donnell, L. "Longitudinal Wave Transmission and Impact," Trans. ASME, LII (1930), 153.

14. Fischer, H. C. "Stress Pulse in a Bar with Neck or Swell," Appl. Sci. Res., Ser. A, IV (1954), 317-328.

15. Folk, R., Fox, G., Shook, C., and Curtis, C. "Elastic Strain Produced by Sudden Application of Pressure to One End of a Cylindrical Bar," J. Acous. Soc. Am., XXX (1958), 552.

16. Fox, L. Numerical Solution of Ordinary and Partial Differential Equations. p. 218. Oxford: Pergamon Press, 1962.

17. Giebe, E. von, and Blechschmidt, E. "Experimentelle und Theoretische Untersuchungen über Dehnungseigenschwingungen von Stäben und Rohren," Ann d. Physik, XVIII (1933), 417.

18. Godunov, S. K., and Ryabenki, V. S. Theory of Difference Schemes. p. 21 and 26. New York: John Wiley and Sons, 1964.

19. Goldsmith, W. Impact. London: Edward Arnold, Ltd., 1960.

20. Heimann, J. H., and Kolsky, H. "The Propagation of Elastic Waves in Thin Cylindrical Shells," Div. Appl. Math. Brown Univ. Tech. Rep. No. AM-20, Dec. 1965.

21. Herrmann, G. "Forced Motions of Elastic Rods," J. Appl. Mech., XXI (1954), 221-224.

22. Hudson, G. E. "Dispersion of Elastic Waves in Solid Circular Cylinders," Phys. Rev., LXIII (1943), 46-51.

23. Hueter, T. F. "Ultrasonic Velocity Dispersion in Solid Rods," J. Acoust. Soc. Am., XXII (1950), 514.

24. Hughes, D. S., Pondrom, W. L., and Mims, R. L. "Propagation of Elastic Pulses in Metal Rods," Phys. Rev., LXXV (1949), 1552.

25. Kolsky, H. "The Propagation of Longitudinal Elastic Waves along a Cylindrical Bar," Phil. Mag., Ser. 7, XLV (1954), 712.

26. Kolsky, H. Stress Waves in Solids. p. 56. New York: Dover Publications, Inc., 1963.

27. Lloyd, J., and Miklowitz, J. "On the Use of Double Integral Transforms in the Study of Dispersive Elastic Wave Propagation," Proceedings of the Fourth U.S. National Congress of Applied Mechanics. p. 255. New York: ASME, 1960.

28. Love, A. E. H. Mathematical Theory of Elasticity, p. 428. New York: Dover Publications, 1944.

29. McSkimin, H. J. "Propagation of Longitudinal Waves in Cylindrical Rods at High Frequencies," J. Acous. Soc. Am., XXVIII (1956), 484.

30. Miklowitz, J. "Recent Developments in Elastic Wave Propagation," Appl. Mech. Rev., XIII (1960), 865.

31. Miklowitz, J. "Traveling Compressional Waves in an Elastic Rod according to the More Exact One-Dimensional Theory," Proceedings of the Second U.S. National Congress of Applied Mechanics. p. 179. 1954.

32. Miklowitz, J., and Nisewanger, C. R. "The Propagation of Compressional Waves in a Dispersive Elastic Rod," J. Appl. Mech., XXIV (1957), 237.

33. Mindlin, R. "Waves and Vibrations in Isotropic, Elastic Plates," Proceedings of the First Symposium on Naval Structural Mechanics. p. 199. 1960.

34. Mindlin, R., and Herrmann, G. "A One-Dimensional Theory of Compressional Waves in an Elastic Rod," Proceedings of the First U.S. National Congress of Applied Mechanics. p. 187. 1952.

35. Mindlin, R., and McNiven, H. "Axially Symmetric Waves in Elastic Rods," J. Appl. Mech., XXVII (1960), 145.

36. Mirsky, I. "Wave Propagation in Transversely Isotropic Circular Cylinders," J. Acous. Soc. Am., XXXVII (1965), 1016.

37. Neumann, J. von, and Richtmyer, R. "A Method for the Numerical Calculation of Hydrodynamic Shocks," J. Appl. Phys., XXI (1950), 232.

38. Onoe, M., McNiven, H., and Mindlin, R. "Dispersion of Axially Symmetric Waves in Elastic Rods," J. Appl. Mech., XXIX (1962), 729.

39. Organick, Elliot I. A Fortran Primer. p. 169. Reading, Mass.: Addison-Wesley Publishing Company, Inc., 1963.

40. Petersson, S. "Investigation of Stress Waves in Cylindrical Steel Bars by Means of Wire Strain Gages," Trans. Roy. Inst. Tech. (Stockholm) LXII (1952), 21.

41. Pochhammer, L. J. f. Math. (Creele), Bd. 81 (1876), 324. (See Love, The Mathematical Theory of Elasticity. p. 289. New York: Dover Publications, 1944.)

42. Prescott, J. "Elastic Waves and Vibrations of Thin Rods," Phil. Mag., XXXIII, Ser. 7 (1942), 703.

43. Rayleigh, J. W. S. The Theory of Sound. I, Chap. 4. New York: Dover Publications, 1945.

44. Richtmyer, R. Differences Methods for Initial-Value Problems. New York: Interscience Publishers, Inc., 1957.

45. Ripperger, E. A. "The Propagation of Pulses in Cylindrical Bars--An Experimental Study," Proceedings of the First Midwestern Conference on Solid Mechanics. p. 29. Urbana, Illinois: 1953. Also, "The Propagation of Pulses in Cylindrical Bars; An Experimental Study," Stanford Univ. Div. of Engr. Mech. Tech. Rept. No. 13, 1953.

46. Ripperger, E. A., and Abramson, H. N. "Reflection and Transmission of Elastic Pulses in a Bar at a Discontinuity in Cross Section," Proceedings of the Third Midwestern Conference on Solid Mechanics. University of Michigan. 1957.

47. Rohrich, K. "Ausbreitungsgeschwindigkeit Ultraakustischer Schwingungen in Zylindrischen Stäben," Z. f. Physik, LXXIII (1932), 813.

48. Rosenfeld, R., and Miklowitz, J. "Wave Fronts in Elastic Rods and Plates," Proceedings of the Fourth U.S. National Congress of Applied Mechanics. p. 293. 1960.

49. Schoeneck, H. "Experimentelle Untersuchungen der Schwingungen Zylindrischer Einselkristalle bei Hohen Elastischen Frequezen," Z. f. Physik, XCII (1934), 390.

50. Shear, S. K., and Foche, A. F. "The Dispersion of Supersonic Waves in Cylindrical Rods of Polycrystalline Silver, Nickel and Magnesium," Phys. Rev., LVIII (1940), 532.

51. Skalak, R. "Longitudinal Impact of a Semi-Infinite Circular Elastic Bar," J. Appl. Mech., XXIV (1957), 59.

52. Timoshenko, S., and Goodier, J. N. Theory of Elasticity. p. 10. New York: McGraw-Hill Book Company, Inc., 1951.

53. Tu, L., Brennan, J., and Sauer, J. "Dispersion of Ultrasonic Pulse Velocity in Cylindrical Rods," J. Acoust. Soc. Am., XXVII (1955), 550.

54. Wilkins, M. "Calculations of Elastic-Plastic Flow," Univ. of California, LRL, Contract No. W-7405-eng-48, 1963.

APPENDIX A

NOMENCLATURE

NOMENCLATURE

A	constant in P.C.S.
A	surface area
C	constant in P.C.S.
c	phase velocity
c_D	phase velocity of a dilation wave
$c_o = \sqrt{E/\rho}$	phase velocity for the elementary bar
c_S	phase velocity of a shear wave
d	outside bar diameter
E	Youngs modulus
$\bar{\bar{E}}$	strain tensor
$G = \lambda/(\lambda + 2\mu)$	
h	constant in P.C.S.
h'	constant in P.C.S.
$\bar{\bar{I}}$	unit or identity matrix
$i = \sqrt{-1}$	
k	constant in P.C.S.
k'	constant in P.C.S.
L	finite bar length
P	pressure applied at $z = 0$
p	frequency of a harmonic wave in P.C.S.
R	outside radius of cylindrical bar
r	radial cylindrical polar coordinate
$\bar{\bar{S}}$	stress tensor

t	time
U	finite difference notation for u_r
$\widetilde{U}(r)$	radial distribution of u_r in P.C.S.
$\vec{u}$	deformation vector
$\vec{V}$	velocity vector
W	finite difference notation for u_z
$\widetilde{W}(r)$	radial distribution of u_z in P.C.S.
z	axial cylindrical polar coordinate
$\alpha = \Delta z/\Delta r$	
γ	wave number of the harmonic wave used in P.C.S.
δ_{ij}	Kronecker delta
ε_{ij}	component of strain
ζ	function used in the stability discussion
η	function used in the stability discussion
θ	dilation
k	wave number
λ	Lamés constant
λ'	wave length of a harmonic wave
μ	Lamés constant
ν	Poisson ratio
ρ	mass density
σ_{ij}	component of stress
τ	volume
φ	angular cylindrical polar coordinate
ψ	function used in stability discussion
ω	angular velocity
$\vec{\omega}$	rotation vector

Δr	radial increment
Δt	time increment
Δz	axial increment

APPENDIX B

JUSTIFICATION OF THE ACCELERATION APPROXIMATION

JUSTIFICATION OF THE ACCELERATION APPROXIMATION

The acceleration approximation ($D\vec{V}/Dt = \partial^2\vec{u}/\partial t^2$) must be justified for both the harmonic and step inputs at $z = 0$. For the harmonic end condition, the numerical solution is tested to determine if it converges to the P.C.S. Since the above linearization is used for the P.C.S., the approximation is justified for the numerical procedure. Besides, the deformations can be made as small as desired and the second order terms can certainly be neglected.

However, for the step end condition, the numerical solution is tested to determine if it agrees with experimental data. Thus, this approximation must be more carefully justified for the step change in stress at $z = 0$.

For the conditions of the experiment for a step input of pressure the reader is referred to Chapter VI. The pressure is described as "approximately 300 psi" or 2.065×10^{-5} Mbar, also $E = 0.72395$ Mbar, therefore, $\varepsilon_{zz} \approx 3 \times 10^{-5}$ cm/cm and since $\varepsilon_{rr} \approx -\nu\varepsilon_{zz}$, $\varepsilon_{rr} \approx -1 \times 10^{-5}$.

For the axi-symmetric case without torsion, the components of velocity are obtained as follows:

$$\vec{V} = \frac{D\vec{u}}{Dt} = \frac{\partial\vec{u}}{\partial t} + (\vec{V}\cdot\nabla)\,\vec{u}$$

thus,

$$V_r = \frac{\partial u_r}{\partial t} + V_r \frac{\partial u_r}{\partial r} + V_z \frac{\partial u_r}{\partial z}$$

$$V_z = \frac{\partial u_z}{\partial t} + V_r \frac{\partial u_z}{\partial r} + V_z \frac{\partial u_z}{\partial z}$$

and,

$$\frac{\partial u_r}{\partial t} = V_r(1 - \frac{\partial u_r}{\partial r}) - V_z \frac{\partial u_r}{\partial z}$$

$$\frac{\partial u_z}{\partial t} = V_z(1 - \frac{\partial u_z}{\partial z}) - V_r \frac{\partial u_z}{\partial r}$$

where the spatial derivatives have the following orders of magnitude:

$$\frac{\partial u_z}{\partial z} = \varepsilon_{zz} = \mathcal{O}(10^{-5})$$

$$\frac{\partial u_r}{\partial r} = \varepsilon_{rr} \approx - \nu\varepsilon_{zz} = \mathcal{O}(10^{-5})$$

$$\frac{\partial u_r}{\partial z} = 2\varepsilon_{rz} - \frac{\partial u_z}{\partial r} = \mathcal{O}(10^{-5})$$

$$\frac{\partial u_z}{\partial r} = 2\varepsilon_{rz} - \frac{\partial u_r}{\partial z} = \mathcal{O}(10^{-5}).$$

Employing these orders of magnitude:

$$\frac{\partial u_r}{\partial t} \approx V_r(1 - 10^{-5}) - V_z \times 10^{-5}$$

$$\frac{\partial u_z}{\partial t} \approx V_z(1 - 10^{-5}) - V_r \times 10^{-5}.$$

Since the components of velocity are the same order of magnitude, the following can be written with reasonable accuracy:

$$\frac{\partial u_r}{\partial t} = V_r$$

$$\frac{\partial u_z}{\partial t} = V_z.$$

Similarly, the components of acceleration are obtained:

$$\vec{a} = \frac{D\vec{V}}{Dt} = \frac{\partial \vec{V}}{\partial t} + (\vec{V}\cdot\nabla)\,\vec{V}$$

$$a_r = \frac{\partial V_r}{\partial t} + V_r \frac{\partial V_r}{\partial r} + V_z \frac{\partial V_r}{\partial z}$$

$$a_z = \frac{\partial V_z}{\partial t} + V_r \frac{\partial V_z}{\partial r} + V_z \frac{\partial V_z}{\partial z}$$

$$\frac{a_r}{c} = \frac{1}{c}\frac{\partial V_r}{\partial t} + \frac{V_r}{c}\frac{\partial}{\partial t}\left(\frac{\partial u_r}{\partial r}\right) + \frac{V_z}{c}\frac{\partial}{\partial t}\left(\frac{\partial u_r}{\partial z}\right)$$

$$\frac{a_z}{c} = \frac{1}{c}\frac{\partial V_z}{\partial t} + \frac{V_r}{c}\frac{\partial}{\partial t}\left(\frac{\partial u_z}{\partial r}\right) + \frac{V_z}{c}\frac{\partial}{\partial t}\left(\frac{\partial u_z}{\partial z}\right).$$

But, from the elementary bar solution, $V_z = \sigma c/E$ or $V_z = \varepsilon_{zz} c$. Therefore:

$$\frac{V_z}{c} \approx \varepsilon_{zz} = \mathcal{O}(10^{-5}) \text{ and } \frac{V_r}{c} = \mathcal{O}(10^{-5}).$$

Substituting the magnitude orders:

$$\frac{a_r}{c} \approx \frac{\partial}{\partial t}\left[10^{-5}\frac{\partial u_r}{\partial r} + 10^{-5}\frac{\partial u_r}{\partial z} + \frac{V_r}{c}\right]$$

$$\frac{a_z}{c} \approx \frac{\partial}{\partial t}\left[10^{-5}\frac{\partial u_z}{\partial r} + 10^{-5}\frac{\partial u_z}{\partial z} + \frac{V_z}{c}\right].$$

But,

$$\mathcal{O}\left(\frac{\partial u_r}{\partial r}\right) = \mathcal{O}\left(\frac{\partial u_r}{\partial z}\right) = \mathcal{O}\left(\frac{V_r}{c}\right) = \mathcal{O}(\varepsilon_{zz})$$

and,

$$\mathcal{O}\left(\frac{\partial u_z}{\partial r}\right) = \mathcal{O}\left(\frac{V_z}{c}\right) = \mathcal{O}\left(\frac{\partial u_z}{\partial z}\right) = \mathcal{O}(\varepsilon_{zz}).$$

So, the following can be written and the acceleration approximation is justified for an accuracy of about five significant figures:

$$a_z = \frac{\partial V_z}{\partial t} = \frac{\partial^2 u_z}{\partial t^2}$$

$$a_r = \frac{\partial V_r}{\partial t} = \frac{\partial^2 u_r}{\partial t^2}$$

and

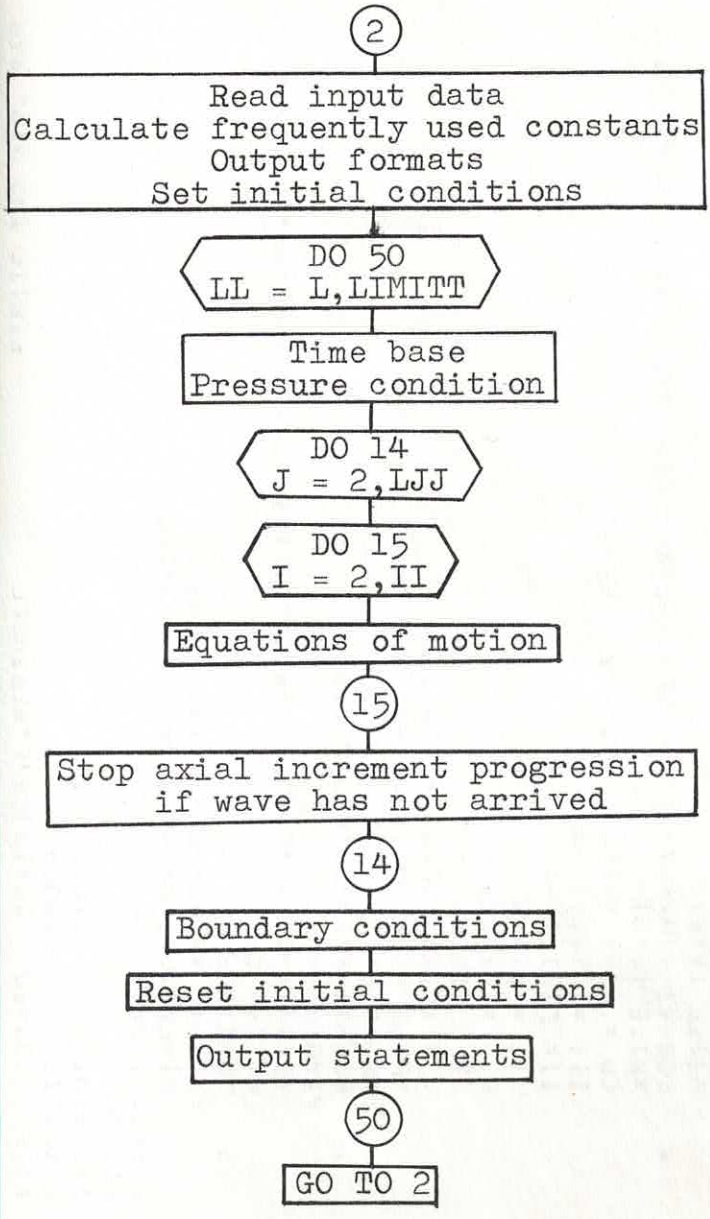
$$\vec{a} = \frac{D\vec{V}}{Dt} = \frac{\partial^2 \vec{u}}{\partial t^2}.$$

APPENDIX C

COMPUTER PROGRAM

COMPUTER PROGRAM

Block Diagram



Card Numbers	
2DBAR003	
2DBAR004	2DBAR036
2DBAR037	
2DBAR038	2DBAR040
2DBAR041	
2DBAR042	
2DBAR043	2DBAR066
2DBAR067	
2DBAR068	2DBAR071
2DBAR072	
2DBAR074	2DBAR177
2DBAR178	2DBAR184
2DBAR185	2DBAR198
2DBAR199	
2DBAR201	

```
$JOB   S0745D   20,IBJOB,L.BERTHOLF                FINITE TWO DIM. BAR
$EXECUTE        IBJOB
$*OUTPUT        PAGES   100
$IBJOR
$IBFTC TODBAR                                                                2DBAR000
      DIMENSION  U(12,200,3) , W(12,200,3) ,          A(30,30), B(30),2DBAR001
     6X(30), AA(30,30), BB(30) , XX(30)                                      2DBAR002
   2  CONTINUE                                                              2DBAR003
      KKKKK= 0                                                              2DBAR004
      READ (5,1) MM,LIMITI,LIMITT,LIMITZ,JZCAL,JZWRT,P0,IBCD,DT,DR,DZ,     2DBAR005
     6XNU,E,RHO                                                             2DBAR006
   1  FORMAT (6I3,F9.4,I1, 6F7.6)                                           2DBAR007
      XMU = E/(2. *(1. + XNU))                                              2DBAR008
      XLAMB = E*XNU/(( 1. -2. *XNU)*(1. + XNU))                             2DBAR009
      G = XLAMB/(XLAMB + 2.* XMU)                                           2DBAR010
      LJ = LIMITZ                                                           2DBAR011
      LJJ = LIMITZ -1                                                       2DBAR012
      DTT = DT**2                                                           2DBAR013
      II= LIMITI -1                                                         2DBAR014
      III = LIMITI -2                                                       2DBAR015
      CD = SQRT ((XLAMB + 2.* XMU)/RHO)                                     2DBAR016
      WRITE (6,3)                                                           2DBAR017
   3  FORMAT (1H1,2X, 44HDISPLACEMENTS, U(R) AND U(Z) IN CENTIMETERS.)      2DBAR018
      WRITE (6,5)                                                           2DBAR019
   5  FORMAT (/3X,21HTIME IN MICROSECONDS.  )                               2DBAR020
      WRITE (6,6)                                                           2DBAR021
   6  FORMAT(/3X,23HR AND Z IN CENTIMETERS.  )                              2DBAR022
      WRITE (6,7)  XNU                                                      2DBAR023
   7  FORMAT(/3X,18HPOISSON-S RATIO IS,F6.3,1H. )                           2DBAR024
      WRITE (6,9)  E                                                        2DBAR025
   9  FORMAT(/3X,17HYOUNGS MODULUS IS,F6.3,8H(MBARS).)                      2DBAR026
      WRITE (6,11)  RHO                                                     2DBAR027
  11  FORMAT(/3X,10HDENSITY IS, F6.3, 8H(GM/CC).  )                         2DBAR028
      WRITE (6,12)                                                          2DBAR029
  12  FORMAT(//////// ,3X,4HTIME,5X,1HR,6X,1HZ,12X,4HU(R), 16X,            2DBAR030
     64HU(Z), 15X, 6HSTRAIN,//,)                                            2DBAR031
      DO 4 I= 1,LIMITI                                                      2DBAR032
      DO 4 J= 1,LIMITZ                                                      2DBAR033
      DO 4 K= 1,3                                                           2DBAR034
      W(I,J,K) = 0.                                                         2DBAR035
   4  U(I,J,K) = 0.                                                         2DBAR036
      DO 50 LL= 1,LIMITT                                                    2DBAR037
```

```
      N=LL-1                                                                2DBAR038
      FM= N                                                                 2DBAR039
      P = P0                                                                2DBAR040
      DO 14 J= 2,LJJ                                                        2DBAR041
      DO 15 I= 2,II                                                         2DBAR042
      R= DR*FLOAT(I-1)                                                      2DBAR043
      UU222 = U(I,J,2)                                                      2DBAR044
      WW222 = W(I,J,2)                                                      2DBAR045
C     THIS IS THE BEGINNING OF THE DIFFERENTIAL EQUATIONS                   2DBAR046
C     THIS IS THE BEGINNING OF THE DIFFERENTIAL EQUATIONS                   2DBAR047
      U(I,J,3) = 2.* UU222     - U(I,J,1) + DTT*(                           2DBAR048
     6 (1.    /(4.* DZ*DR ))*((XLAMB + XMU)/RHO) *                          2DBAR049
     6 (W(I+1, J+1,2) - W(I-1, J+1,2) -W(I+1, J-1, 2) + W(I-1,J-1,2))      2DBAR050
     6  +(XMU/RHO)*(1.    /DZ**2)*(U(I,J+1 ,2) + U(I,J-1,2) - 2.*UU222      2DBAR051
     6  ) - ((XLAMB+2.*XMU)/RHO)* (1.    /R**2)*UU222                       2DBAR052
     6  +((XLAMB+ 2.*XMU)/RHO)*(1.    /DR**2)*                             2DBAR053
     6 ( U(I+1, J,2) + U(I-1, J,2) -2.* UU222 )                            2DBAR054
     6 +((XLAMB+ 2.*XMU)/RHO)*(1.    /(2.*R*DR))*                          2DBAR055
     6 ( U(I+1,J,2) - U(I-1,J,2)))                                         2DBAR056
      W(I,J,3) = 2.* WW222     - W(I,J,1) + DTT*(                           2DBAR057
     6 (1.    /(4.* DZ*DR ))*((XLAMB + XMU)/RHO) *                          2DBAR058
     6 (U(I+1, J+1,2) - U(I-1, J+1,2) -U(I+1, J-1, 2) + U(I-1,J-1,2))      2DBAR059
     6 +((XLAMB+ XMU)/RHO)*(1.    /(2.*R*DZ))*                             2DBAR060
     6  (U(I,J+1,2) -U(I,J-1,2))          +                               2DBAR061
     6 (XMU/RHO)*(1.    /DR**2)*                                           2DBAR062
     6 (W(I+1, J, 2) + W( I-1, J, 2) - 2.* WW222    )                      2DBAR063
     6 +(XMU/RHO)*(1.    /(2.*R*DR ))* (W(I+1,J,2) - W(I-1,J,2))           2DBAR064
     6 +((XLAMB +2.*XMU)/RHO) *(1.    /DZ**2)*                             2DBAR065
     6  ( W(I,J+1,2)  +W(I,J-1,2) -2.*WW222    ))                         2DBAR066
  15  CONTINUE                                                              2DBAR067
C     THIS IS THE     END   OF THE DIFFERENTIAL EQUATIONS                   2DBAR068
C     THIS IS THE     END   OF THE DIFFERENTIAL EQUATIONS                   2DBAR069
      JJJ =1.25* CD*EM*DT/DZ                                                2DBAR070
      IF ( J .GT. JJJ + J7CAL) GO TO 18                                     2DBAR071
  14  CONTINUE                                                              2DBAR072
  18  CONTINUE                                                              2DBAR073
      JJ=J +1                                                               2DBAR074
      INC = 11                                                              2DBAR075
C     THIS IS THE BEGINNING OF THE BOUNDARY CONDITIONS                      2DBAR076
C     THIS IS THE BEGINNING OF THE BOUNDARY CONDITIONS                      2DBAR077
C     BOUNDARY CONDITIONS FOR R=0                                           2DBAR078
```

```
      DO 89 J= 1,LIMITZ                                                 2DBAR079
      W(1,J,3) = W(2,J,3)                                               2DBAR080
   89 U(1,J,3) = 0.                                                     2DBAR081
C     BOUNDARY CONDITIONS FOR R=0                                       2DBAR082
      IF(IBCD .EQ. 1) GO TO 799                                         2DBAR083
C     BOUNDARY CONDITIONS FOR FIXED END AT Z = L                        2DBAR084
      DO 35 I= 1,LIMITI                                                 2DBAR085
      W(I,LIMITZ, 3) = 0.                                               2DBAR086
   35 U(I,LIMITZ,3) = U(I,LJJ,3)                                        2DBAR087
C     BOUNDARY CONDITIONS FOR FIXED END AT Z = L                        2DBAR088
  799 CONTINUE                                                          2DBAR089
      IF (IBCD .NE. 1) GO TO 789                                        2DBAR090
C     BOUNDARY CONDITIONS FOR  FREE END AT Z = L                        2DBAR091
      LLL = LL +1                                                       2DBAR092
      IF (LLL .LT. LIMITZ) GO TO 3000                                   2DBAR093
      KKKKK = KKKKK + 1                                                 2DBAR094
      BB(1) = W(1,LJJ,3)                                                2DBAR095
      BB(22) = DR/DZ*G*W(11,LJJ,3)                                      2DBAR096
      DO 3333 I= 2,11                                                   2DBAR097
      BB(I) = W(I,LJJ,3)                                                2DBAR098
      BB(I+10) = U(I,LJJ,3)                                             2DBAR099
 3333 CONTINUE                                                          2DBAR100
      INN = 2                                                           2DBAR101
      IF (KKKKK . GT. 2) GO TO 4032                                     2DBAR102
      INN = 1                                                           2DBAR103
      DO 8888 I= 1,30                                                   2DBAR104
      DO 8888 J= 1,30                                                   2DBAR105
 8888 AA(I,J) = 0.                                                      2DBAR106
      AA(1,1) = 1.                                                      2DBAR107
      AA(1,12) = 2.*G*DZ/DR                                             2DBAR108
      AA(22,22) = 1.                                                    2DBAR109
      AA(22,21) = G/10. -1.                                             2DBAR110
      AA(22,10) = G*DR/DZ                                               2DBAR111
      DO 6655 I= 2,11                                                   2DBAR112
      AA(I,I-1) = 1.                                                    2DBAR113
      AA(I,I+11) = G*DZ/DR                                              2DBAR114
      AA(I,I+10) = G*DZ/DR*(1./FLOAT(I-1) -1.)                          2DBAR115
      AA(I+10,I+10) = 1.                                                2DBAR116
      AA(I+10,1) = DZ/DR                                                2DBAR117
      AA(I+10,I-1) =-DZ/DR                                              2DBAR118
 6655 CONTINUE                                                          2DBAR119
 4032 CONTINUE                                                          2DBAR120
```

```
      CALL SSOLVE (22, AA, BB, INN, 1.E-08, 10, XX, ITT)                2DBAR121
      DO 3005 I= 1,11                                                   2DBAR122
      W(I+1, LJ, 3) = XX(I)                                             2DBAR123
      U(I+1,LJ, 3) =XX(I+11)                                            2DBAR124
 3005 CONTINUE                                                          2DBAR125
      U(1, LJ, 3) = 0.                                                  2DBAR126
      W(1,LJ,3) =  W(2,LJ,3)                                            2DBAR127
 3000 CONTINUE                                                          2DBAR128
C     BOUNDARY CONDITIONS FOR  FREE END AT Z = L                        2DBAR129
  789 CONTINUE                                                          2DBAR130
C     BOUNDARY CONDITIONS FOR A PRESSURE APPLIED AT Z=0                 2DBAR131
      B(1) = -P*G*DZ/XLAMB - W(1,2,3)                                   2DBAR132
      B(22) = -G*DR/DZ*W(11,2,3)                                        2DBAR133
      DO 2000 I= 2,11                                                   2DBAR134
      B(I) = -P*G*DZ/XLAMB - W(I,2,3)                                   2DBAR135
      B(I+10) = - U(I,2,3)                                              2DBAR136
 2000 CONTINUE                                                          2DBAR137
      IN = 2                                                            2DBAR138
      IF ( N.GT. 2 ) GO TO 2003                                         2DBAR139
      IN = 1                                                            2DBAR140
      DO 654 I= 1,30                                                    2DBAR141
      DO 654 J= 1,30                                                    2DBAR142
  654 A(I,J) = 0.0                                                      2DBAR143
      A(1,1) = -1.                                                      2DBAR144
      A(1,12) = G*2.*DZ/DR                                              2DBAR145
      A(22,22) = 1.                                                     2DBAR146
      A(22,21) = -1. + G/10.                                            2DBAR147
      A(22,10) = - G*DR/DZ                                              2DBAR148
      DO 6555 I=2,11                                                    2DBAR149
      A(I, I-1) = -1.                                                   2DBAR150
      A(I,I+11) = G*DZ/DR                                               2DBAR151
      A(I,I+10) = G*DZ/DR*(1./FLOAT (I-1)  - 1.)                        2DBAR152
      A(I+10, I) = DZ/DR                                                2DBAR153
      A(I+10, I-1) = - DZ/DR                                            2DBAR154
      A(I+10,I+10) = -1.                                                2DBAR155
 6555 CONTINUE                                                          2DBAR156
 2003 CONTINUE                                                          2DBAR157
      CALL SOLVE (22, A, B, IN, 1.E-08, 10,X,IT)                        2DBAR158
      DO 2005 I= 1,11                                                   2DBAR159
      W(I+1,1,3) = X(I)                                                 2DBAR160
      U(I+1,1,3) = X(I+11)                                              2DBAR161
```

```
 2005 CONTINUE                                                          2DBAR162
      U(1,1,3) = 0.                                                     2DBAR163
      W(1,1,3) = W(2,1,3)                                               2DBAR164
C     BOUNDARY CONDITIONS FOR A PRESSURE APPLIED AT Z=0                 2DBAR165
C     BOUNDARY CONDITIONS FOR RADIAL SURFACE                            2DBAR166
      DO 78 J= 2,JJ                                                     2DBAR167
      IF (J .EQ. LIMITZ) GO TO 567                                      2DBAR168
      U(LIMITI,J,3) = U(II ,J,3)-    G*U(II,J,3)/FLOAT(III)             2DBAR169
     6-   G*(DR/DZ)*(W(II,J+1,3) -W(II,J,3))                           2DBAR170
   78 W(LIMITI,J,3) = W(II ,J,3) -    DR/DZ*(U(II,J+1,3) -U(II,J,3))    2DBAR171
  567 CONTINUE                                                          2DBAR172
C     BOUNDARY CONDITIONS FOR RADIAL SURFACE                            2DBAR173
      IF (IBCD .NE. 1)  U(LIMITI,LJ,3) = U(II , LJ,3) - G   *U(II,LJ,3) 2DBAR174
     6/FLOAT(III) -   G*DR/DZ*(W(II,LJ,3) -W(II,LJJ,3))                 2DBAR175
C     THIS IS THE    END    OF THE BOUNDARY CONDITIONS                  2DBAR176
C     THIS IS THE    END    OF THE BOUNDARY CONDITIONS                  2DBAR177
      DO 30 I= 1,LIMITI                                                 2DBAR178
      DO 30 K= 1,JJ                                                     2DBAR179
      U(I,K,1) = U(I,K,2)                                               2DBAR180
      W(I,K,1) = W(I,K,2)                                               2DBAR181
      U(I,K,2) = U(I,K,3)                                               2DBAR182
   31 W(I,K,2) = W(I,K,3)                                               2DBAR183
   30 CONTINUE                                                          2DBAR184
      IF (N.GT. LIMITT - 4) INC = 1                                     2DBAR185
      IF (N .LT. 15 .AND. IBCD .EQ. 1) INC = 1                          2DBAR186
      MMM = MM*(N/MM)                                                   2DBAR187
      IF(N .NE. MMM )   GO TO 41                                        2DBAR188
      TIME =DT* FM                                                      2DBAR189
      DO 40 K= 1,JJ,JZWRT                                               2DBAR190
      DO 40 I= INC, LIMITI, INC                                         2DBAR191
      Z=DZ*FLOAT(K-1)                                                   2DBAR192
      R=DR* FLOAT(I-1)                                                  2DBAR193
      EPS = (W(I,K+1, 2) - W(I,K,2))/DZ                                 2DBAR194
      WRITE (6,45)  TIME, R, Z, U(I,K,2) , W(I,K,2)   ,EPS              2DBAR195
   45 FORMAT( 1X,3(F7.3) ,3(E20.8), 20X)                                2DBAR196
   40 CONTINUE                                                          2DBAR197
   41 CONTINUE                                                          2DBAR198
   50 CONTINUE                                                          2DBAR199
   60 CONTINUE                                                          2DBAR200
      GO TO 2                                                           2DBAR201
      RETURN                                                            2DBAR202
```

```
      END                                                                2DBAR203
C     SUBROUTINES SSLOVE AND SOLVE ARE PLACED HERE
$DATA
  1 12124 21  8  1.0000206520.100  0.127  0.127  0.3125 0.723952.7135
-     END OF FILE
```

DISPLACEMENTS, U(R) AND U(Z) IN CENTIMETERS.

TIME IN MICROSECONDS.

R AND Z IN CENTIMETERS.

POISSON'S RATIO IS 0.312.

YOUNGS MODULUS IS 0.724 (MBARS).

DENSITY IS 2.713(GM/CC).

TIME	R	Z	U(R)	U(Z)	STRAIN
0.	1.270	0.	0.10108650E-05	0.33003810E-05	-0.25987252E-04
0.	1.270	0.127	0.	0.	0.
0.	1.270	0.254	0.	0.	0.
0.	1.270	0.381	0.	0.	0.
0.	1.270	0.508	0.	0.	0.
0.	1.270	0.635	0.	0.	0.
0.	1.270	0.762	0.	0.	0.
0.	1.270	0.889	0.	0.	0.
0.	1.270	1.016	0.	0.	0.
0.	1.270	1.143	0.	0.	0.
0.100	1.270	0.	0.10624410E-05	0.39699524E-05	-0.25999943E-04
0.100	1.270	0.127	0.37883148E-08	0.66795969E-06	-0.52595251E-05
0.100	1.270	0.254	-0.	-0.	-0.
0.100	1.270	0.381	-0.	-0.	-0.
0.100	1.270	0.508	-0.	-0.	-0.
0.100	1.270	0.635	-0.	-0.	-0.
0.100	1.270	0.762	-0.	-0.	-0.
0.100	1.270	0.889	-0.	-0.	-0.
0.100	1.270	1.016	-0.	-0.	-0.

Program Details

Input data (cards 005-007)

MM is the number of time increments the program computes before output is again obtained.

LIMITI is the number of radial zones.

LIMITT is the total number of time increments.

LIMITZ is the number of axial zones.

JZCAL is the approximate number of axial increments that are computed beyond the front of the wave.

JZWRT is the number of axial increments the program computes before output is again obtained.

PO is the magnitude of the step in pressure at z = 0.

IBCD either equals 1 or 2
IBCD = 1 for a free end at z = L
IBCD = 2 for a fixed end at z = L

XNU is the Poisson ratio.

Frequently used constants (cards 008-016)

Output formats (cards 017-031)

These statements produce the output shown at the top of the preceding page.

Set initial conditions (cards 032-036)

Time base (cards 038-039)

TIME = FM*DT

Pressure condition (card 040)

Although it is not shown, this card allows the use of a time dependent pressure at z = 0.

Equations of motion (cards 043-066)

Cards 048-066 are equations (40) of the text.

Boundary conditions (cards 074-177)

JJ is the largest number of axial increments for which boundary conditions are necessary.

Cards 078-082 are the r = 0 conditions for proper behavior.

Cards 084-088 are the boundary conditions for a fixed end at z = L. These are equations (88) and (89) of the text.

Cards 091-129 are the boundary conditions for a free end at z = L. These are equations (86) of the text. These equations are rewritten in the following system:

$$(AA)\ (XX) = (BB)$$

where XX(I) is defined as shown in cards 122-125. This linear system is solved by using the subroutine SSOLVE.[1]

Cards 131-165 are the boundary conditions for a pressure at z = 0. These are equations (80) and (81) of the text which are rewritten in the system (A) (X) = (B). The method is the same as used for a free end at z = L. In fact, the same subroutine was used with a different name--SOLVE.[1] This is done so that the inverse for each matrix can be calculated and stored separately.

Cards 166-173 are the boundary conditions at r = R. These cards are equations (44) of the text.

Reset initial conditions (cards 178-184)

Output statements (cards 185-198)

These statements yield the values shown on the first output page included immediately after the program.

INC (see card 075) is like the number of radial increments the program computes before output is again obtained. For INC = 11, only the surface values are given in the output.

GO TO 2 (card 201)

This allows the solution of more than one problem (by adding another data card). After the last data card, the program (card 005) reads the end of file card and a normal program halt occurs.

---

[1]Subroutines SSOLVE and SOLVE were obtained from the Share Distribution Agency under the name of STUSOLV and number of 3194. The only change made in this subroutine was to increase the dimension of the system from 20 to 30.

APPENDIX D

NUMERICAL VALUES FOR POCHHAMMER-CHREE SOLUTION

TABLE 4

Numerical Values for Pochhammer-Chree Solution

d/λ'	ν	r/R	U/U_{max}	W/W_{max}
0.30	0.25	0	0.00000	1.00000
		0.1	0.11401	0.99854
		0.2	0.22712	0.99419
		0.3	0.33845	0.98699
		0.4	0.44715	0.97702
		0.5	0.55236	0.96439
		0.6	0.65329	0.94924
		0.7	0.74919	0.93173
		0.8	0.83935	0.91206
		0.9	0.92314	0.89044
		1.0	1.00000	0.86711
0.35	0.25	0	0.00000	1.00000
		0.1	0.11960	0.99874
		0.2	0.23792	0.99137
		0.3	0.35372	0.98070
		0.4	0.46578	0.96598
		0.5	0.57292	0.94742
		0.6	0.67407	0.92527
		0.7	0.76820	0.89987
		0.8	0.85441	0.87156
		0.9	0.93190	0.84076
		1.0	1.00000	0.80790
0.40	0.25	0	0.00000	1.00000
		0.1	0.12630	0.99690
		0.2	0.25086	0.98765
		0.3	0.37198	0.97242
		0.4	0.48801	0.95147
		0.5	0.59740	0.92517
		0.6	0.69871	0.89399
		0.7	0.79065	0.85847
		0.8	0.87211	0.81924
		0.9	0.94213	0.77699
		1.0	1.00000	0.73247

TABLE 4--Continued

d/λ'	ν	r/R	U/U_{max}	W/W_{max}
0.45	0.25	0	0.00000	1.00000
		0.1	0.13406	0.99571
		0.2	0.26583	0.98291
		0.3	0.39307	0.96189
		0.4	0.51363	0.93307
		0.5	0.62553	0.89704
		0.6	0.72694	0.85456
		0.7	0.81627	0.80650
		0.8	0.89221	0.75385
		0.9	0.95369	0.69771
		1.0	1.00000	0.63923
0.50	0.25	0	0.00000	1.00000
		0.1	0.14261	0.99427
		0.2	0.28232	0.97722
		0.3	0.41628	0.94925
		0.4	0.54180	0.91099
		0.5	0.65639	0.86335
		0.6	0.75783	0.80743
		0.7	0.84423	0.74452
		0.8	0.91406	0.67608
		0.9	0.96622	0.60369
		1.0	1.00000	0.52900
0.55	0.25	0	0.00000	1.00000
		0.1	0.15143	0.99269
		0.2	0.29932	0.97093
		0.3	0.44019	0.93527
		0.4	0.57079	0.88660
		0.5	0.68813	0.82611
		0.6	0.78958	0.75532
		0.7	0.87293	0.67596
		0.8	0.93648	0.58999
		0.9	0.97904	0.49951
		1.0	1.00000	0.40671
0.60	0.25	0	0.00000	1.00000
		0.1	0.15978	0.99112
		0.2	0.31540	0.96470
		0.3	0.46283	0.92142
		0.4	0.59828	0.86236
		0.5	0.71826	0.78901
		0.6	0.81977	0.70321
		0.7	0.90029	0.60710
		0.8	0.95790	0.50305
		0.9	0.99134	0.39360
		1.0	1.00000	0.28139

TABLE 4--Continued

d/λ'	ν	r/R	U/U_{max}	W/W_{max}
0.90	0.25	0	0.00000	1.00000
		0.1	0.17532	0.98742
		0.2	0.34565	0.94972
		0.3	0.50607	0.88701
		0.4	0.65173	0.79946
		0.5	0.77793	0.68724
		0.6	0.88013	0.55046
		0.7	0.95398	0.38910
		0.8	0.99527	0.20290
		0.9	1.00000	-0.00875
		1.0	0.96423	-0.24697
1.20	0.25	0	0.00000	1.00000
		0.1	0.16446	0.99006
		0.2	0.32568	0.95971
		0.3	0.48024	0.90731
		0.4	0.62437	0.83003
		0.5	0.75374	0.72353
		0.6	0.86318	0.58171
		0.7	0.94635	0.39618
		0.8	0.99532	0.15556
		0.9	1.00000	-0.15538
		1.0	0.94740	-0.55697
1.50	0.25	0	0.00000	1.00000
		0.1	0.14536	0.99484
		0.2	0.28979	0.97828
		0.3	0.43204	0.94696
		0.4	0.57012	0.89480
		0.5	0.70087	0.81211
		0.6	0.81926	0.68440
		0.7	0.91749	0.49032
		0.8	0.98369	0.19883
		0.9	1.00000	-0.23502
		1.0	0.93984	-0.87622
2.00	0.25	0	0.00000	0.60888
		0.1	0.10984	0.61202
		0.2	0.22214	0.62052
		0.3	0.33901	0.63136
		0.4	0.46179	0.63848
		0.5	0.59024	0.63095
		0.6	0.72134	0.58974
		0.7	0.84702	0.48235
		0.8	0.95051	0.25374
		0.9	1.00000	-0.18867
		1.0	0.93799	-1.00000

TABLE 4--Continued

d/λ'	ν	r/R	U/U_{max}	W/W_{max}
5.0	0.25	0	0.00000	0.01736
		0.1	0.00931	0.01915
		0.2	0.02151	0.02504
		0.3	0.04049	0.03679
		0.4	0.07234	0.05781
		0.5	0.12725	0.09363
		0.6	0.22187	0.15148
		0.7	0.38078	0.23405
		0.8	0.62880	0.30866
		0.9	0.93905	0.18014
		1.0	1.00000	-1.00000
10.0	0.25	0	0.00000	0.00004
		0.1	0.00005	0.00006
		0.2	0.00019	0.00015
		0.3	0.00059	0.00042
		0.4	0.00186	0.00126
		0.5	0.00599	0.00393
		0.6	0.01945	0.01254
		0.7	0.06359	0.04006
		0.8	0.20529	0.12161
		0.9	0.60898	0.26524
		1.0	1.00000	-1.00000
0.3936	0.29	0	0.00000	1.00000
		0.1	0.12549	0.99673
		0.2	0.24929	0.98697
		0.3	0.36975	0.97090
		0.4	0.48528	0.94881
		0.5	0.59437	0.92108
		0.6	0.69563	0.88820
		0.7	0.78781	0.85077
		0.8	0.86984	0.80945
		0.9	0.94080	0.76498
		1.0	1.00000	0.71816
1.8701	0.29	0	0.00000	0.80793
		0.1	0.12431	0.80936
		0.2	0.24999	0.81259
		0.3	0.37802	0.81409
		0.4	0.50851	0.80705
		0.5	0.63998	0.77962
		0.6	0.76815	0.71203
		0.7	0.88412	0.57184
		0.8	0.97122	0.30605
		0.9	1.00000	-0.17138
		1.0	0.91999	-1.00000

LONGITUDINAL ELASTIC WAVE PROPAGATION IN FINITE CYLINDRICAL BARS

ABSTRACT

by Larry D. Bertholf, Ph.D.
Washington State University, 1966

Chairman: Harry A. Sorenson

The partial differential equations of motion for three-dimensional dynamic elasticity are derived and simplified for the study of longitudinal waves in cylindrical bars. The conditions for proper behavior at r = 0 are examined and a stress-free surface is used at r = R.

The equations of motion and boundary conditions are formulated in terms of deformations and the derivatives are approximated by finite differences. The finite difference equations are integrated for different end conditions with the aid of a digital computer. Stable and accurate numerical solutions are obtained without using the artificial viscosity approximation. The computer program and a detailed explanation are included.

The Pochhammer-Chree solution for an infinite bar is traced. The resulting frequency equation is solved numerically for many wave lengths and the radial distributions of the deformations are presented.

A numerical solution of the differential equations is compared with the Pochhammer-Chree solution for $d/\lambda' = 0.3$. A

harmonic axial deformation condition is imposed numerically at $z = 0$ and the comparison is made after numerical values are obtained for large values of z and t. Agreement of the solutions is obtained for distances greater than four diameters from $z = 0$ and times greater than $(z + 6\ d)/c_o$.

A numerical solution is obtained also for a step change in pressure at $z = 0$. The numerical results exhibit a time-dependent region that corresponds to the one-dimensional strain solution. For large values of time the solution approaches the one-dimensional stress solution. At one and two diameters from the application of the pressure, the numerical results are compared with experimental data obtained by Miklowitz and Nisewanger at the radial surface. The important features of these data are reproduced by the numerical solution.

Numerical solutions are obtained for reflections in finite bars by including difference approximations for the boundary conditions at $z = L$. A step change in pressure is imposed numerically at the $z = 0$ end of a one-inch diameter aluminum bar and four separate problems are considered: (1) bar length of one diameter with a stress free end at $z = L$, (2) bar length of one diameter with a fixed end at $z = L$, (3) bar length of two diameters with a stress-free end at $z = L$, and (4) bar length of two diameters with a fixed end at $z = L$. In the shorter bar, numerical results are obtained for reflections from both ends; that is, the $z = L$ and the $z = 0$ ends. The numerical solution qualitatively agrees with the elementary bar solution. Numerical values for the time

dependence of the axial strain at the radial surface are presented at several axial positions.